Title
NUCLEAR STRUCTURE, FISSION, AND SUPERHEAVY ELEMENTS. LECTURE NOTES

Author
Nilsson, Sven Gosta.

Publication Date
1968-08-01

UCRL-18355 Rev.

Cy. 2

Lecture notes:

NUCLEAR STRUCTURE, FISSION, AND SUPERHEAVY ELEMENTS

Sven Gösta Nilsson

INSTITUT D'ETUDES SCIENTIFIQUES DE CARGÈSE (CORSICA)

SUMMER INSTITUTE ON NUCLEAR PHYSICS

September 2-28, 1968

LAWRENCE RADIATION LABORATORY
UNIVERSITY of CALIFORNIA BERKELEY

Cy. 2

UCRL-18355 Rev.

DISCLAIMER

To be presented at Institut d'Etudes Scientifiques
de Cargése (Corsica)

UCRL-18355-Rev.-
Preprint

UNIVERSITY OF CALIFORNIA

Lawrence Radiation Laboratory
Berkeley, California

AEC Contract No. W-7405-eng-48

Lecture notes:

NUCLEAR STRUCTURE, FISSION, AND SUPERHEAVY ELEMENTS

Sven Gösta Nilsson

INSTITUT D'ETUDES SCIENTIFIQUES DE CARGÉSE (CORSICA)

SUMMER INSTITUTE ON NUCLEAR PHYSICS

September 2- 28, 1968

NUCLEAR STRUCTURE, FISSION, AND SUPERHEAVY ELEMENTS*

S. G. Nilsson**

Lawrence Radiation Laboratory
University of California
Berkeley, California 94720

October 1968

INTRODUCTION

The intention behind these lecture notes is to present some material relevant to half-life determinations of fissioning actinide and superheavy elements. In order to deal with this subject at all systematically, we first outline briefly the general problem of nuclear stability as seen from the view-point of the semiempirical mass formula. Furthermore we consider the modifications brought about by the deformation dependent shell model. Finally, we discuss the most critical mode of decay of very heavy elements – spontaneous fission – first from the point of view of statics, the character of the nuclear potential energy surface, secondly, from the point of view of dynamics, aiming at the description of the penetration of the fission barrier and the estimate of the inertial mass associated with the penetration.

---

* Work supported by the U.S. Atomic Energy Commission, based on investigations in cooperation with C. F. Tsang, Lawrence Radiation Laboratory; Z. Szymanski, A. Sobiczewski and S. Wycech, University of Warsaw, Warsaw, Poland; P. Möller, and C. Gustafson, Lund Institute of Technology, Lund, Sweden. A common publication is forthcoming.

** On leave of absence from Department of Mathematical Physics, Lund Institute of Technology, Lund, Sweden.

I. NUCLEAR STABILITY FROM THE POINT OF VIEW OF THE SEMIEMPIRICAL MASS FORMULA

The nuclear binding energy $B(N,Z)$ is defined in the following way

$$m(N,Z) = \frac{1}{c^2} E(N,Z) = NM_N + ZM_Z - \frac{1}{c^2} B(N,Z)$$

where $m(N,Z)$ is the actual mass of a nuclide, corresponding to neutron number N and proton number Z, and M_N and M_Z the free neutron and proton masses. From an analysis of available nuclear masses (now numbering approximately 1200) already in the 1930's V. Weizsächer[1] and Bethe and Backer[2] were able to identify four leading terms that relatively well accounted for the variation of B with N and Z:

$$B = b_{vol} A - b_{surf} A^{2/3} - \frac{1}{2} b_{sym} \frac{(N-Z)^2}{A} - \frac{3}{5} \frac{Z^2 e^2}{R} \quad .$$

The first two terms are formally the same as those employed to describe a liquid drop. The charge term is also the same provided the liquid is homogeneously charged. A straight-forward generalization of this formula to describe other shapes of the nucleus than the spherical equilibrium one is usually called the liquid-drop model of the nucleus.

Let us discuss briefly each one of these four terms. The first and dominant term, the volume energy, reflects the nearly linear A-dependence of the nuclear volume or the A-independence of the nuclear density. Every nucleon appears to interact basically with the nearest of its neighbors. Most authors give $b_{vol} \simeq 16$ MeV. This is the binding energy per particle of nuclear matter, the latter so defined that surface effects are negligible

and Coulomb interaction nonexistant. Furthermore, there are equal numbers of neutrons and protons, by definition, in nuclear matter.

The second term, the surface energy, proportional to the nuclear surface area, represents the loss of binding suffered by the particles in the surface layer due to the lower density (fewer neighbors) there. On the other hand the average kinetic energy in a realistic nuclear surface is less than that in the nuclear bulk.* A fit to mass data gives approximately $b_{surf} \approx 18\text{-}20$ MeV.

The third term, the symmetry energy, reflects the fact that, nuclear forces favor equal numbers of neutrons and protons, or $N = Z$. In the case $N = Z$ the limitations brought about by the Pauli principle are reduced to a minimum. With a b_{sym} of ≈ 50 MeV, this term decides the width of the mass valley and together with the Coulomb term the stability line.

The last term, the electric repulsion term, corresponds to the electrostatic energy of a homogeneously charged sphere of radius R_c. One may regard this quantity as an available mass formula parameter. One should, however, expect it to approximate the value normally assumed for the nuclear radius. The half-density radius $R_{1/2}$, defined as the radius where the density is half of that in the center, is assumed to be[3]

$$R_{1/2} \simeq 1.1 \times A^{1/3} \text{ fm} .$$

*On this latter point see W. J. Swiatecki, Proc. Phys. Soc. A., 64 (1951) 226.

The commonly employed rms-radius, defined as

$$R_{rms} = \sqrt{5/3}\ \langle r^2 \rangle \simeq 1.2 \times A^{1/3}\ \text{fm}$$

is consistent with $R_{1/2} \simeq 1.1 \times A^{1/3}$ fm, provided there is a certain depth of diffuseness, and for this depth one assumes

$$d = R(\rho = 10\%) - R(\rho = 90\%) \approx 2\text{-}3\ \text{fm} \quad .$$

The value of R_c employed to fit mass data is usually near $R_c \simeq 1.25 \times A^{1/3}$ fm. The excess of R_c over $R_{1/2}$ is roughly consistent with the quoted diffuseness of the charge distribution. However, if one adds a specific diffuseness correction term and an exchange correction term to the electrostatic energy as follows (see e.g., W. D. Myers and W. J. Swiatecki, Ref. 4)

$$E_c = \frac{3}{5}\ \frac{Z^2 e^2}{R_c}\ \left(1 - \frac{\pi^2}{2}\ \frac{5}{3} \left(\frac{a}{R_c} \right)^2 - \frac{0.7636}{Z^{2/3}} \right)$$

where the diffuseness parameter a is related to d by $d \simeq 2a \ln 9$, one should expect to use an R_c value near to $R_{1/2}$. Instead the mass fit* by Myers and Swiatecki[4] gives $R_c = 1.2249 \times A^{1/3}$ fm, a fact which hints that the Coulomb energy term in their semiempirical mass formula hides some additional effect otherwise not explicitly accounted for.

*See second paper quoted under Ref. 4.

Some of the different terms of the mass formula are clearly discernible in Fig. 1. Thus, one sees that the nuclear matter limit of 16 MeV is never reached, not even approached. Still the binding energy per nucleon is roughly constant (~ 8 MeV) for $A \geq 40$. Below this A-value the surface energy dominates. The negative slope for $A \gtrsim 60$ reflects the growing importance of the Coulomb energy term.

It has been argued that not only the volume energy,* but also the surface energy should be isospin dependent. Thus one has added a symmetry dependent term to the surface energy which is now written

$$E_s = b'_{surf} A^{2/3} \left(1 - \gamma \left(\frac{N-Z}{A} \right)^2 \right)$$

where Ref. 4 gives $b'_{surf} = 17.944$ MeV, $\gamma = 1.7826$. (In this reference** furthermore $b_{vol} = 15.494$ MeV, $b_{sym} = 55.24$ MeV.) To these terms there is finally added a pairing energy term $P(N,Z)$ usually taken equal to $(-\Delta, 0, \Delta)$ for even-even, odd-A, and odd-odd nuclei, respectively, where

*The symmetry energy earlier introduced is such a term proportional to

$$A \cdot \left(\frac{N-Z}{A} \right)^2$$ or to the nuclear volume. See Ref. 4.

**We have in the present investigation employed the values cited, taken from the second paper quoted under Ref. 4.

$$\Delta \approx 12 / \sqrt{A} \text{ MeV}^{*}.^{5}$$

In terms of this semiempirical mass formula, where no account is made for a possible deviation from a purely spherical shape, one may now study the region of nuclear stability with respect to various break-ups and transformation phenomena such as beta-decay, neutron- and proton-emission, spontaneous fission, and alpha-decay.

The trend of the mass valley (beta-stability line) is obtained from the condition

$$\left(\frac{\partial m}{\partial N}\right)_{A = \text{const}} = 0 \quad .$$

This leads to the relation[5] below for $\gamma = 0$

$$N - Z = \frac{\frac{3}{10}\frac{e^2}{R_c} A - (M_n - M_p)c^2}{\frac{b_{sym}}{A} + \frac{3}{10}\frac{e^2}{R_c}} \quad .$$

*P. E. Nemirovsky and Yu. V. Adamchuk (Nucl. Phys. 39 (1962) 551) give for the average odd-even mass difference the expression $\Delta = 11.56/A^{0.552}$ MeV applying to both protons and neutrons. (The authors also propose two alternative, slightly different functions of A.) One may in addition note in the empirical data a weak but systematic excess of Δ_p over Δ_n.

For very large A, Green[6] has found an alternative and simpler approximate relation

$$N - Z = \frac{0.4 \times A^2}{A + 200} \quad .$$

The heaviest attainable neutron isotope of a given element corresponds to zero neutron separation energy, or

$$\left(\frac{\partial B}{\partial N}\right)_{Z = \text{const}} = 0 \quad .$$

The so-called neutron "drip line" is of great astrophysical interest. The corresponding proton "drip line" corresponds to the condition

$$\left(\frac{\partial B}{\partial Z}\right)_{N = \text{const}} = 0 \quad .$$

Instability with respect to alpha decay and spontaneous fission set additional limits to the availability of nuclides. Especially the limit of availability for a heavy-A nucleus is largely decided by the spontaneous fission process. The largest binding energy per particle is realized for systems near $^{56}_{26}Fe$, and all nuclei with A > 100-120 are unstable against fission. The lifetimes are, however, so long that the fission process is unimportant for normal nuclides of A < 230. The spontaneous fission half-life of $^{230}_{90}Th$ is approximately 10^{17} years, while the same for $^{240}_{94}Pu$ is $\simeq 10^{11}$ years, for $^{254}_{102}No$ 10 sec, and for $^{260}_{104}Ku$ 0.3 sec. The fall-off of half-lives with A is thus very rapid. The liquid drop model (see below) makes Z^2/A the

one relevant parameter for the fission process, and it has been inferred that the quantity Z^2/A being ≈ 41 should correspond to half-lives in the region of seconds (which in the $Z = 100$ region is a rather appropriate estimate).

The use of the semiempirical mass formula defines only rough boundaries to the regions of long-lived or stable nuclei (see Fig. 2). The mass valley boundaries are in their details connected with nuclear shell structure that gives modifications in the binding energy relative to the predictions of the semiempirical mass formula of the order of $\pm$ 10 MeV for heavy nuclei. The problem of a possible island of relative stability beyond the short-lived heavy nuclei of $Z = 102$-105 recently under investigation is directly connected with the existence of nuclear magic numbers (in this case $Z = 114$, $N = 184$).

A comparison of empirical nuclear masses with the semiempirical mass formula, fit in terms of five free mass parameters, b_{vol}, b_{surf}, b_{sym}, γ, and R_c, as determined by Myers and Swiatecki,[4] is exhibited in Fig. 3. The plot is constructed in terms of neutron number N and the sharp increase in binding connected with $N = 28$, 50, 82, and 126 is clearly visible.

Although it is tempting, one cannot employ the mass formula for much larger or very different systems than those encountered in the neighborhood of the beta-stable mass valley. Thus, e.g., it cannot answer the problem as to whether finite masses of pure neutron matter are stable. For this, a discussion of the nuclear matter problem, the reader is referred to other lecture series offered in this summer school.

Even if neutron matter has a negative nuclear binding, the superposition of the gravitational attraction may finally make a large assembly of neutrons stable (a neutron star). Essentially employing the undeterminancy relation

to estimate the nuclear energy associated with the location of nucleons within a box of measure r_o, the space alloted to a nucleon in a close-packed neutron star, one can estimate[5] the critical mass number of such a star as

$$A_{crit} \simeq \left(\frac{\hbar^2}{GM^3 r_o} \right)^{3/2} \simeq 10^{56}$$

where G is the gravitational constant. This mass number corresponds to a mass of about 1/10 of the solar mass. It has been suggested that matter in this state could possibly be associated with the white dwarf state of stellar evolution.[5]

II. THE NUCLEAR POTENTIAL

Nuclear shell structure affects mainly the binding of the last few nucleons and gives rise to fluctuations relative to the smooth behavior of the mass formula of the order of 10 MeV (see Fig. 3). Although this represents a small quantity ($\approx 1\%$) compared to, e.g., the nuclear surface energy, shell structure is responsible for the existence of nonspherical equilibrium shapes, shape isomers and for nuclear spectra in general.

The condition for a Fermi gas model to be valid is that the mean free path of a nucleon inside the nucleus is larger than the average internucleon distance. For a shell model field to be appropriate it is required that the mean free path is larger than the dimensions of the entire nucleus.[5] Experimentally, even this latter condition appears to be fulfilled.

From the fact that the nucleon separation energy is approximately 10 MeV and the nucleon kinetic energy (which can be estimated from the Fermi gas model) is about 40 MeV one may conclude that the potential depth should be of the order of -50 MeV. Actually, a detailed study shows that the potential is somewhat momentum dependent and the effective potential, V, due to the velocity dependence of the nuclear two-body force, is somewhat deeper for particles far below the Fermi surface and somewhat shallower for the ones far above. One may thus write the potential as a first order expansion in the nucleon kinetic energy

$$V = V(\epsilon_{kin} = 0) + a \cdot \epsilon_{kin} + \text{----} \quad .$$

The second term can then formally be included in the single-particle kinetic

energy term through an effective mass M^* defined by

$$\frac{M}{M^*} = 1 + a \quad .$$

From the nuclear level density encountered experimentally it appears that it is appropriate to use $M \approx M^*$ near the Fermi surface while M^* approaches $M/2$ for the states near the bottom of the potential.

In heavy nuclei the nuclear potential felt by neutrons and protons becomes somewhat different due to the excess in numbers of neutrons over protons. On account of the Pauli principle there is less probability for two like nucleons to come within the range of strong attraction than for two unlike ones. The neutron potential is therefore largely generated by the protons and vice versa. The isospin dependent part of the potential is reflected in the mass formula in the symmetry energy term. We may write for the potential

$$V = V_o + \frac{1}{2} t_3 \times \frac{N-Z}{A} \times V_1 \qquad \begin{cases} t_3 = \frac{1}{2} & \text{(neutron)} \\ t_3 = -\frac{1}{2} & \text{(proton)} \end{cases} \quad .$$

The last term, when evaluated in the independent-particle approximation, leads to the following symmetry energy term

$$(E_{sym})_{pot} \approx \frac{1}{8} \frac{(N-Z)^2}{A} \langle V_1 \rangle \quad .$$

It is generally assumed that half of the symmetry energy term derives from potential energy and half from kinetic energy.[5] This would correspond to

$$V_1 \approx 2\, b_{sym} \approx 100 \text{ MeV} .$$

For ^{238}U the difference between the neutron and proton potential (representing strong interactions) amounts to about 15 MeV. For the protons, however, this difference is more than compensated for by the repulsive Coulomb potential.

As pointed out by Lane[10] the empirically derived charge dependent term of the potential can be recognized as the main part of a more general term proportional to the scalar product of $\vec{t}$, the nucleon isospin, and $\vec{T}_{A-1}$, the isospin vector of the rest of the nucleus. Due to the well-known alignment of the nuclear wave functions in isospace, only the 3-components of this scalar product contribute significantly, resulting in a term proportional to t_3 (N-Z).

A. Nuclear Potentials Employed in Literature

The potentials that have been employed are limited by what is mathematically convenient or manageable. With the advent of present day computers a more complicated potential "ansatz" can be explored. From the analysis of a large body of scattering data for spherical near-closed shell nuclei the parameters of a spherical potential of the Woods-Saxon type have been determined. As an example we quote the Woods-Saxon potential fitted by Rost[11] to reproduce the observed single-particle level order near N = 126, Z = 82 (see below, Figs. 6a and 6b), as well as observed relative stripping

cross-sections. (This potential is in fair agreement with those employed by Blomquist and Wahlborn[12] and Sliv.[13])

We quote here the parameters of the potential employed

$$V_c = \overset{o}{V}_c \, f(r)$$

where

$$f(r) = \frac{1}{1 + e^{\frac{r-R_{1/2}}{a}}}$$

and

$$R_{1/2} = r_o \times A^{1/3}$$

for protons and neutrons, respectively; Rost finds $r_o = 1.275$ fm for protons and $r_o = 1.347$ fm for neutrons and a diffuseness parameter $a = 0.70$ fm for both neutrons and protons. Optimum $\overset{o}{V}_c$ is found to equal -58.7 MeV for protons and -40.6 MeV for neutrons.

The spin-orbit term is defined as

$$V_{so} = -2\lambda \, \overset{o}{V}_c \left(\frac{\hbar}{2Mc} \right)^2 (\vec{\ell} \cdot \vec{s}) \, \frac{1}{r} \, \frac{d}{dr} f(r)$$

where $f(r)$ is a term of the same character as above, with $a_{so} = a = 0.70$ fm and furthermore $r_{so} = r_o$. The parameter λ is chosen differently for protons and neutrons, 17.8 and 31.5, respectively, according to Rost.

To cite another of many examples, Gareev, Ivanova, and Kalinkin[14] employ the same type of potential in the deformed case but assume the range parameters r_o and a to be the same for neutrons and protons.

For $\overset{o}{V}_c$ they assume

$$\overset{o}{V}_c = -53\left(1 \pm 0.63 \times \frac{N-Z}{A}\right) \text{ MeV} \qquad \begin{cases} \text{protons} \\ \text{neutrons} \end{cases}$$

and for the spin-orbit term

$$\lambda \sim 1 + 2 \times \frac{N-Z}{A} \quad (\text{protons } \underline{\text{and}} \text{ neutrons}) \quad .$$

Provided the difference in range for neutrons and protons could be neglected in the Rost case the corresponding numbers, cited above, would be

$$\overset{o}{V}_c = -49.65\left(1 \pm 0.86 \times \frac{N-Z}{A}\right) \text{ MeV}$$

and

$$\lambda \sim \left(1 \mp 1.31 \times \frac{N-Z}{A}\right)$$

where the upper sign applied to protons and the lower sign to neutrons. Thus, the greatest difference lies in the treatment of the spin-orbit term, the Rost potential suggesting a somewhat smaller spin-orbit splitting strength for protons than for neutrons for heavy nuclei while for the scheme of Ref. 14 the reverse is true.

B. Oscillator Potential, Spherical and Deformed

The Woods-Saxon potential in principle lends itself to the treatment of distorted shapes. One may thus (see Ref. 16) use $a = \text{const}$ and let $R_{1/2}$ be angle dependent, thus,

$$R_{1/2} \sim \overset{\circ}{R}_{1/2} (1 + \beta_2 Y_{20} + \beta_4 Y_{40} + \beta_6 Y_{60}) \quad .$$

However, the resulting numerical problem of finding single-particle orbitals is there formidable unless some expansion of V_c is employed. To the extent that large β_2-values are involved (quadrupole distortions) the expansion of the potential is essentially nonconvergent* beyond, say, $\beta_2 \approx 0.4$. All calculations at large distortions have been made in terms of a modified harmonic oscillator potential. For equilibrium distortions in the rare earth and actinide regions, where energy levels and single-particle wave functions both from a modified oscillator and from an expanded Woods-Saxon potential are available, no significant advantage of the one compared to the other are apparent, as far as single-particle level order is concerned. Strangely enough this holds true even for relative stripping cross-section prediction.

*N. K. Glendenning, private communication. By employing suitable coordinates the large quadrupole term in the Woods-Saxon potential can be transformed away. The kinetic energy term, in turn becoming asymmetric, can easily be handled.[16]

For this reason we have found it advantageous to base an analysis of the probability for spontaneous fission on the modified harmonic oscillator model.

Let us first consider the simple quadrupole terms introduced by the non-isotropy of the oscillator potential assumed

$$V_{osc} = \frac{M}{2} \left[\omega_\perp^2 (x^2 + y^2) + \omega_z^2 z^2 \right]$$

with[16]

$$\omega_z = \omega_o(\epsilon)(1 - \tfrac{2}{3} \epsilon)$$

$$\omega_\perp = \omega_o(\epsilon)(1 + \tfrac{1}{3} \epsilon) \quad .$$

This leads to a distortion dependent part of the potential proportional to $\epsilon(1 - \frac{1}{6} \epsilon)r^2P_2(\cos \theta)$.

It turns out to be advantageous to use stretched coordinates $\sqrt{M\omega_\perp/\hbar}\ x = \xi$, etc. With the help of these one may transform away coupling terms of $r^2P_2(\cos \theta)$ between shells N and $N \pm 2$.

The spin-orbit term is an essential feature of the central potential. In the deformed case it is reasonable[5] to generalize this term into a term proportional to $\vec{s} \cdot (\vec{p} \times \vec{\nabla} V)$. As $\vec{s}$, $\vec{v}$, and grad V are the only three available vectors of the nucleon motion, this is the simplest invariant term one may construct.

If one were to derive a spin-orbit term from the deformed harmonic oscillator using the above prescription one would find

$$V_{so} = \lambda M\omega_o^2 \left[\left(\frac{\omega_z}{\omega_\perp} \right)^{1/3} (\vec{\ell}_T \cdot \vec{s}) + \left\{ \left(\frac{\omega_\perp}{\omega_z} \right)^{2/3} - \left(\frac{\omega_z}{\omega_\perp} \right)^{1/3} \right\} \ell_3 s_3 \right]$$

$$\sim \vec{\ell}_T \cdot \vec{s}$$

where the last term in the bracket, for moderate deformation, is very small and where $\vec{\ell}_T$ is defined in terms of the "stretched-all-the-way" coordinates

$$a = \sqrt{\frac{M\omega_o}{\hbar}} \frac{\omega_\perp}{\omega_o} \quad x \quad \text{etc.}$$

(which transform the harmonic oscillator ellipsoid into a sphere).

Presently we have been content with going half the way in this direction by replacing $\vec{\ell} \cdot \vec{s}$ by $\vec{\ell}_t \cdot \vec{s}$, where $\vec{\ell}_t$ is defined in the stretched coordinates mentioned, $\xi \sim \sqrt{\omega_\perp} \cdot x$ etc. The Hamiltonian then takes for form[16]

$$H_{sp} = T + \frac{1}{2} \hbar\omega_o \left[- \Delta_\rho + \rho^2 - \frac{2}{3} \epsilon\rho^2 P_2 (\cos \theta_t) \right.$$

$$\left. + \frac{2}{3} \epsilon \frac{1}{2} \left(2 \frac{\partial^2}{\partial\zeta^2} - \frac{\partial^2}{\partial\xi^2} - \frac{\partial^2}{\partial\eta^2} \right) \right] + C \vec{\ell}_t \cdot \vec{s} \quad .$$

Here ρ^2 is defined as

$$\rho^2 = \xi^2 + \eta^2 + \zeta^2 \quad .$$

To this we have added terms proportional to* (cf. Ref. 9).

$$\epsilon_4\rho^2 P_4(\cos\theta), \quad \epsilon_6\rho^2 P_6(\cos\theta), \quad \text{and} \quad \epsilon_3\rho^2 P_3(\cos\theta) \quad .$$

We will return to these terms below.

It is well-known that one cannot fit the deformed level spectra by this potential without a correction term that truncates the potential more and more with increasing A. It is natural to consider an expansion of the radial dependence of the potential, of which the r^2 (oscillator) term is to be considered the lowest-order term. One might think of adding first an r^4 or a ρ^4 term, which latter somewhat better adjusts to the deformed shape, or rather – and this might appear a more consistent approach – a

*Distortions of the nuclear potential in connection with the equilibrium state have recently been considered by P. Vogel, Phys. Letters 25B (1967) 65 (P_3 deformations) and C. Brihage and G. Reidemeister, Nucl. Phys. A100 (1967) 65 (P_4 deformations).

term proportional to V_{osc}^2.* The matrix elements of a term ρ^4 within one shell are actually the same as those of $\left(-\frac{1}{2}\vec{\ell}^{\,2}\right)$ apart from constants. Thus, one has

$$\langle N\ell'\Lambda'|\rho^4|N\ell\Lambda\rangle = \delta_{\ell\,\ell'}\,\delta_{\Lambda\,\Lambda'}\left[\frac{3}{2}N(N+3) - \frac{1}{2}\ell(\ell+1) + \frac{15}{4}\right] .$$

C. The Oscillator Frequency and the Respective Radii of Proton and Neutron Matter

The oscillator parameter $\overset{o}{\omega}_o$ is usually determined from the condition that the nuclear radius be reproduced. From a simple application of the Thomas-Fermi model to the spherical case, or by simply summing matrix elements of $\langle r^2\rangle$ for the pure harmonic oscillator, one obtains[16]

$$\hbar\omega_o = 41\, A^{-1/3} \text{ MeV} .$$

With the wave functions available we may then go back and calculate $\langle\overline{r^2}\rangle$ for protons and neutrons. One then finds[17,18] for this value of $\hbar\omega_o$ at spherical shape

*Preliminary results along this latter line are, however, somewhat discouraging (P. Möller, private communication).

$$\langle \overline{r^2} \rangle_p \simeq \frac{3}{5} (0.95 \rightarrow 0.98)\, r_o^2\, A^{2/3}$$

$$\langle \overline{r^2} \rangle_n \simeq \frac{3}{5} (1.05 \rightarrow 1.09)\, r_o^2\, A^{2/3} \quad .$$

To obtain the average radius correctly it is found that $A^{1/3} \cdot \hbar\omega \simeq 40$ MeV is a somewhat better value than 41 MeV. Furthermore one is not confined to employing the same value of $\hbar\omega_o$ for neutrons and protons. One may let the different neutron and proton potentials and the Coulomb repulsion on the protons be reflected in the use of $\omega_n \neq \omega_p$. Indeed one can fulfill the requirement of

$$\langle r^2 \rangle_n \simeq \langle r^2 \rangle_p$$

approximately by choosing

$$\overset{o}{\omega}_n = \overset{o}{\omega}_o \left(1 + \frac{1}{3} \frac{N-Z}{A} \right)$$
$$\overset{o}{\omega}_p = \overset{o}{\omega}_o \left(1 - \frac{1}{3} \frac{N-Z}{A} \right) \quad .$$

This corresponds to an isospin vector term

$$V_1 = \frac{1}{2} M\omega_o^2 r^2 \frac{4}{3} \frac{N-Z}{A} \cdot t_3 \quad .$$

This term, whose average value is

$$\langle V_1 \rangle = \langle \frac{1}{2} M\omega_o^2 r^2 \rangle \frac{4}{3} \frac{N-Z}{A} t_3$$
$$\simeq 20 \frac{N-Z}{A} t_3 \text{ (MeV)}$$

represents the difference between the repulsive Coulomb energy term and the additional attractive contribution to the proton potential (originating from the strong interaction).

It is presently not clear whether one wants as much excess in the neutron radius as corresponds to the use of $\overset{o}{\omega}_n = \overset{o}{\omega}_p$ or whether requiring $\langle\overline{r^2}\rangle_n = \langle\overline{r^2}\rangle_p$ is more desirable. Calculations carried out with the alternative assumptions exhibit only small relative differences as to equilibrium shapes and barrier heights.*

*Recently a fit to the differential electron scattering cross-section for ^{208}Pb on the basis of a charge distribution obtained from nuclear wave function has been interpreted by L. R. B. Elton, Phys. Letters 26B (1968) 689, to imply a roughly 10% larger value of the r.m.s. radius for neutrons than for protons. Recent experiments on Kaon absorption, assumed to reflect on conditions in the nuclear skin region, indicate a large excess of neutrons over protons for ^{79,81}Br and ^{107,109}Ag (E. H. S. Burhop, Nucl. Phys. 131 (1967) 438). On the other hand, earlier pion absorption experiments (A. Abasian, R. Cool, and J. W. Cronin, Phys. Rev. 104 (1956) 855) giving the ratio $\sigma(\pi^-,p)/\sigma(\pi^+,p)$ at 700 MeV claim to have set a limit of $R_n^{1/2} - R_p^{1/2} = -(0.25 \pm 0.20)$ fm. The determination by J. A. Nolen, J. P. Schiffer, and N. Williams (Phys. Letters 27B (1968) 1) of the neutron r.m.s. radius for ^{208}Pb from the charge r.m.s. radius and from the Coulomb displacement energy of the isobaric analog state gives an excess in the r.m.s. radius for neutrons of 0.07 ± 0.03 fm. We presently tend to interpret the seemingly contradicting situation as indicating more a larger diffuseness for neutrons than an actual difference in the half-radius or even r.m.s. radius.

D. The Condition of Conservation of Equipotential Surfaces

An important problem is the formulation of an auxiliary condition that corresponds to the fact that the nuclear "liquid" at various deformations retains on the average the same density. Hence, due to the short-range nature of the nuclear two-body interaction, the nuclear field should also extend over the same volume in space. One way to formulate this condition mathematically is to require that the volume enclosed by a given equipotential surface be conserved. Implicitly assumed is that the oscillator bottom remains fixed, i.e., that the force field at the very center is left unaffected by changes near the surface.

Consider the surface in x, y, z space spanned by all the points of the same potential energy

$$\frac{M}{2}\left[\omega_\perp^2(x^2+y^2) + \omega_z^2 z^2\right] = \text{const} = V_o \quad .$$

The volume inside this surface is the following

$$\text{vol} = \left(\frac{2V_o}{M}\right)^{3/2} \frac{4\pi}{3} \left(\frac{1}{\omega_\perp}\right)^2 \cdot \frac{1}{\omega_z}$$

which is a constant, provided the condition

$$\omega_z \omega_\perp^2 = \text{const} = \overset{o}{\omega}{}_o^3$$

is fulfilled. It should be emphasized that for a pure harmonic oscillator the same condition applied to all equipotential surfaces.

It can now be noted that a similar volume conservation condition is easy to formulate also when the terms proportional to ϵ_3, ϵ_4, and ϵ_6 are added. Our total potential is then written

$$V_d = \frac{1}{2}\hbar\omega_o(\epsilon, \epsilon_4, \ldots)\rho^2(1 - \frac{2}{3}\epsilon P_2 + 2\epsilon_3 P_3 + 2\epsilon_4 P_4 + 2\epsilon_6 P_6 + \ldots) .$$

The relation between the distortion coordinates ϵ and ϵ_4 on the one hand and α_2 and α_4 defined by the radius vector

$$R(\theta) = R_o(\alpha_2, \alpha_4)(1 + \alpha_2 P_2 + \alpha_4 P_4)$$

on the other hand is illustrated in Fig. 4. It should be noted that the spheroid itself contains, in addition to P_2 and P_4, also P_6, P_8, etc. Such terms are, however, neglected in the diagram. Calculating the volume inside the surface, defined by the next to the last equation above one finds

$$\frac{\omega_o^3}{\omega_o^3} = \frac{1}{(1 + \frac{1}{3}\epsilon)(1 - \frac{2}{3}\epsilon)^{1/2}} \int_{-1}^{1} \frac{\frac{1}{2}\, d(\cos\theta)}{(1 - \frac{2}{3}\epsilon P_2 + 2\epsilon_3 P_3 + 2\epsilon_4 P_4 + 2\epsilon_6 P_6)^{3/2}} .$$

This condition still holds independently of which equipotential surface we choose to consider, and the relative simplicity of the expression above is one reason for adding $\rho^2 P_4$ rather than, e.g., $r^4 P_4$ or $\rho^4 P_4$ to our potential. The same argument holds for the P_3 and P_6 parts of the potential.

Added terms that can be written as powers of V_d can obviously be included in the same volume conservation condition on $\omega_o(\epsilon, \epsilon_4, \ldots)$. However, ρ^4 does not qualify as such a conveniently handled term, nor does the term proportional to $\vec{\ell}_t \cdot \vec{s}$. As the effect of these latter terms is to bring down levels from other shells, it is to be expected that their effect on the volume conservation condition is not negligible. To correct for this neglect without modifying the volume conservation condition above we have subtracted the average value of these terms for each shell. As $\langle \vec{\ell}_t \cdot \vec{s} \rangle$ for each shell has a vanishing mean value, the entire modification* consists of replacing ρ^4 with $\rho^4 - \langle \rho^4 \rangle_N$, or $\vec{\ell}_t^{\,2} - \langle \vec{\ell}_t^{\,2} \rangle_N$.

Actually, the addition of ρ^4 alone tends to push the shells apart beyond the oscillator spacing $\hbar\omega_o$. This corresponds to the fact that the added ρ^4 term makes the well narrower. A subtraction of $\langle \rho^4 \rangle_N$ restores the width of the potential for each shell but still causes the potential walls to rise faster locally than do the pure oscillator walls. The addition of $-\vec{\ell}_t^{\,2}$ on the other hand, lowers the effective oscillator spacing below $\hbar\omega_o$, while $(-\vec{\ell}_t^{\,2} + \langle \vec{\ell}_t^{\,2} \rangle_N)$ restores the spacing to $\hbar\omega_o$. This is possible only with the introduction of the peculiarity that each shell is given its own potential shape. In spite of this artifice, orthogonality is still preserved as long as <u>one</u> entire matrix is diagonalized.

---

*Obviously within one N-shell the matrix elements of $-\frac{1}{2}(\vec{\ell}_t^{\,2} - \langle \vec{\ell}_t^{\,2} \rangle_N)$ and $(\rho^4 - \langle \rho^4 \rangle_N)$ are identical.

E. Single-Particle Energies

In Figs. 2-5 of Ref. 9 we exhibit the energy eigenvalues as functions of ϵ, for ϵ_3, ϵ_4, ϵ_6, equal to zero, for the two important regions of deformed nuclei. These diagrams are roughly adequate for $165 < A < 175$ and $245 < A < 260$. As hexadecapole distortions are important at the beginning and the end of the rare earth and the beginning and end of the actinide regions, we exhibit diagrams (Figs. 5a-h) valid for nuclei with $150 < A < 165$, $175 < A < 190$, $225 < A < 235$, $250 < A < 260$, where $\epsilon = -0.04$, 0.04, -0.04, and 0.04, respectively. More complete level diagrams will be given elsewhere. Slight improvement of the level schemes is noticeable particularly for rare-earth neutron levels.

By this device we have established a fair reproduction of the order of the observed single-particle levels. Presently stripping data of, e.g., (d,p) and (He^3,d) type, giving distribution strengths over the different members of a rotational band, have become of increasing importance (among a large number of relevant references see, e.g., Ref. 19). From these data, orbital "finger prints" identify the single-particle orbits experimentally beyond any doubt among available orbitals of given spin and parity. With almost no exception, earlier assignments, based on alpha-, beta-, and gamma-spectroscopic data, have been confirmed. However, new levels of considerably higher excitations have been observed, in addition. It is to be emphasized that, to describe conditions at fission saddle distortions, the positions of the shell crossings due to deformation are decisive. Thus, for the actinide elements we want to know safely the position of, e.g., the proton levels [505 11/2], [400 1/2], [651 1/2], and [770 1/2] and

the neutron levels [606 13/2], [501 1/2], [761 1/2], and [880 1/2], see cited figures.

In Fig. 5i, we note in passing the magic numbers predicted by the potential chosen. As other authors[7,8] we predict $Z = 114$ to be a fairly good magic number.[9] On the neutron side, there does not appear anything clearly "magic" for the shell parameters appropriate to the actinide region. As the parameters κ and μ are extrapolated into the $A \simeq 300$ region (see Figs. 6a,b), the $N = 164$ subshell disappears entirely while the shell closing at $N = 184$ may be said to approach magicness (as also $N = 196$).

In the latter figure we display the spherical level ordering obtained by the modified oscillator potential and the Woods-Saxon potential as employed by Rost.[11] The extrapolation procedure employed by us to describe masses near $A \approx 300$ is the following. The shell parameters κ and μ are optimized for the regions centered around $A = 165$ and $A = 242$. By these two sets of choice of the κ and μ parameters the entire rare earth and actinide regions are fairly adequately described. It is then assumed that one may extrapolate the encountered variation in κ and μ linearly with A. As a check the spectrum obtained by interpolation for κ and μ to $A = 208$ is plotted.

The agreement with the single-hole levels of ^{207}Tl and ^{207}Pb is encouraging. On the other hand, the spectra of ^{209}Bi and ^{209}Pb are less well reproduced. The levels in the latter cases start at a binding energy of only 3-4 MeV, and the insufficiency of the oscillator well is therefore expected to become increasingly important with excitation energy in the ^{209}Bi and ^{209}Pb spectra.

For comparison we have included in the same figures the level schemes obtained by Rost according to similar extrapolation rules outlined in Ref. 11. Although in details there are considerable disagreements, there is an overall agreement in the prediction of low level density for the spherical shape for $A = 114 - 126$ and for $N = 178 - 184$. As detailed calculations bear out, this situation is favorable to the establishment of a spherical ground state and a large barrier against fission.

III. THE PAIRING FORCE

Of relatively minor importance to the equilibrium distortion is the pairing force. When pairing is taken into account, the single-particle energy sum is replaced by the following expression

$$E = \sum_{\nu} e_{\nu} 2V_{\nu}^2 - G\left(\sum_{\nu} U_{\nu} V_{\nu}\right)^2 - G \sum_{\nu} V_{\nu}^4$$

where e_{ν} are the single-particle energies and U_{ν} and V_{ν} the pairing factors, and where the sum is taken separately over neutrons and protons, for each with a different pairing matrix element G_n and G_p.

The previously employed prescription has been to assume the pairing matrix element as proportional to a constant divided by A, or G_n/A for neutrons and G_p/A for protons.

The pairing force was originally introduced by Bohr, Mottelson and Pines[20] to simulate the short range interaction not included in the potential field. It was basically thought of as being a simplified representation of the δ-force but additionally limited to acting only between pairs of time-reversed states. The factor $1/A$ is a volume factor and is assumed to reflect the fact that the overlap integral, in lieu of any other correlation, should be inversely proportional to volume. The entering matrix element is for a δ-force

$$G \sim \int \Psi_{\nu}^{*} \Psi_{\bar{\nu}}^{*} \Psi_{\mu} \Psi_{\bar{\mu}} \, d\tau \quad .$$

It should be obvious that the overlap between μ and ν orbitals is weakened by μ and ν being in different magic shells, or, e.g., representing very different asymptotic quantum numbers.

Relative to a certain level ν the matrix elements for scattering into a state μ should fall off with energy (and e.g., angular and radial quantum number differences between ν and μ). In the simplified version of pairing theory, one employs one single average pairing matrix element and a corresponding choice of the cut-off energy above and below the Fermi level. To some extent a higher cut-off can be compensated by a smaller matrix element within a given region of A. However, one has in addition the empirical finding that the odd-even mass difference, in the simple pairing theory equal to Δ, depends on A as

$$\Delta = \frac{12.0}{\sqrt{A}} \text{ MeV} .$$

The magnitude of Δ and its A-dependence appear to set some limits on the freedom of choice (see below).

The neutron and proton collision velocities depend on the depths of the neutron and proton potentials. These depths in turn depend not only on A but also on Z. As the S-state interaction depends critically on the colliding energy, it is natural to assume for the pairing force matrix element an isospin dependence to lowest order in (N-Z) of the following type

$$G' \times A = g_o \pm g_1 \frac{N-Z}{A}$$

where the plus sign holds for protons and the minus sign for neutrons. It was found that the empirical odd-even mass differences were reproduced for constant g_o and g_1 over a wide mass range, from $A \simeq 150$ to $A \simeq 250$, by including $\sqrt{15Z}$ states below and equally many states above the proton Fermi surface. The corresponding cut-off was employed for neutrons. This corresponds roughly to the inclusion of three neutron and three proton oscillator shells. As emphasized some of these prescriptions are arbitrary. Other authors confine themselves to a constant number of states and cover a less wide region of masses. A wide range of prescriptions are therefore available.

With present prescriptions we find $g_o = 19.2$, $g_1 = 7.4$ MeV.* The fit to odd-even mass differences in the rare earth region achieved may be studied in Figs. 7a,b.

The effect of the inclusion of pairing relative to a simple summation of single-particle energies is exhibited in Fig. 8 for the case of ^{254}Fm mostly for the pure spheroid case ($\epsilon_4 = 0$). While the pairing energy is about 14 MeV for $\epsilon = 0$ it is reduced to about 1 MeV at the equilibrium distortion and thereafter exhibiting strong fluctuations. The variation in

*We have presently limited the number of free parameters by prescribing g_o and g_1 the same for neutrons and protons. From Figs. 7a and 7b it appears that an improved fit may be obtained by using somewhat different values of g_o and g_1 for neutrons and protons.

Δ_n and Δ_p with ϵ for ^{254}Fm may be studied in Fig. 9. To account for the indication of an energy gap at the fission saddle point[21a] of about 2 MeV for ^{240}Pu and of about 3-4 MeV at the fission saddle point for ^{218}Po one must, as Stepien and Szymanski,[21b] assume an increase of G with distortion. Such an assumption receives support from the energy gap calculation based on the "slab model" by Kennedy, Wilets and Henley.[22] We have in separate calculations assumed G constant with deformation and proportional to the surface area, respectively. The latter assumption appears to account better for fission half lives as well as for the apparent large energy gap at the fission saddle point.

Setting G directly proportional to S corresponds to the simplified assumption that the contribution to the pairing from the inner regions of the nucleus is negligible and that the surface region is entirely responsible for the pairing. The assumption that pairing is largely a surface phenomena is based on the fact that at the large collision velocities encountered in the center of the nucleus, the ^{1}S phase shift becomes very small and ultimately changes sign. The slab model calculations[22] bear out that Δ is proportional to $S^{3/2}$ while the simple assumption of $G \sim S$ leads to $\Delta \sim S^3$ as borne out by Fig. 10. The surface dependence of G suggested by the slab model thus appears to fall half-way between the assumptions of G = const and $G \sim S$.

IV. THE COULOMB ENERGY

The Coulomb energy involves quantum mechanically the following expression

$$E_c = \sum \sum_{i>j} \int \Psi^*(\bar{r}_1 \cdots \bar{r}_Z) \frac{e^2}{|\bar{r}_i - \bar{r}_j|} \Psi(\bar{r}_1 \text{ --- } \bar{r}_Z)\, d\tau_1 \text{ --- } d\tau_Z$$

where, if correlations are neglected, Ψ is the Slater determinant of single-particle states. Furthermore provided that anti-symmetrization is neglected and Ψ replaced by a simple product wave function, E_c takes the simple form

$$E_c = \sum \sum_{i>j} \iint \rho_i(\vec{r}_i)\, \rho_j(\vec{r}_j) \frac{e^2}{|\vec{r}_i - \vec{r}_j|} \, d\tau_i \, d\tau_j$$

where the single-particle density ρ_i is defined as

$$\rho_i = \psi_i^* \psi_i \quad .$$

As our program calculates single-particle wave functions ψ_i, this expression can in principle be evaluated.* Presently we have been content with the simplification of assuming a homogeneous charge density within an

*Preliminary results of such calculations by J. Bang and A. Stenholm Jensen are reported in Conf. Int. Symp. Nucl. Str., Dubna (1968) 98.

equipotential surface enclosing a volume equal to $\frac{4\pi}{3} R_c^3$. Thus

$$E_c \simeq \frac{Z^2}{2} \iint^{R(\theta)} \rho(\vec{r}_1)\ \rho(\vec{r}_2)\ \frac{e^2}{|\vec{r}_1 - \vec{r}_2|}\ d\tau_1\ d\tau_2$$

where thus ρ is the total nuclear charge density, which is constant out to a radius $R(\theta)$, depending on the distortion parameters ϵ, ϵ_4, ϵ_6, etc., assumed.

In principle this is a six-dimensional integral. It can, however, be reduced (see e.g., J. R. Nix[23]) to a two-dimensional integral where elliptic functions appear in the integrand. The two-dimensional integral can then be evaluated numerically for an axially symmetric but otherwise arbitrary shape.

We have, in addition, introduced corrections for surface diffuseness and exchange energy. These are of the order of a few percent. One may then write the Coulomb energy form

$$E_c = \frac{3}{5}\ \frac{Z^2 e^2}{R_c} \left[\ g(\epsilon\ ,\ \epsilon_4,\ \ldots\ ) - \frac{\pi^2}{2}\ \frac{5}{3}\ \left(\frac{a}{R_c}\right)^2 - \frac{0.7636}{Z^{2/3}}\ \right] .$$

In this equation $g(\epsilon, \epsilon_4, \ldots)$ assumes the value one for a pure sphere and has otherwise to be evaluated numerically.

The diffuseness correction contains the diffuseness parameter a (taken equal to 0.546 fm). It is shown (Myers and Swiatecki[4]) that, to lowest order in the diffuseness parameter a, this expression is correct for

an arbitrarily shaped drop. No shape-dependence is thus connected with this term. Finally, the third term representing an approximate correction, as derived by Bethe and Bacher,[2] to take into account the extra correlation of the protons that is implied by the requirement of antisymmetry of the nuclear wave function. In the evaluation of the Coulomb integral on the preceding page the uncorrelated density should be replaced by the correlated two-particle density function, which can be evaluated for a simple Fermi gas as

$$\rho(\vec{r}_1)\ \rho(\vec{r}_2)\ [1 - \tfrac{1}{2}\, C^2\ (k_F r_{12})]$$

where k_F is the Fermi momentum

$$k_F = \frac{9\pi}{4}\ \left(\frac{Z}{R_c^3}\right)^{1/3}$$

and

$$C(x) = \frac{3}{x^2}\ \left(\frac{\sin x}{x} - \cos x\right) \quad .$$

The second term in the density function gives the antisymmetrization energy term

$$-\frac{Z^2 e^2}{R_c}\ 3\left(\frac{3}{16\pi Z}\right)^{2/3} \approx -\frac{3}{5}\ \frac{Z^2 e^2}{R_c}\ 0.76\ Z^{-2/3} \quad .$$

From the derivation of this term, one may verify that it represents a volume energy and is thus independent of the nuclear shape. Because the exchange term is the result of short-range correlations, the correction to this term resulting from the finite size of the nucleus is proportional to the nuclear surface area and is smaller by $A^{1/3}$ than the leading term given above. This surface correction to the exchange term has not been included.

V. EQUILIBRIUM DISTORTIONS

With the inclusion of the Coulomb energy the total energy takes the form

$$E(\epsilon, \epsilon_4, \ldots) = \sum_\nu 2e_\nu(\epsilon, \epsilon_4, \ldots) V_\nu^2 - G\left(\sum_\nu U_\nu V_\nu\right)^2$$

$$- G\left(\sum_\nu V_\nu^4 - \sum_\nu{}' 1\right) + E_c(\epsilon, \epsilon_4, \ldots) \quad .$$

The minima of the energy surface are obtained from the condition

$$\frac{\partial E}{\partial \epsilon} = \frac{\partial E}{\partial \epsilon_4} = \ldots = 0 \quad .$$

Equilibrium distortions of ϵ, ϵ_4, ϵ_6 have been calculated according to this prescription. Often the corresponding experimental quantities do not relate directly to any singular one of these. Thus the quadrupole moment receives a large contribution from the interference of the ϵ_4 and ϵ distortions. For nuclear quadrupole moments, which are presently accurately measured in the deformed regions via Coulomb excitation cross-sections, one may employ the nucleonic wave functions to compute the expectation value

$$\langle \Psi(\epsilon, \epsilon_4, \ldots) \left| \sum 2r^2 P_2 \right| \Psi(\epsilon, \epsilon_4, \ldots) \rangle_{eq} = Q_2 \quad .$$

A comparison with data shows the so determined quadrupole moments to be well reproduced as to their A-dependence. As to the absolute magnitudes the

theoretical values are generally 5-10% too small, however.[17] We do not exhibit any comparison as earlier results in the field are essentially reproduced.[24-27]

In the case of ϵ_4 distortions (and ϵ_6 distortions) an interesting area of comparison is presently available. A detailed analysis of inelastic alpha-scattering data (involving a large set of energies and angles) has recently been carried out by Hendrie et al.[15] on the basis of an optical-potential. The optical Woods-Saxon potential assumed has equipotential surfaces given by*

$$R_{1/2} = \overset{o}{R}_{1/2}(1 + \beta_2 Y_{20} + \beta_4 Y_{40} + \beta_6 Y_{60}) \quad .$$

The differential cross-sections involving the populations of rotational bands of even-even deformed nuclei up to and including 6^+ (and sometimes 8^+) are fitted by a combination of β_2, β_4, and β_6 (see Fig. 11). In this analysis it is furthermore assumed that the nucleus is a perfect rotor (i.e., that Coriolis coupling and stretching may be neglected). The parameters β_2 and β_4 are determined in this way with an accuracy of about $\pm$ 0.01 from the data (see Fig. 12).

*The relation between the coordinates α_λ and β_λ is given by

$$\beta_\lambda = \sqrt{4\pi/(2\lambda+1)}\ \alpha_\lambda \quad .$$

The last parameter β_6 is less accurately determined. It appears, however, safe to say that in general and over the whole region studied, $152 \leq A \leq 178$, numerically small and negative β_6-values are favored (see Fig. 13 for comparison with theoretical values). One is thus lead to assume the existence of stable hexäkontatettara-pole shapes for the nucleus.

Returning to Fig. 12 the agreement between theoretical and empirical β_4-values appears remarkable. It turns out that the β_4-values encountered correspond roughly to the β_4-distortion already present to zeroth order by the prescribed filling of levels in the deformed well. This has been pointed out by the author in Ref. 28 and by Bertsch.[29] Thus the first few outside-of-closed-shell spheroidal orbitals ($N = n_z$) have a large positive contribution to β_4. The same is true of the last filled ones ($n_z = 0$). On the other hand, those near the middle of the shell ($n_z \simeq \frac{1}{2} N$) have a large negative contribution to β_4. This suffices to explain the trend of the encountered variation of β_4 between closed-shell nuclei. It must be emphasized that polarization (coupling between shells $N \rightarrow N \pm 2$) enlarges the effect by a factor of 2 or 3.* Coulomb interaction generally favors positive β_4. Finally, pairing has a smearing trend and therefore tends to counteract the

*Actually the inclusion of couplings within the N-shell reduces the distortion somewhat relatively to that obtained from keeping the diagonal contributions only as in Ref. 30. (For a discussion of the different contributions see Ref. 17.)

effects of polarization and Coulomb interaction. For this reason, earlier calculations that neglected the effects of pairing, polarization, and Coulomb repulsion gave still rather similar results.[30,31]

In Figs. 14a and 14b we exhibit the theoretical distortion parameters ϵ and ϵ_4 associated with the nuclides in the rare earth and actinide regions, respectively. These diagrams should be consulted prior to the employment of the single-particle diagrams.

VI. DISTORTIONS BEYOND THE EQUILIBRIUM SHAPE AND THE STRUTINSKY NORMALIZATION METHOD

The total potential-energy surface is presently studied between $\epsilon = -0.2$ (sometimes -0.5) and $\epsilon = 0.95$ (sometimes $\epsilon = 0.9$) and for ϵ_4 between -0.08 and $\epsilon_4 = 0.16$ (sometimes 0.12). With the application of the volume conservation condition alone, as can be seen from Fig. 15, the behavior is unsatisfactory for large ϵ. One may note that the restoring energy introduced by the volume conservation condition is a term of very large magnitude, being roughly proportional to $\frac{1}{9}\epsilon^2$ times the total nuclear energy, or for $\epsilon = 0.9$ of the order of 1000 MeV. As, unfortunately, not the entire nuclear potential is included in the volume conservation condition, "small" corrections to the geometry of the potential-energy surface are not unexpected. (In particular the unrenormalized ρ^4 or $\vec{\ell}^2$ term appears responsible for the improper behavior at large $|\epsilon|$. See Ref. 28.) On the other hand, the topological character of the surface may be correctly reproduced as the correct level order is reproduced.

Such a renormalization of the surface is brought about by the introduction of the Strutinsky procedure.[32] The basic idea is the following. The average behavior of nuclear binding energies as a function of the nuclear charge and size is well reproduced by the so-called liquid-drop model (see Section I) with empirically determined parameters. One then surmises that on the <u>average</u> this model also adequately describes deformation.*

---

*This is, of course, what is conjectured in the original application of the model to the theory of fission in the classical paper by N. Bohr and J. A. Wheeler (Phys. Rev. <u>56</u> (1939) 426).

The relative success of the liquid-drop theory of fission may be taken as a warrant for this. One should therefore require that on the average – the average taken over so many nuclei that shell effects are averaged out – the total energy has the same distortion dependence as that of a liquid-drop. This requirement is enforced by subtracting out of the total energy an averaged energy and replacing the latter by the liquid-drop energy. The main problem consists in forming this average in a satisfactorily unique way.

To this end Strutinsky first defines a smoothed level density $g(e)$ by smearing the calculated single-particle levels e_ν over a range γ, where γ is an energy of the order of the shell spacing. Let us first define an uncorrected level density $g_o(e)$, where

$$g_o(e) = \frac{1}{\gamma\sqrt{\pi}} \int_{-\infty}^{\infty} de' \exp\left[- \left(\frac{e-e'}{\gamma} \right)^2 \right] \cdot G(e')$$

$$= \frac{1}{\gamma\sqrt{\pi}} \sum_\nu \exp\left[- \left(\frac{e-e_\nu}{\gamma} \right)^2 \right]$$

where $G(e') = \sum_\nu \delta(e' - e_\nu)$ is the calculated single-particle level density. Assume that there are short-range fluctuations in $G(e')$ with ranges $\lambda < \hbar\omega$ and a long-range variation of order $L > \hbar\omega$. The problem is now to average out the short-range variations without affecting the long-range dependence on energy. Obviously this puts limits on the choice

of γ as $\lambda \ll \gamma \ll L$. With the condition on γ upheld, one may correct for errors introduced by the folding (averaging) procedure by introducing a modified averaging function. Thus, an improved averaged level density function $g(e)$, in second order suggested by Strutinsky[32] and in its more general form derived by Tsang,[33] can be written as

$$g(e) = \frac{1}{\gamma\sqrt{\pi}} \sum_{\nu} f_{corr} \exp\left[- \left(\frac{e-e_\nu}{\gamma} \right)^2 \right]$$

where f_{corr} is defined as

$$f_{corr} = 1 + \left(\frac{1}{2} - u_\nu^2 \right) + \left(\frac{3}{8} - \frac{3}{2} u_\nu^2 + \frac{1}{2} u_\nu^4 \right)$$

$$+ \left(\frac{5}{16} - \frac{15}{8} u_\nu^2 + \frac{5}{4} u_\nu^4 - \frac{1}{6} u_\nu^6 \right) + \text{---} \quad .$$

In the latter expression we have introduced the simplified notation

$$u_\nu = \frac{e-e_\nu}{\gamma} \quad .$$

The second term in f_{corr} represents a second-order correction and ensures that a (smooth) polynomial $G(\epsilon)$ of second order in ϵ is preserved after the folding transformation. Using the listed terms up to the sixth order the long-range dependence of $G(\epsilon)$ is restored up to sixth order in energy.

In Fig. 16, valid for Pb^{208}, we display the shell energy* E_{shell}, representing the finally obtained shell structure correction to the liquid drop energy, as given below. It is obvious that the keeping of terms in f_{corr} up to 4th order makes E_{shell} rather γ-independent while the second-order approximation introduces a serious folding error.**

Based on the averaged level density function $g(e)$ one may now calculate an averaged total energy $E(g)$ e.g., for neutrons

$$E(g) = \int^{\bar{\lambda}_n} 2e\, g_n(e)\, de$$

where the neutron Fermi energy $\bar{\lambda}_n$ is determined from the condition

$$N = \int^{\lambda_n} 2g_n(e)\, de \quad .$$

The averaged proton energy is obtained similarly. The sum of energies due to pairing and shell structure is obtained from the equation

$$E_{shell} + E_{pair} = \sum_\nu e_\nu\, 2V_\nu^2 - \Delta^2/G - G\left(\sum_\nu V_\nu^4 - \sum_\nu 1 \right) - E(g) - \langle E_{pair} \rangle .$$

*In figure this quantity is denoted N-dshell, referring to neutrons.

**In the present calculation correction terms were included up to the sixth order.

The two parts of this sum, relating to neutrons and protons respectively, have to be evaluated separately. In order to be able to connect to the liquid-drop model we have in the expression above subtracted the average pairing energy $\langle E_{pair} \rangle$, where the average is taken over the shell.* This average turns out to be A-independent. One now obtains the renormalized total energy by adding to the expression above the surface and Coulomb energies (the symmetry energy is usually assumed deformation-independent in the liquid drop model, so its addition is irrelevant for the deformation dependence). We have thus

$$E = E_{surf} + E_c + E_{shell} + E_{pair} - \langle E_{pair} \rangle \quad .$$

In summary, we have thus replaced the smoothed total energy behavior with that of the liquid-drop model.** All local shell structure variations originally obtained are retained, on the other hand.

It is thus important to verify that the equilibrium deformations, shown earlier to be in agreement with experiments, remain the same. Indeed the changes in ϵ and ϵ_4 are usually less in absolute value than 0.01.

---

*The average is formed at the equilibrium distortion. The systematic growth in pairing energy due to the assumption of G being proportional to S is not subtracted out. This is a feature associated solely with very large distortions which is assumed not to be built into the liquid-drop model.

**With parameters as of Ref. 4.

This appears to imply that the model used previously, with the volume conservation condition applied, for small distortions has the gross behavior, stiffness etc., of the liquid drop model. The difference first appears at $\epsilon \gtrsim 0.4$ and corresponds more to a change in "geometry" while the "topology" of the energy surface is retained.

One may estimate the small quantity $\langle E_{pair} \rangle$, employed in the final expression for the total energy, from the following approximate relations

$$E_{pair} \simeq - \left(\frac{1}{2} \rho_n \Delta_n^2 + \frac{1}{2} \rho_p \Delta_p^2 \right) .$$

We have chosen G_n and G_p such that (see p. 29)

$$\langle \Delta_n \rangle \approx \langle \Delta_p \rangle \approx \frac{12}{\sqrt{A}} \text{ MeV} .$$

The level densities can be estimated for the simple oscillator model as

$$\rho_n \simeq \rho_p \simeq \frac{\frac{1}{2} \left(\frac{3}{2}\right)^{2/3}}{\hbar\omega} A^{2/3} \ (\text{MeV}^{-1}) .$$

In this way one obtains

$$E_{pair} \approx - 2.3 \text{ MeV}$$

independently of A.

To the extent $\langle E_{pair} \rangle$ is independent of A, its absolute value is, of course, largely irrelevant. In the comparison of calculated masses with empirical ones, we have thus arbitrarily set $\langle E_{pair} \rangle = - 2.3$ MeV. The comparison will be further discussed below.

VII. PREDICTION OF NUCLEAR MASSES

In Fig. 17 we compare empirical and theoretical masses with reference to the liquid drop mass prediction for zero distortions $M_{LD}(0)$. Thus above in Fig. 17 we plot $M_{exp} - M_{LD}(0)$ in units of MeV. Immediately below we plot the theoretical value of E at equilibrium distortion, E_{eq}, which thus contains all effects of shell structure and distortion. These latter contributions are obviously not contained in the liquid-drop energy evaluated for a pure spherical shape, which latter is taken as a reference point. The difference between $M_{exp} - M_{LD}(0)$ and E_{eq}, exhibited as the third and lowest graph in this figure, reflects on the appropriateness both of the liquid-drop parameters chosen and on the nuclear shell and pairing fields. Although the local trends exhibit encouraging agreement, there are two important points of deviation:

(i) the over-all trend appears to be towards too small theoretical masses with large A-values.

(ii) There appear relatively large discrepancies connected with the doubly-closed shells of ^{208}Pb. The theoretical binding appears underestimated by about 2 MeV below and at $A \approx 208$.

First, a slight readjustment of the Myers-Swiatecki[4] mass parameters may be desirable, particularly as these were obtained on the basis of a conjectured shell structure term; e.g., a different choice of the Coulomb radius may affect the masses of deformed and spherical nuclei differently and thereby also affect the deviation near $A = 208$. Alternatively, the underestimate of binding near doubly closed shells may reflect on details of the single-particle level scheme, or to some extent it may indicate the

existence of an additional correlation energy not reproduced by the pair correlation energy, which latter, on the contrary, collapses near closed shells. Finally we have neglected the rotational asymmetry degree of freedom γ, which may be important for ground state masses between $A = 190$ and $A = 200$.

For the moment we have been content with the performance of the semi-empirical mass parameters on the basis of this comparison. However, a redetermination of these parameters on the basis of the experimental masses is being planned.*

---

*Our calculations of masses are similar to those reported by P. A. Seeger and R. C. Perisho, Los Alamos Scientific Laboratory Report, LA-3751, 1967. These authors neglect, however, the P_4 degree of freedom and represent the liquid drop barrier by a cubic in ϵ. On the other hand, they allow for an adjustment of the liquid drop parameters. Our inclusion of the P_4 degree of freedom appears to improve the mass fit considerably.

VIII. POTENTIAL-ENERGY SURFACES AND THE FISSION ISOMER STATES*

Two representative energy surfaces are exhibited in Figs. 18 a,b. The separate contributions from the liquid-drop terms and the shell plus pairing energies are exhibited in Figs. 19 and 20. The employment of ϵ and ϵ_4 and the range of these parameters chosen in the calculations appear adequate to map the general trend of the fission barrier for elements with $Z \geq 96$. For lighter elements the existence of higher distortion multipoles may be important. Thus the liquid-drop energy alone appears in U to be about 0.6 MeV higher at the liquid-drop saddle point distortion ($\epsilon \approx 0.85$) in the (ϵ, ϵ_4) parametrization than in the more general parametrization used by Nix.[23] Similarly for the Pu saddle point, occurring at $\epsilon \approx 0.75$ in the liquid drop model, the error due to the insufficient number of parameters appears to be at least 0.3 MeV. Beyond Cm the difference at the liquid-drop saddle point falls, however, below 0.1 MeV. This reflects the fact that for larger Z^2/A the liquid drop saddle point occurs at smaller quadrupole distortion, where higher shape multipoles are less significant. (One might attempt to introduce an ad hoc correction of the barrier based on this comparison, but presently we use these numbers as a measure of the inaccuracy of the parametrization at large distortions.)

---

*The recent results by Yu. A. Muzichka, V. V. Pashkevich, and V. M. Strutinsky, Joint Institute of Nuclear Research, Dubna, preprint P7-3733, are in good agreement with those reported here concerning the barriers of the actinide and super-heavy-element region, although the ϵ_4 degree of freedom is neglected in the reference above.

For the $Z = 114$ region the parametrization appears adequate as the barrier rarely extends beyond $\epsilon \approx 0.7$. Actually the double-hump saddle points are situated at very moderate distortions. In the super-heavy element case the great uncertainty enters due to the extrapolation to higher A-regions of the nuclear potential while the parametrization may be adequate.

In the actinide region, on the other hand, the nuclear potential seems well known, at least for the equilibrium region of distortions. Representative topographical maps are given for a few nuclei exhibiting the entire (ϵ, ϵ_4) plane covered in the calculations. As is seen from these, the importance of the ϵ_4-degree of freedom increases with increasing ϵ. Although equilibrium shapes of both positive and negative ϵ_4-values are represented, the saddle always occurs for a positive ϵ_4, representing a small waistline on the spheroid. As ϵ increases, the waistline develops rapidly, as expected.

In Fig. 8 one may study the effect of the ϵ_4 degree of freedom on the barrier of ^{254}Fm. Obviously its inclusion is decisive. In Figs. 21a-h we exhibit the barriers obtained for isotopes $Z = 92$ to $Z = 106$ for the two alternative assumptions of $G = \text{const}$ and G proportional to the surface area.* This type of plot represents a cut through the two-dimensional topographic map in the (ϵ, ϵ_4) plane such that for each ϵ-value we have

*We believe the second assumption to be more adequate (see below).

employed the ϵ_4 for which the energy is minimum.*

One should note the general trend in the actinide nuclei for the formation of a double-hump barrier, as was first emphasized by Strutinsky.[32] As A grows from 230 to 250, the innermost barrier rises from a very small hump to be the dominant barrier while the second barrier hump diminishes. For common Z ≈ 100 isotopes the second barrier is very low (and with the inclusion of neglected degrees of freedom it appears likely that it vanishes altogether). The second barrier hump in U, Pu, and Cm comes out much too high theoretically, unless the surface dependent G matrix element is employed. In this latter case the barrier heights are within one or a few MeV of that obtained from experimental data analyzed in terms of the one-hump barrier theory.**

The empirical evidence for the two-hump fission barrier is now fairly convincing and is connected with the following recent findings. First among these were the discovery of the spontaneous-fission isomers, which correspond to excited states of nuclei in the region $236 \leq A \leq 246$. These isomeric

---

*The oblate minimum, as has been shown by D. A. Arseniev, L. A. Malov, V. V. Pashkevich, and V. G. Soloviev, preprint Dubna, E4-3703 (1968), is unstable with respect to the γ degree of freedom and directly leads to the ground state minimum. It can therefore not be associated with any shape isomerism.

**The inclusion of the gamma degree of freedom appears further to reduce the first hump of the barrier by 0.4 to 2.1 MeV, for nuclei between ^{240}Pu and ^{256}Fm as reported by V. V. Pashkevich, Conf. Int. Symp. Nucl. Str., Dubna (1968) 94.

states are found to decay by spontaneous fission rather than by gamma decay. The first fission isomer, in ^{242}Am, discovered by Polikanov,[34] had a half-life of 140 ms. Later eight other cases have been found[35,36] with half-lives from 6×10^{-5} sec (^{238}Am) to 5×10^{-9} sec (^{240}Pu). The known excitation energies appear to lie between 2 and 3 MeV. Indeed these latter half-lives and excitation energies are consistent with the assumption that these isomeric states represent a shape isomerism and are connected with the secondary barrier minimum. (The marked additional hindrance for ^{242}Am may be connected with the single-particle orbitals involved in this odd-odd case.)

Additional evidence appears to support the existence of states associated with the barrier indentation. This evidence[36] is based on the study of the variation of the cold-neutron fission cross section for elements in the region $231 \leq A \leq 242$. Superposed on the fine structure of, say, about 1 eV, occurring at about 6-7 MeV of excitation, and relating to compound states associated with an equilibrium shape, there appears a sequence of resonances with a spacing of, on the average, about 100 eV and a width of a few eV.* D_{II}/D_I varies from about 500 in ^{235}U to about 50 in ^{241}Pu; D_{II} referring to

*These numbers being relevant for the particular case of ^{235}U are obviously rather different in odd-A, odd-odd or even-even cases. For a discussion on the ^{241}Pu resonance spectrum, see A. Kerman and H. Fashbach, Comments on Nuclear and Particle Physics 2 (1968) 125.

the spacing of the resonance type states and D_I to the spacing of the normal equilibrium shape states. Presently one interprets the resonance states as the states of the second energy minimum as suggested by Lynn.[36] Using the standard level density formulas one may estimate the second minimum to lie 1.5 - 3 MeV above the ground state for the various nuclei between ^{235}U and ^{242}Am. All these facts appear to be in qualitative agreement with the predictions of these present model calculations. This seems all to give further confidence to our description of the actinide barriers.

A. Region of Superheavy Elements

For elements $Z = 102 - 108$ with $A < 280$ presently studied the equilibrium shape corresponds to $\epsilon \approx 0.2 - 0.25$ and the barrier appears to show a simple one-hump character.

For these elements and for others with larger Z, as N approaches 184 the lowest minimum becomes spherical and the barrier becomes again of double-hump character. The barrier minimum occurs near $\epsilon \approx 0.3$. Actually the transition from a deformed to a spherical ground state takes place for $N \simeq 176 - 178$ for $Z = 102 - 114$, according to present preliminary investigations. Thus for $Z = 102$, e.g., already $A = 280$ is spherical according to our calculations. The deepest spherical minimum and the highest barrier seems to occur for the double-magic nucleus[38] $Z = 114$, $N = 184$, $A = 298$ (see Figs. 22 a-d). It was conjectured by Swiatecki,* that there might be a

*As quoted in Ref. 45.

region of relative stability (half-life $\gtrsim$ 1s) against spontaneous fission (see below) bounded by the approximate mass valley boundaries of $A \approx 308$, $A \approx 288$ and $N-Z = 76$ and $N-Z = 62$. It now appears that this region may be connected with the very neutron rich actinide element region along $N = 184$. Thus $N = 178$ to N-values beyond $N = 184$ appear to favour sphericity. For a more detailed investigation into the fission process, in terms of which the boundaries of this region are determined, we next turn to the problem of the barrier penetration.

IX. THE BARRIER PENETRATION PROBLEM*

A problem of foremost importance in connection with the fission barriers is that of the dynamical inertial mass associated with the penetration of the barrier leading to fission. (For a general review of the problem of nuclear fission see the monograph by Wilets.[38])

Let us assume for the moment that the problem were a one-dimensional one and ϵ the relevant parameter. According to simple WKB theory the penetration probability for the penetration of a barrier is given by the expression

$$P = \exp\left\{ -\frac{2}{\hbar} \int_{\epsilon'}^{\epsilon''} \sqrt{2B(W(\epsilon) - E)}\, d\epsilon \right\} \equiv \exp(-K) \quad .$$

There exists an improved expression, as shown by P. O. Fröman and N. Fröman,[39]

$$P = (1 + \exp K)^{-1} \quad .$$

This expression differs from that above mainly for small K-values. Maybe one is more familiar with the corresponding expression for the case that ϵ is replaced by x and B by the penetrating-particle mass M. In our case B takes the dimension of mass times length,[2] or moment of inertia,

*I have in the following exploited Prof. Z. Szymanski's notes on the penetration problem, as well as the lecture notes by A. Bohr and B. Mottelson[5] on the time-dependent treatment of the analogous problem of vibrational motion.

as ϵ is dimensionless. The quantity $W(\epsilon)$ represents the potential-energy surface considered in the foregoing. To make things simple, let us assume B to be a constant, while in the actual case it turns out to be ϵ-dependent. One usually assigns to B its value at the saddle point, where the contribution to the integral is expected to be the largest. The quantity P is defined as the probability of penetration through the barrier for a given "assault". To relate to the fission half-life, we also need an expression for the number of assaults on the barrier per second. Thus number n is usually equated to the frequency of the beta-vibrational motion at the equilibrium point. One may therefore set $n = 10^{21}$, corresponding to a vibrational frequency of $\hbar\omega_{vib} \cong 1$ MeV. We have thus, in units of sec.

$$\tau \simeq \frac{1}{n} \cdot \frac{1}{P} \simeq 10^{-21} \exp K \quad .$$

Consider a parabolic barrier of height S over the energy minimum

$$W(\epsilon) = S - \frac{1}{2} C(\epsilon - \epsilon_S)^2$$

where

$$\epsilon_S = (\epsilon' + \epsilon'')/2$$

and

$$C = 8S/(\epsilon' - \epsilon'')^2 \quad .$$

Introducing

$$\omega_f = \sqrt{C/B}$$

one obtains

$$K = 2\pi(S-E)/\hbar\omega_f \quad .$$

Using the Fröman[39] expression for the penetration probability P one finally obtains

$$P = (1 + \exp 2\pi(S-E)/\hbar\omega_f)^{-1} \quad .$$

This actually equals the exact expression derived by Hill and Wheeler[40] valid specifically for a parabolic shape. In this formula S represents the barrier height, while the frequency ω_f contains both the barrier curvature C and the inertial parameter B.

From the Hill-Wheeler expression we obtain $P = 1/2$ for zero barrier. The zero barrier point accordingly is the point where, as a function of the excitation energy E, the penetrability has diminished to 1/2 of that of infinite excitation. It is also the point of maximum change in penetrability with E. Indeed from the dependence of the penetrability on E not only S but also an average $\hbar\omega_f$ appears experimentally accessible. Experimental analysis gives S as dropping from 8 to 4 MeV when A goes from 230 to 250. Various empirical values of $\hbar\omega_f$ are available centered around about 500 KeV. However, recently all such experimental determinations are somewhat in question as they are based on an analysis in terms of a one-hump and not a two-hump barrier.

A. Microscopic Theory of the Fission Process

In the preliminary discussion above we used a one-dimensional description, and furthermore B entered as a completely phenomenological parameter. Let us for the moment, for the sake of simplicity, continue to disregard all except one degree of freedom, but try to obtain a value of B in terms of the microscopic nuclear model developed here on the preceeding pages. The adiabatic treatment employed is largely analogous to the treatment of vibrations around an equilibrium point. The usual procedure is to consider small deviations from the equilibrium. It is our aim to find an expression for the total energy of the following kind valid around the equilibrium point*

$$T + V = E_o + \frac{1}{2} B \dot{a}^2 + \frac{1}{2} C(a - a(0))^2$$

which represents the lowest-order terms in an expansion in $\dot{a}$ and in $(a - a(0))$, where $a(0)$ is the equilibrium value of the distortion coordinate a.

We thus expect the microscopic model to determine for us the parameters C, the curvature parameter of the potential around the stationary point, and B, the inertial mass parameter. It is assumed that in the vicinity of the stationary point one may introduce an energy operator of the following type

*We have employed a and not ϵ to denote a general distortion coordinate.

$$\hat{\mathcal{H}} = H_0 - \frac{\kappa}{2} \hat{\alpha} \hat{\alpha}$$

where H_0 is the single particle Hamiltonian appropriate at the saddle point (being a stationary point). Let us for simplicity assume that $\hat{\alpha}$ is the distortion mass quadrupole moment relative to the stationary value Q_0

$$\hat{\alpha} = \hat{Q} - Q_0 = \sum \hat{q}_i - Q_0$$

$\hat{q}_i$ being the single-particle mass quadrupole moment operator. We have thus, for the time being, while the more general case involves both ϵ and ϵ_4 as free parameters (see below), assumed that the quadrupole moment is the relevant distortion parameter.

The momentary total quadrupole moment $Q(t)$ is $\langle\hat{\alpha}\rangle + Q_0$. For simplicity of notation, let us denote $\langle\hat{\alpha}\rangle$ by α. The corresponding wave functions are generated by a <u>generator Hamiltonian</u> of the form

$$H_{gen} = H_0 - \kappa \alpha \hat{\alpha} - \mu(t)\hat{\alpha} \equiv H_0 - \kappa \alpha_V(t) \hat{\alpha}$$

where thus

$$\alpha_V(t) \equiv \alpha - \mu(t)/\kappa \quad .$$

The second term in the middle expression is the field generated by the nuclear two-body force. The third term, added in the form of a Lagrangian multiplier, accounts for the inertial effects of the vibrational motion at a non-equilibrium point. It is the addition of this term that assures that the

expectation value of the operator $\hat{\alpha}$ taken with respect to the wave functions, calculated from the generator Hamiltonian above, comes out to be the value of α that in the first place enters the generator Hamiltonian.

To obtain the inertial mass parameter we have to consider time-dependent deformations $\alpha_V(t)$ of the potential relative to the stationary saddle point. Hence we seek solutions of the time-dependent Schrödinger equation

$$i\hbar \frac{\partial}{\partial t} \psi(t) = (H_0 - \kappa \alpha_V(t) \hat{\alpha}) \psi(t) \quad .$$

As solutions we consider expansions

$$\psi(t) = C_o|0\rangle e^{-i \frac{E_o t}{\hbar}} + \sum_{i \neq 0} C_i|i\rangle e^{-i \frac{E_i t}{\hbar}}$$

where $|0\rangle$ and $|i\rangle$ are the ground and excited state solutions of H_0 with eigenvalues E_o and E_i. The coefficients $C_i(t)$ are considered small compared to C_o. The following expressions for C_i are obtained

$$C_{i\neq 0} \simeq \left[\frac{\kappa \alpha_V \langle i|\hat{\alpha}|0\rangle}{E_i - E_o} + i\hbar \dot{\alpha}_V \frac{\langle i|\hat{\alpha}|0\rangle}{(E_i - E_o)^2} \right] e^{i \frac{E_i - E_o}{\hbar} t} \quad .$$

This is obtained by partial integration of the equation

$$i\hbar \dot{C}_i = - \kappa \alpha_V(t) \sum_j C_j \langle i|\hat{\alpha}|j\rangle e^{i \frac{E_i - E_j}{\hbar} t}$$

under the assumption that $\dot{\alpha}_V(t) \approx$ const.* The total energy is obtained as the expectation value of $H_o - \frac{\kappa}{2} \hat{\alpha} \hat{\alpha}$ with respect to the wave functions above, expressed in terms of $\alpha_V(t)$ and $\dot{\alpha}_V(t)$. The field $\alpha_V(t)$ is eliminated from the expressions by the use of the self-consistency condition

$$\alpha \equiv \langle \psi(t) | \hat{\alpha} | \psi(t) \rangle = \sum_{i \neq 0} \langle 0 | \hat{\alpha} | i \rangle \; C_i \; e^{-i \frac{E_i - E_o}{\hbar} t} + \text{c.c.}$$

With the expressions for C_i inserted we obtain

$$\alpha(t) = \sum_i \frac{2\kappa \, \alpha_V |\langle i | \hat{\alpha} | 0 \rangle|^2}{E_i - E_o} \equiv 2\kappa \; \alpha_V(t) \sum_1 .$$

Taking the derivative of this expression we obtain

$$\dot{\alpha}(t) = 2\kappa \; \dot{\alpha}_V(t) \sum_1 .$$

---

*Alternatively this boundary condition of constant rate of change of field at the equilibrium point may be replaced by the requirement of a solution of the form: $\alpha_V(t) = \overset{o}{\alpha}_V \exp(\gamma \, t/\hbar)$.

Using the above relations to eliminate α_V and $\dot{\alpha}_V$ we obtain* for $\mathcal{E}$

$$\mathcal{E} = E_o + \frac{1}{2}\left(\frac{1}{2\sum_1} - \kappa\right)\alpha^2 + \frac{1}{2}\cdot\frac{\hbar^2}{2}\,\frac{\sum_3}{\left(\sum_1\right)^2}\,\dot{\alpha}^2 \quad .$$

In the last three equations we have employed the short-hand notation:

$$\sum_n = \sum_i \frac{|\langle i|\hat{\alpha}|0\rangle|^2}{(E_i - E_o)^n} \quad .$$

Taking pairing into account and replacing $\hat{\alpha}$ by $\sum_i \hat{q}_i$ we finally obtain

$$\sum_n = \sum_{\mu,\nu} \frac{|\langle\mu|q|\nu\rangle|^2}{(E_\mu + E_\nu)^n}\,(U_\mu U_\nu + V_\mu V_\nu)^2$$

where $\langle\mu|q|\nu\rangle$ is the single-particle quadrupole matrix element. In the expression for $\mathcal{E}$ above we can identify the inertial mass term B as

*Use has also been made of the commonly employed "Hartree approximation" that the expectation value $\langle\hat{\alpha}\,\hat{\alpha}\rangle$ can be replaced by $\langle\hat{\alpha}\rangle\ \langle\hat{\alpha}\rangle$.

$$B_Q = \frac{\hbar^2}{2} \frac{\sum_3}{\left(\sum_1\right)^2} \quad .$$

It is to be noted that in the equation above $\mathcal{E}$ also contains an improved expression for the potential energy surface in the immediate neighborhood of the saddle point. Presently we have not attempted to correct the potential energy surface as obtained by our normalized single-particle energy summation.

Concerning B, thus obtained, we have to note that this is really B_Q, the quantity associated with Q. To obtain B_ϵ we have to employ the approximate relation

$$\sqrt{B_Q}\ dQ = \sqrt{B_Q}\ \frac{dQ}{d\epsilon}\ d\epsilon = \sqrt{B_\epsilon}\ d\epsilon \quad .$$

Some results of the calculations of B_ϵ, performed by Szymanski, Sobiczewski and Wycech, are given in Table I. It is seen that B_ϵ depends rather strongly on ϵ. However, the value at $\epsilon = 0.5$ should be the most relevant for the penetration problem.* Furthermore B_ϵ is relatively sensitive to the value of the pairing strength G.

*In fact B_ϵ is roughly proportional to ϵ for moderate deformations. Column 3 in Table I is computed on the basis of a linear variation of B with ϵ between the two points for which B has been evaluated.

B. Consideration of Other Degrees of Freedom

For the potential energy surface we have concluded ϵ_4 to be a most important degree of freedom. If this and other distortions are included in the dynamical picture, the energy expansion around the saddle equilibrium point becomes

$$T + V = E_o + \frac{1}{2} \sum_{\lambda,\lambda'} B_{\lambda\lambda'} \dot{a}_\lambda \dot{a}_{\lambda'} + \frac{1}{2} \sum_{\lambda,\lambda'} C_{\lambda\lambda'}(a_\lambda - a_\lambda(0))(a_{\lambda'} - a_{\lambda'}(0)) \quad .$$

Due to the fact that $B_{\lambda\lambda'}$ is a positive definite expression, one can always find coordinates that bring the previous expression into a normal form

$$T + V = \frac{1}{2} \sum_{\mu} B_\mu \dot{b}_\mu^2 + \frac{1}{2} \sum_{\mu} C_\mu b_\mu^2 \quad .$$

Of the coefficients C_μ only one is negative for a proper saddle point direction in which the fission process proceeds.

In the microscopic picture the different a_λ-coordinates are replaced by different multipoles Q, Q_4, Q_6 etc. Sobiczewski, Szymanski and Wycech are presently investigating the more formidable two-dimensional problem associated with Q and Q_4. Indications are, however, that the modified-one-dimensional treatment of the problem as of above is rather adequate in view of the other uncertainties entering.

X. FISSION HALF LIVES

We return to the penetration formula

$$P = [1 + \exp(K)]^{-1} \simeq \exp(-K) = \exp\left[- \int_{\epsilon''}^{\epsilon'} 2\sqrt{\frac{2B}{\hbar^2}(W(\epsilon) - E)}\, d\epsilon \right].$$

In this expression let us take the variable B outside of the integral sign and replace it by its value at the saddle point.* For $W(\epsilon)$, the total static energy, we have in the preliminary estimates made the simplifying assumption that the ϵ_4-degree of freedom is maximally exploited without regard for dynamics in such a way that for each ϵ the path goes through the value of ϵ_4 that gives minimum potential energy W. For E, the energy of assault, we have been content with the rough prescription of adding 0.5 MeV to the minimum energy, this figure representing the zero-point vibrational energy corresponding to beta-vibrations. We had earlier

$$\tau = 10^{-21}\, e^{K} .$$

If we replace the life-time τ (sec) by $t_{1/2}$, the half life, use years as units instead of seconds, and furthermore take the logarithm base 10 on both sides, we obtain the approximate relation

*In the case of a double-hump barrier this procedure appears particularly questionable.

$$^{10}\log t_{1/2} \simeq -28.66 - 1.228 \cdot \sqrt{\frac{B}{\hbar^2}} \cdot F$$

where F is the barrier integral

$$F = \int_{\epsilon''}^{\epsilon'} \sqrt{W(\epsilon) - E}\, d\epsilon \quad .$$

A. Actinide Region, Even-Even Isotopes

Fission half-lives are available for even-even nuclei (Fig. 23) in this region up to $Z = 102$ (Nobelium), with several isotopes, and for $Z = 104$ (Kurchatovium), with just one isotope measured, ^{260}Ku. The barrier extends to larger distortions than those for which our parameterization is adequate in the cases of $_{90}$Th, $_{92}$U, and $_{94}$Pu. With some extrapolation most isotopes of $_{96}$Cm, $_{98}$Cf and all of $_{100}$Fm and $_{102}$No can be handled. In Table I we list the theoretical B values obtained by Sobiczewski, Szymanski, and Wycech[42] (for G = const.) for $\epsilon = 0.2$, $\epsilon_4 = 0.0$ and for $\epsilon = 0.5$, $\epsilon_4 = 0.02$, respectively. Assuming a linear ϵ - dependence based on these points we have evaluated the integral K theoretically. An experimental K-value is obtained from fission half lives. A theoretical, corrected K-value, K_{corr}, is obtained simply by adding to E the error in the equilibrium mass value. Good agreement between the experimental K-value and K_{corr} is obtained for $Z = 100$ and $Z = 102$. The correction applied is most likely an overestimate as the error should propagate at least through the first part of the barrier. The good agreement for the light actinides in all likelihood reflects on the overestimate

of the second hump in the fission barrier (largely due to an insufficient number of deformation parameters).

B. Superheavy Region

To exhibit the sensitivity of the predicted half-lives in the superheavy element region, centered around $Z = 114$, $N = 184$, to the value of B assumed, we presented in Ref. 37 the result in the form of Fig. 24. This figure shows $^{10}\log t_{1/2}$ as a function of $\sqrt{B/\hbar^2 \cdot A^{-5/3}}$ for various isotopes of $Z = 114$. The straight lines pass through the constant value -28.7 and their slopes are given as $(1.23) \cdot A^{5/6}$ times the barrier integral F. The microscopic calculations give definite B-values, depending on both N and Z. However, in this figure we replaced them for simplicity by an average value (the right thick vertical line).

For comparison we have in this figure also shown other estimates of B. To the left is the liquid-drop value corresponding to the assumption of irrotational flow. This is given as[23]

$$B_{\alpha}^{irr} = \frac{3}{10} \, AMR_o^2 (1 + \frac{9}{7} \alpha^2 + \dots)$$

while

$$B_{\epsilon}^{irr} = \frac{2}{15} \, AMR_o^2 (1 + \frac{4}{5} \epsilon + \dots) \quad .$$

The ratio of the microscopic value to the irrotational-flow value at $\epsilon \approx 0.5$ varies between 6 and 11 for different nuclei. This is a somewhat larger figure than the corresponding ratio for the rotational moment of inertia

for deformed nuclei and the ratio for the quadrupole vibrational mass. On the whole, however, the irrotational-flow value should only be considered as a lower limit.

The shaded regions in this figure correspond to semiempirical estimates based on empirical fission half-lives in the actinide region. Two such estimates of B are displayed in this figure. The higher one, which should be considered the more reliable value together with the microscopic value, was obtained by Moretto and Swiatecki[41] from an analysis of fission half-lives in the actinide region. This analysis was based on the theoretical fission barriers obtained in accordance with Ref. 4. These are the liquid-drop fission barriers modified by a shell structure correction term. We now further assume that this range of B-values obtained for deformed actinide nuclei is valid also for spherical superheavy nuclei after scaling by the simple $A^{5/3}$ factor, correcting only for an increase in size.*

The scaling problem is also relevant for the second shaded region, marked "semiempirical I".

The latter B-values were obtained from an analysis of actinide fission half-lives in terms of a cubic barrier with its minimum value for spherical

---

*The sensitivity of the calculated B_ϵ-values to the value of ϵ used makes the procedure of employing just a scaling factor $A^{5/3}$ somewhat doubtful. It is to be noted that the saddle shape for $Z = 114$ isotopes is less distorted than for actinide elements.

shape and with the liquid-drop curvature at the saddle point. This prescription probably overestimates the barrier thickness systematically and when applied to fission half-lives in turn underestimates the corresponding B-values. These values should therefore be given less weight.

C. Limits of Superheavy Region of Relative Stability

Using a value of $B/A^{5/3}$ intermediate between the average microscopic estimate and the estimate of Ref. 41, it appears possible to make the rough prediction that there is a region of elements with fission half-lives in excess of 1 sec for $290 < A \lesssim 310$ for $Z = 114$, $290 < A \lesssim 306$ for $Z = 112$, $288 < A \lesssim 304$ for $Z = 110$ etc. This refers specifically to the spontaneous fission half-lives.

The next test for the "survival of the fittest" is that of alpha decay half-lives. On the basis of the calculated masses, one obtains easily alpha Q-values.[43] From these in turn alpha half-lives have been calculated.[44]

In general, alpha decay energies, representing a derivative function of the mass valley, are expected to be smallest for Z and N just below the magic numbers 114 and 184 respectively. Longevity thus favors the $N < 184$, $Z < 114$ quadrant. Due to the fact that for these very heavy nuclei the direction of the stability line forms a considerable angle with the direction of the alpha decay arrow in the mass chart, the neutron rich side of the stability line is the most favorable. Indeed, for $Z = 110$, $N = 184$ we calculate $Q_\alpha = 5.76$ MeV, which should correspond to an alpha half-life of the order of 10^8 years. Roughly in this region of elements $Q_\alpha = 5.5$ MeV corresponds to 10^{10} years, 6.0 MeV to 10^7 years, 6.5 MeV to 10^4, and 7.0 to

10 years. As a rough rule an increase in Q_α by 0.05 MeV decreases the half-life by factor of two and 0.5 MeV by a factor of 10^3. A test of Q_α values in the Pb region shows agreement with empirical ones within ±0.5 MeV. However, in the quadrant in question the theoretical energies are generally overestimated by about 0.5 MeV. This corresponds to a factor 10^3 in alpha half-lives. Assuming the errors in Q_α-values, in the region to which we have extrapolated our potential, to behave similarly one may hold out a certain probability for a pocket of alpha-longevity around the nucleus mentioned.

The survival-of-the-fittest test finally concerns beta-decay. From the masses calculated the following relevant even-even isotopes with masses $286 \leq A \leq 302$ appear to be beta stable (Z = 108, A = 286, 288), (Z = 110, A = 288, 290, 292, 294), (Z = 112, A = 292, 294, 296), and (Z = 114, A = 298, 300, 302) and the following odd-A ones (Z = 109, A = 287), (Z = 110, A = 289, 291), (Z = 111, A = 293), (Z = 112, A = 295) and (Z = 113, A = 297).

D. Surviving Elements

The candidates for long-range survival appear to be located around (Z = 110, N = 184), which element is estimated to have a half-life against spontaneous fission of about 10^{11} years, against alpha decay of 10^8 years (with probable errors of several powers of ten), and appears to be beta-stable.

If these elements were produced somewhere in the universe at some past time, the chance that we may still trace them at present lies in two directions. One is in the incoming cosmic radiation. The other lies in the chemical isolation of such a surviving element from its chemical relatives in natural

ores.* As pointed out by G. Seaborg in his review of Elements Beyond 100, Present Status and Future Prospects[45] Z = 114 should have the chemical properties of Pb, Z = 113 those of Tl, Z = 112 those of Hg, Z = 110 those of Pt, etc. (see Fig. 25). It appears likely that such a remnant element would most easily be found among its chemical relatives, Pt, Au, Os, etc.

*This possibility was first pointed out to us by Dr. S. G. Thompson.

XI. POSSIBLE PRODUCTION OF SUPERHEAVY ELEMENTS*

A. Heavy Ion Reactions

The heaviest elements presently produced ($Z > 100$) are all synthesized by bombardment of target elements of sufficiently high atomic number with beams of heavy ions. The heaviest ion employed appears to be $^{40}_{18}Ar$, but in the future as heavy ions as $_{92}U$ may be available.

By heavy ion reactions one tends to reach elements far off on the neutron deficient side of the stability line. This is so because the stability line bends more and more relative to its initial $45°$ direction in the N-Z mass plane. Both target and projectile are therefore less neutron-rich than the center of the superheavy region ($Z = 114$, $N = 184$), near to which the stability line happens to pass. Even by the choice of neutron-rich targets as $^{248}_{96}Cm$ and neutron-rich projectiles as $^{40}_{18}Ar$ one falls short of the limits of the superheavy region as for example,

$$^{248}_{96}Cm + ^{40}_{18}Ar \rightarrow ^{284}114 + 4n \quad .$$

The unfortunate loss of boil-away neutrons is due to the excessive energy needed to penetrate the Coulomb barrier between the heavy ions and the target nuclei.

---

*The subject matter under this heading is covered in detail in Ref. 45. The remarks here contained are in a large measure based on this very broad review article.

Slightly more promising future prospects are

$$^{244}_{94}Pu + ^{48}_{20}Ca \rightarrow ^{288}_{}114 + 4n$$

or

$$^{248}_{96}Cm + ^{48}_{20}Ca \rightarrow ^{292}_{}116 + 4n \quad .$$

Both reactions require the exclusive ^{48}Ca projectiles, which at the present are difficult to strip. An even more distant prospect is

$$^{248}_{96}Cm + ^{64}_{28}Ni \rightarrow ^{308}_{}124 + 4n$$

which may be additionally promising as $Z = 124$ also appears associated with a minor shell closing. Reference 37 gives a half-life of the order of seconds.

B. Neutron Capture Reactions

Two other avenues seem presently open, namely exposure of available heavy isotopes to the large neutron fluxes in special (high flux) reactors and in so-called "nuclear explosive devices". In the former case the largest neutron flux achieved up to now[45] is 6×10^{15} and in the latter about 10^{31} neutrons/cm^2 sec. If the material is exposed for, say, a few years in such a fast reactor, the integrated exposure is 10^{23} neutrons/cm^2, which is somewhat less than the integrated flux from the nuclear explosive device, the latter being approximately 10^{25} neutrons/cm^2.

One should compare this with the possibly available neutron fluxes in the heavenly laboratories responsible for the "slow" neutron capture process (the s-process) associated with the red giant phase of stellar evolution[46,47] where the flux is estimated at 10^{16} neutrons/cm^2 sec, the duration of the order of 10^3 years, and the integrated flux around 10^{26} neutrons/cm^2. The corresponding numbers for the "fast" neutron capture process (the r-process), first associated with supernovae and more recently with extended or quasi-stellar radio sources* where the corresponding numbers are $>10^{27}$ neutrons/cm^2 sec, 1-1000 sec, and $>10^{27}$ neutrons/cm^2.

The nuclear explosive devices have produced less heavy elements than expected. Indeed $^{257}_{100}$Fm corresponds to the largest Z- and A-numbers recently produced.[45] However, the neutron capture path followed is sensitive to e.g., the flux duration, the target elements present, the neutron spectrum, etc.

The neutron flux supposedly present in the r-process, although somewhat resembling the flux from nuclear explosive devices, has still a 10^6 - 10^8 times longer time scale. This may, in spite of the results from the "device" experiments, lead to an r-path in the very neutron rich region, that eventually

*As recently pointed out by F. Hoyle and W. A. Fowler (Nature 197 (1967) 533) and P. A. Seeger, W. A. Fowler and D. D. Clayton (Astrophys. Jour. Suppl. 97 (1965) 121) the neutron flux and temperatures associated with the r-process appear to require such large stellar objects of $10^4 \rightarrow 10^6$ solar masses.

will populate the $Z = 114$, $N = 184$ region. Residues of these nuclei, a few of these with rather long alpha half-lives, may occur around $Z = 110$, $N = 184$, which might possibly, if occurring half-lives are longer than a few times 10^8 years, be present in earthly matter. If half-lives are shorter than that by a few powers of ten, such elements could still reach us in the cosmic radiation as messengers of more recent cosmic experiments.

ACKNOWLEDGMENTS

The author is grateful to Dr. Isadore Perlman, head of the Nuclear Chemistry Division of Lawrence Radiation Laboratory, for the warm hospitality granted.

I am indebted to Dr. Ben Mottelson and Dr. Larry Wilets for suggestions and critical comments on the isospin and surface dependence of the basic pairing matrix element. The great interest in this work shown by Dr. Glenn Seaborg, Dr. Wladyslaw Swiatecki and Dr. Stanley Thompson has been decisive for its line of direction. In recent months the great burden of the work reported here was in a large measure carried by Mr. Chin Fu Tsang of LRL on the problem of the potential energy surface, and, on the penetration problem, by Drs. Zdrislaw Szymanski, Adam Sobiscewski, and Slavomir Wycech. Important contributions to the present investigation have earlier been made by Mr. Björn Nilsson of Lund and Dr. Raymond Nix, now at Los Alamos. In Lund further work on the P_6 and P_3 degrees of freedom is in progress by Mr. Peter Möller and Mr. Christer Gustafson.

REFERENCES

1. C. F. von Weizsächer, Z. Physik 96 (1935) 431.
2. H. A. Bethe and R. F. Backer, Rev. Mod. Phys. 8 (1936) 193.
3. L. R. B. Elton, Nuclear Sizes, (Oxford University Press, Oxford, 1961).
4. W. D. Myers and W. J. Swiatecki, Nucl. Phys. 81 (1966) 1; see also Proc. International Symposium on Why and How Should We Investigate Nuclei Far Off the Stability Line, Lysekil, Sweden, 1966, (Almqvist and Wiksell, Stockholm, 1967), p. 343; and Arkiv Fysik 36 (1967) 593.
5. A. Bohr and B. R. Mottelson, monograph, to be published.
6. A. Green, Nuclear Physics (McGraw-Hill Book Co., New York, 1955).
7. H. Meldner, Lysekil Symposium, 1966, op. cit., p. 593; and Arkiv Fysik 36 (1967) 593.
8. A. Sobiczewski, F. A. Gareev, and B. N. Kalinkin, Phys. Letters 22 (1966) 500.
9. C. Gustafson, I. L. Lamm, B. Nilsson and S. G. Nilsson, Lysekil Symposium, 1966, op. cit., p. 613; and Arkiv Fysik 36 (1967) 613.
10. A. M. Lane, Nucl. Phys. 35 (1962) 676.
11. E. Rost, Phys. Letters 26B (1967) 184.
12. H. Blomquist and S. Wahlborn, Arkiv Fysik 16 (1960) 545.
13. L. A. Sliv and B. A. Volchok, J. Exp. Theor. Phys. 36 (1959) 539.
14. F. A. Gareev, S. P. Ivanova, and B. N. Kalinkin, Joint Institute for Nuclear Research Preprint P4-3451; F. A. Gareev, S. P. Ivanova, B. N. Kalinkin, S. V. Slepnev, and N. G. Ginzburg, Preprint P4-3607.

15. D. L. Hendrie, N. K. Glendenning, B. G. Harvey, O. N. Jarvis, H. H. Duhm, J. Saudinos, and J. Mahoney, Phys. Letters 26B (1968) 127; see also N. K. Glendenning, Proc. of the International School of Physics, Enrico Fermi, Varenna, Course XL, M. Jean editor (Academic Press, New York, 1968).

16. S. G. Nilsson, Mat. Fys. Medd. Dan. Vid. Selsk. 29 (1955) no. 16.

17. B. Nilsson, to be published.

18. I. L. Lamm, to be published.

19. M. Jaskola, N. Nybo, P. O. Tjöm, and B. Elbek, Nucl. Phys. A96 (1967) 52; D. G. Burke and B. Elbek, Mat. Fys. Medd. Dan Vid. Selsk. 36 (1967) no. 6.

20. A. Bohr, B. R. Mottelson, and D. Pines, Phys. Rev. 110 (1958) 936.

21a. H. C. Britt, F. A. Rickey, and W. S. Hall, Los Alamos Scient. Lab. Report LA-DC-9562; L. Moretto and S. Thompson, to be published.

21b. W. Stepień and Z. Szymanski, Phys. Letters 26B (1968) 181.

22. R. C. Kennedy, L. Wilets, and E. M. Henley, Phys. Rev. Letters 12 (1964) 36.

23. J. R. Nix, Ann. Phys. 41 (1967) 52, and private communication.

24. B. R. Mottelson and S. G. Nilsson, Mat. Fys. Skr. Dan Vid. Selsk 1 (1959) no. 8.

25. D. Bés and Z. Szymanski, Nucl. Phys. 28 (1961) 92.

26. Z. Szymanski, Nucl. Phys. 28 (1961) 421.

27. A. Sobiczewski, Nucl. Phys. A93 (1967) 501.

28. S. G. Nilsson, Nucleonic Structure of Equilibrium and Fission Deformations, International School of Physics "Enrico Fermi", Varenna, Course XL, M. Jean editor (Academic Press, New York, 1968).

29. G. F. Bertsch, Phys. Letters 26B (1968) 130.

30. K. Kjällquist, Nucl. Phys. 9 (1958/1959) 163.

31. K. Harada, Phys. Letters 10 (1964) 80.

32. V. M. Strutinsky, Nucl. Phys. A95 (1967) 420.

33. C. F. Tsang, private communication.

34. S. M. Polikanov, V. A. Druin, V. A. Karnaukov, V. L. Mikheev, A. A. Pleve, N. K. Skobolev, V. G. Subotin, G. M. Ter-Akopian, and V. A. Fomichev, Exp. Theor. Phys. 42 (1962) 1464; cf. also S. Björnholm, J. Borggreen, L. Westgaard, and V. A. Karnaukov, Nucl. Phys. A95 (1967) 513.

35. S. Björnholm, private communication.

36. E. Lynn, report at the Conference on Nuclear Structure, Dubna, July, 1968.

37. S. G. Nilsson, R. Nix, A. Sobiczewski, Z. Szymanski, S. Wycech, C. Gustafson, and P. Möller, Nucl. Phys. A115 (1968) 545.

38. L. Wilets, Theories of Nuclear Fission (Clarendon Press, Oxford, 1964).

39. P. O. Fröman and N. Fröman, J.W.K.B. Approximation, Contribution to the Theory (North-Holland Press, Amsterdam, 1965).

40. D. L. Hill and J. A. Wheeler, Phys. Rev. 89 (1953) 1102.

41. L. Moretto and W. J. Swiatecki, private communication.

42. A. Sobiczewski, Z. Szymanski, and S. Wycech, private communication.

43. C. F. Tsang, and S. G. Nilsson, to be published.

44. S. Thompson, private communication.

45. G. T. Seaborg, Elements Beyond 100, Present Status and Future Prospects, to be published in Ann. Rev. Nucl. Sci. (1968).

46. E. M. Burbidge, G. R. Burbidge, W. A. Fowler and F. Hoyle, Rev. Mod. Phys. 29 (1957) 547.

47. W. A. Fowler, Nuclear Astrophysics (Amer. Phil. Soc., Philadelphia, 1967).

FIGURE CAPTIONS

Fig. 1. Binding energy per particle as function of A. The smooth curve represents a mass formula fit. (Figure from A. Bohr, B. R. Mottelson, Ref. 5.)

Fig. 2. Nuclear Valley of Stability (after C. N. Flerov in Why and How Would We Investigate Nuclides Far Off the Stability Line, Almqvist and Wiksell, Stockholm, 1967). The circular mark at $^{298}114$ is the double-closed shell nucleus predicted by the present calculations. The super-heavy region connected with Z = 126, marked in figure, is not directly supported by the present calculations.

Fig. 3. Shell effects evidenced by nuclear masses. Plotted is $M_{exp} - M_{liq}$ in units of MeV. Note deviations associated with shell closure of N = 28, 50, 82 and 126. (Figure is taken from W. D. Myers and W. J. Swiatecki, Ref. 4.)

Fig. 4. Relation between coordinates ϵ, ϵ_4 and a_2, a_4. Note that the pure spheroid shape contains some a_4 (and in addition a_6 etc. not shown in figure).

Fig. 5a. Single-proton levels $150 < A < 165$; $\kappa = 0.0637$, $\mu = 0.600$, $\epsilon_4 = -0.04$.

5b. Single-neutron levels $150 < A < 165$; $\kappa = 0.0637$, $\mu = 0.420$, $\epsilon_4 = -0.04$.

5c. Single-proton levels $175 < A < 190$; $\kappa = 0.0620$, $\mu = 0.614$, $\epsilon_4 = 0.04$.

5d. Single-neutron levels $175 < A < 190$; $\kappa = 0.0630$, $\mu = 0.393$, $\epsilon_4 = 0.04$.

5e. Single-proton levels $220 < A < 240$; $\kappa = 0.0590$, $\mu = 0.639$, $\epsilon_4 = -0.04$.

5f. Single-neutron levels $220 < A < 240$; $\kappa = 0.0635$; $\mu = 0.346$, $\epsilon_4 = -0.04$.

5g. Single-proton levels $250 < A < 260$; $\kappa = 0.0569$, $\mu = 0.656$, $\epsilon_4 = 0.04$.

5h. Single-neutron levels $250 < A < 260$; $\kappa = 0.0635$, $\mu = 0.314$, $\epsilon_4 = 0.04$.

5i. Single-proton levels $A \approx 298$; $\kappa = 0.534$, $\mu = 0.686$, $\epsilon_4 = 0$.

Fig. 6a. Single-proton level diagram for spherical potential. Parameters are fitted to reproduce observed deformed single-particle level order at $A \approx 165$ and 242. Level order at $A = 208$, 290 is extrapolated linearly. E. Rost's predicted level order[11] for $A = 298$ is exhibited for comparison.

6b. Analgous to Fig. 6a, valid for neutrons.

Fig. 7a. Empirical odd-Z-even-Even mass differences compared with theoretical Δ_p in rare earth region.

7b. Empirical odd-N-even-even mass differences compared with theoretical Δ_n in rare-earth region.

Fig. 8. Effect of various terms in total energy as a function of deformation. Long-dashed curve marks simple sum of single-particle energies, for dotted curve Coulomb energy is added, for dot-dashed curve also pairing ($G \sim S$) is included, for short-dashed curve the Strutinsky normalization is applied. In all these cases it is assumed that $\epsilon_4 = 0$. In the last case (solid curve) also the effect of the ϵ_4-degree of freedom is included.

Fig. 9. Gap parameters (left scale) and total pairing energy (right scale) as functions of distortion ϵ for the two cases that G is constant and that G is proportional to the surface area.

Fig. 10. Plot of ratios of calculated Δ_n and Δ_p for the case $G \sim S$ and for the case G = const. The two G-functions are normalized at $\epsilon = 0.25$. It is found that, apart from fluctuations, due to level density variations, Δ varies roughly as S^3 under the assumption $G \sim S$. In the figure we also exhibit for comparison a curve

corresponding to $S^{3/2}$, the $\Delta(S)$ dependence suggested by the "slab model" of Ref. 22.

Fig. 11. Differential cross sections[15] for 50 MeV alpha-particles scattered against ^{154}Sm. Fits to experimental data is made by coupled channel calculations with three alternative sets of β_2 and β_4. The great sensitivity to β_4 in the 4^+ and 6^+ cross sections is clearly borne out.

Fig. 12. Empirical rare earth β_4-values (filled circles) obtained through the analysis of Ref. 15 as illustrated in Fig. 11, compared to the present calculations before the inclusion of the Strutinsky normalization. The effect of the latter is less than 0.01 in magnitude.

Fig. 13. Same as Ref. 12 for equilibrium β_6-values in rare earth region. Errors in empirical β_6-values are at least 0.02. Theoretical β_6-values are sensitive to polarizations due to couplings between shells $N \rightarrow N \pm 4$ not presently included.

Fig. 14a. Equilibrium (ϵ, ϵ_4)-values in the rare earth region as of present calculations (Strutinsky normalization included).

14b. Equilibrium (ϵ, ϵ_4)-values in actinide region.

Fig. 15. Sum of single-particle, pairing and Coulomb energies <u>without Strutinsky normalization</u> as function of ϵ, ϵ_4. At large distortions the energy ultimately rises beyond + 15 MeV (limit for plot).

Fig. 16. Pairing and shell corrections evaluated by the Strutinsky method as a function of the shell-smearing parameter γ. Energies corresponding to three different distortions are considered. For $\gamma \simeq 1.2\ \hbar\omega_0$ it is obvious that with fourth, or better, sixth order correction terms included there is very satisfactory stability with respect to the choice of γ.

Fig. 17. Experimental and theoretical mass values for $150 < A < 310$ plotted relative to the spherical liquid drop value as of Ref. 4.

Fig. 18a. Total-energy surface in (ϵ, ϵ_4) plane for ^{252}Fm after application of the Strutinsky normalization. This figure corresponds to a somewhat earlier calculation and employs $G = \text{const}$ and a different pairing cut-off than described in the present paper. More recent calculations are exhibited in Figs. 21 and 22.

18b. Same as Fig. 18a valid for $^{290}114$.

Fig. 19a. Liquid-drop energy surface for ^{252}Fm.

19b. Liquid-drop energy surface for $^{290}114$.

Fig. 20a. Shell and pairing energy contributions for ^{252}Fm. For further details see Fig. 18a.

20b. Same as Fig. 20a for $^{290}114$.

Fig. 21a. Total energy minimized w.r.t. ϵ_4 for each ϵ as function of ϵ for isotopes of $_{92}$U. Dashed curve corresponds to G set constant while the solid line is based on assumption that G is proportional to the nuclear surface area.

21b. Same as Fig. 21a for isotopes of $_{94}$Pu.

21c. Same as Fig. 21a for isotopes of $_{96}$Cm.

21d. Same as Fig. 21a for isotopes of $_{98}$Cf.

21e. Same as Fig. 21a for isotopes of $_{100}$Fm. The extra dot-dashed curve added for ^{256}Fm represents the new total energy for the case $G \sim S$ when the nuclear potential parameters are modified from those relevant for $A = 242$ to $A = 265$. As can be seen the barrier change is actually very small.

Fig. 21f. Same as Fig. 21a for isotopes of $_{102}$No.

21g. Same as Fig. 21a for isotopes of Z = 104.

21h. Same as Fig. 21a for isotopes of Z = 106.

Fig. 22a. Same as Fig. 21a for isotopes of Z = 114.

22b. Same as Fig. 21a for isotopes of Z = 112.

22c. Same as Fig. 21a for isotopes of Z = 110.

22d. Same as Fig. 21a for isotopes of Z = 108.

Fig. 23. Empirical fission half lives of even-even nuclei plotted against neutron number (taken from A. Ghiorso, University of California, Lawrence Radiation Laboratory Report UCRL-17907). The dotted lines are surmised extrapolations, not necessarily supported by the present work.

Fig. 24. Spontaneous fission half lives of Z = 114 isotopes according to earlier calculations of Ref. 37 as functions of the inertial parameter B for barrier penetration. Four estimates of B are given. The most reliable estimate is placed between the one denoted "semiempirical II" and the one denoted "microscopic". For further explanations, see text.

Fig. 25. Periodic Table exhibiting predicted location of new elements (from G. T. Seaborg, Ref. 45).

Fig. 26. The path of element generation followed by the rapid-neutron capture process (the "r-process") according to P. A. Seeger, W. A. Fowler, D. D. Clayton (Astrophys. Journ. Suppl. XI (1965) 121). The fission break-off line in the upper right corner corresponds to an arbitrary assumption by the authors. Present calculations indicate that this break-off line is associated with much higher A-values.

Table I. Experimental and theoretical fission half-life parameters. The nuclide is identified by Z and A in the first two columns. Columns 3-5 give theoretical and experimental K-values (see section IX), the latter from empirical half-lives. The first K-value is calculated assuming a linear ε-dependence of B between the two calculated points. The second K-value is obtained after a correction for the error in the ground state mass value. The correction is assumed only to affect the equilibrium minimum only. Columns 6-7 give the theoretical B-values calculated for $\varepsilon = 0.2$ ($\varepsilon_4 = 0$) and $\varepsilon = 0.5$ ($\varepsilon_4 = 0.02$).

		Theoretical		Experimental	Theoretical	
Z	A	K	K_{corr}	K	B(0.5)	B(0.2)
92	232	127	99	98	1020	260
	234	132	111	103	1050	240
	236	130	106	104	980	260
	238	127	102	103	910	320
94	236	120	101	88	1077	240
	238	119	103	91	1000	270
	240	118	98	92	920	330
	242	139	97	91	920	380
	244	144	106	90	880	300
96	240	103	76	81	1020	270
	242	117	79	82	930	340
	244	121	89	83	930	390
	246	131	93	83	890	320
	248	131	91	81	860	300
98	246	95	61	74	980	410
	248	114	71	75	920	330
	250	114	72	76	880	320
	252	106	59	71	800	290
100	248	75	33	59	980	450
	250	80	45		910	370
	252	88	40	68	870	360
	254	83	40	66	780	330
	256	86		58	820	420
102	252	47		51	920	330
	254	56	34	61	880	320
	256	53		56	790	280
	258	56		<46	830	370
104	256	46			960	330
	258	45			870	290
	260	58		48	910	390
	262	59			880	470

Z \ N	178	179	180	181	182	183	184	185	186	187	188	189
116	187.87 (1ms) (—.8) 1s (10.14)		190.36 1d (7.1) 1min (9.92)		193.14 10^5y (8.3) 10s (9.71)		196.42 10^{11}y (9.4) $\frac{1}{2}$min (9.58)		201.30 10^{11}y (9.4) 0.1s (10.—)		204.— 1s (10.24)	
115	184.07		187.74 10min (8.89)		188.85 10h (8.58)		192.45 1d (8.45)		197.66 10s (9.59)		203.2 10min (9.11)	
114	178.01 1min (9.4)	180.09	181.00 10^2y (7.0) 10d (7.97)	183.17 1y (7.71)	184.41 10^9y (8.3) 1y (7.55)	186.56 10^2y (7.20)	188.34 10^{16}y (9.6) 10y (7.40)	191.29 100d (7.87)	192.88 10^{11}y (9.4) 1d (8.34)	197.32 .4 (8.49)	199.94 10^{14}y (9.4) 10d (8.09)	203.—2 10d (8.00)
113	174.48		177.84 10y (7.33)		181.57 10^7y (6.89)		185.84 10^7y (6.68)		191.71 1y (7.43)		195.10 10y (7.29)	
112	170.60 10^{-2}s (8.1)	173.03	174.43 1d (5.7) 1y (7.46)	176.93 10^2y (7.17)	178.51 10^6y (6.9) 10^3y (6.83)	180.99 10^4y (6.52)	183.11 10^{12}y (8.1) 10^4y (6.54)	186.40 10^2y (7.10)	189.32 10^{13}y (8.1) 1y (7.50)	193.09 100d (7.—)	195.94 10^{12}y (8.1) 10y (7.—)	199.— 10^{12}y (8.1)
111	168.08		172.34 10y (7.05)		176.83 10^5y (6.38)	179.47	181.75 10^7y (6.03)		188.28 10^2y (6.98)		192.87 10^3y (6.—2)	
110	165.—4 (1ms) (7.2) 10y (7.—)	167.88	169.—2 10min (4.3) 10^3y (6.8—)	172.04 10^4y (6.40)	174.14 10^3y (5.5) 10^6y (6.14)	176.87 10^9y (5.63)	179.39 10^{10}y (6.8) 10^8y (5.76)	183.01 10^5y (6.24)	186.27 10^{10}y (—.7) 10^2y (6.73)	190.— 10^3y (6.8—)	193.—4 10^9y (—.2) 10^4y (—.4—)	197.—8 10^4y (6.—)
109	161.—8		165.02	171.10	173.29	176.18	178.87 10^{11}y (5.24)	182.66	186.08 10^5y (6.21)		189.—8	
108	159.97 10^4y (6.48)	163.71	164.—7 1s (3.2) 10^4y (6.23)	168.81	171.20 1y (4.3) 10^8y (5.57)	174.34	177.11 10^8y (5.8) 10^{13}y (4.89)	181.07 10^9y (5.59)	184.66 10^8y (5.9) 10^6y (5.86)	189.10	192.—0 10^7y (—.9)	
107					171.20	174.49	177.44					
106					169.79 10d (3.9) 10^{11}y (4.97)	173.25	176.37 10^7y (5.3)					

Table II. Table of masses, spontaneous-fission and alpha half-lives near Z = 114, N = 184. The upper number in each square gives the mass relative to the spherical liquid drop value (see Ref. 4) in MeV. In the line below is listed the spontaneous-fission half-life and in parenthesis the barrier height in MeV. The bottom line in each square gives the alpha half-life and the alpha Q-value (in parenthesis). Beta-stable nuclei are underlined.

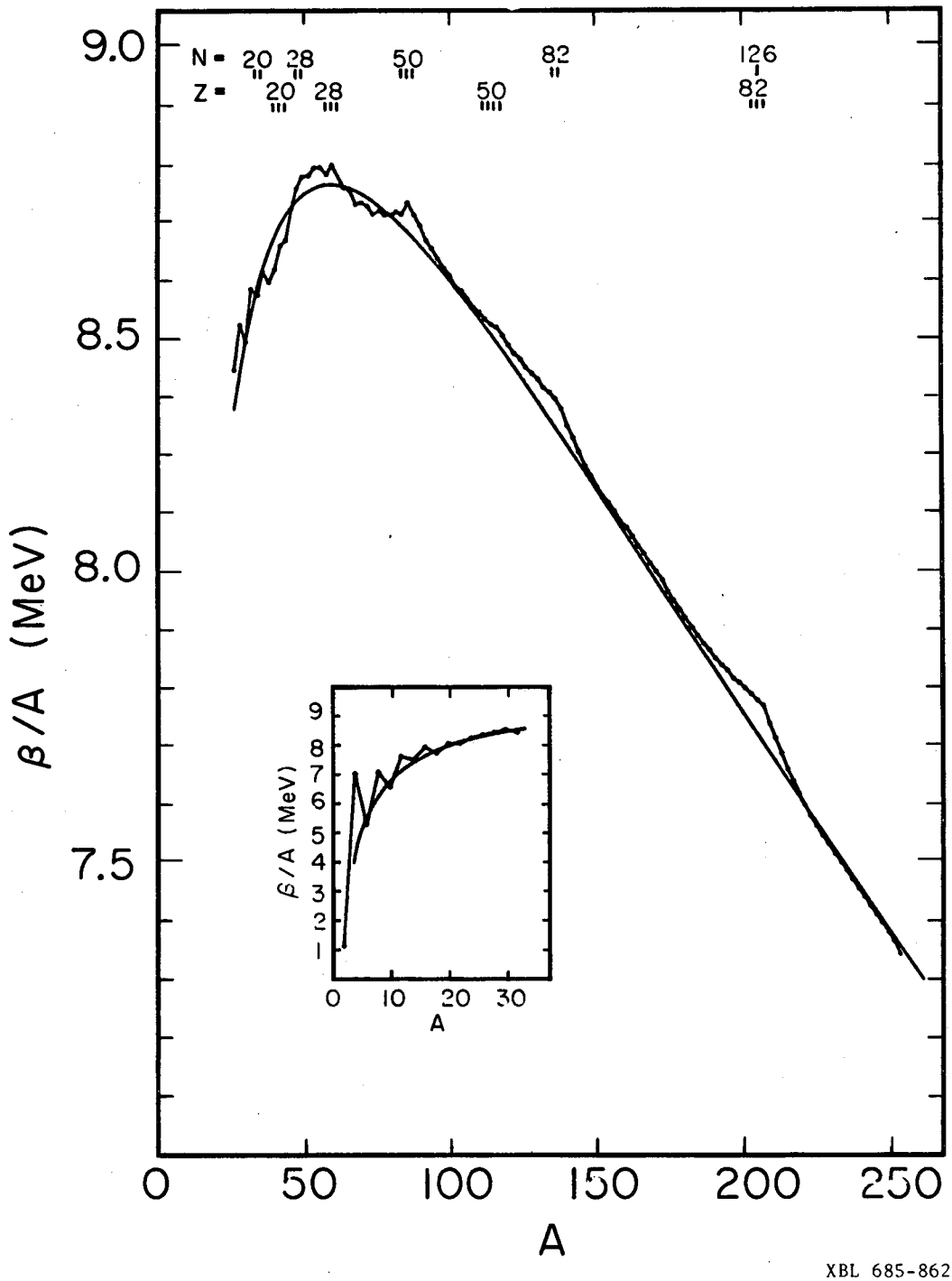
9.0
8.5
8.0
7.5
β/A (MeV)
N = 20 28 50 82 126
Z = 20 28 50 82
0 50 100 150 200 250
A
β/A (MeV)
0 10 20 30
A
XBL 685-862

Fig. 1.

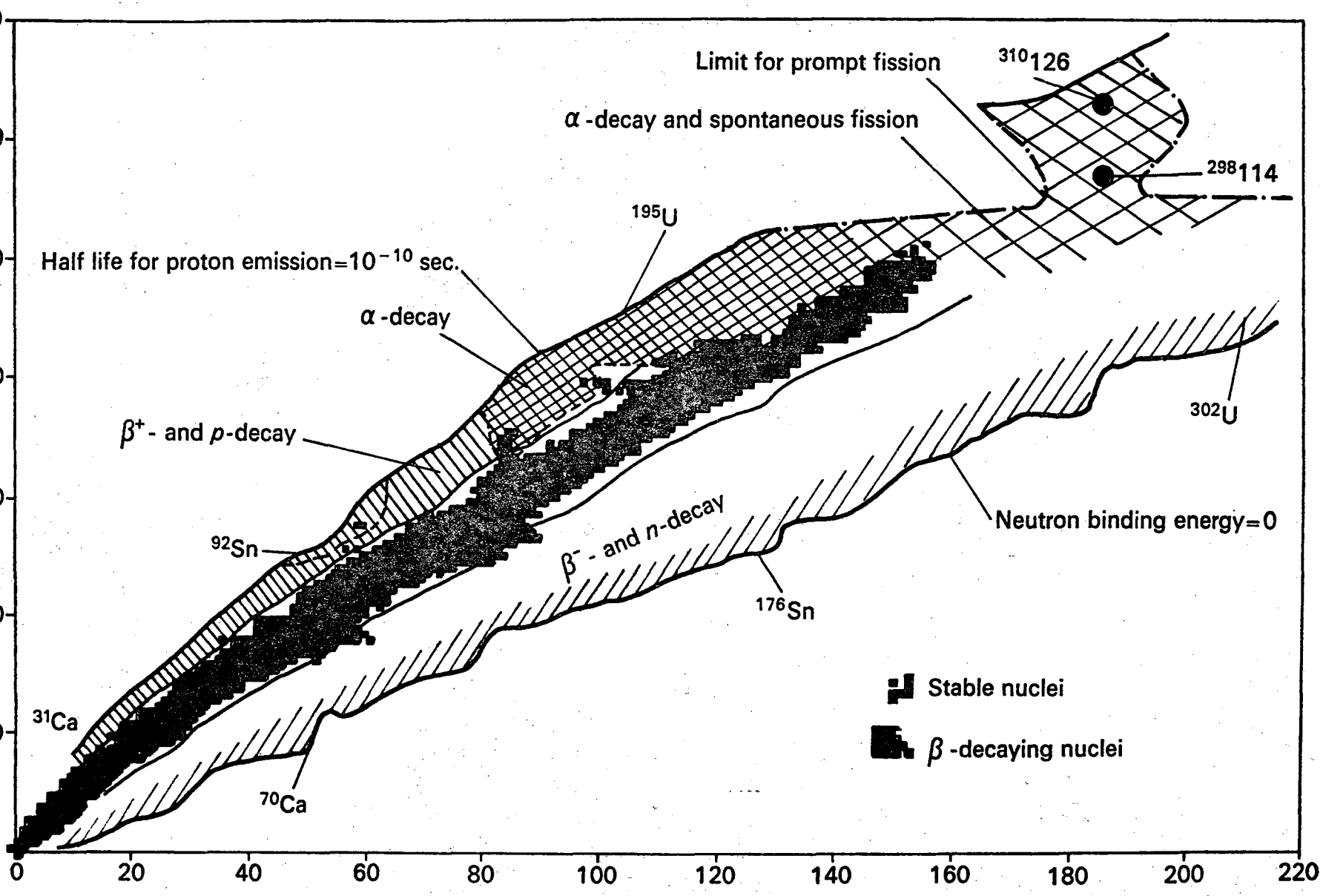
Limit for prompt fission
310126
α -decay and spontaneous fission
298114
195U
Half life for proton emission=10−10 sec.
α -decay
β+- and p-decay
92Sn
β- - and n-decay
176Sn
302U
Neutron binding energy=0
31Ca
70Ca
Stable nuclei
β -decaying nuclei
140
120
100
80
60
40
20
0
20
40
60
80
100
120
140
160
180
200
220

Fig. 2.

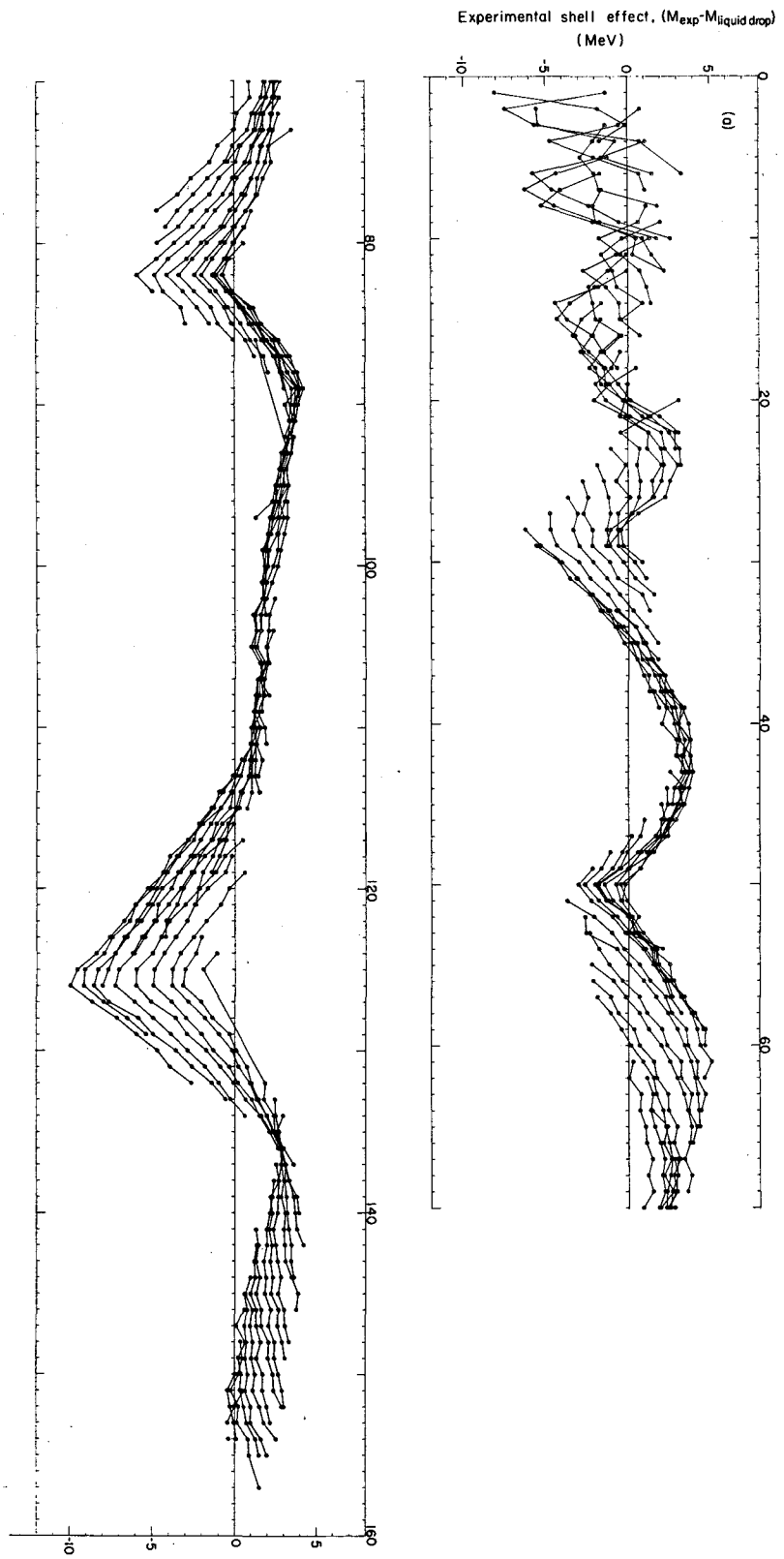
Experimental shell effect, (M_{exp}-$M_{liquid\ drop}$)
(MeV)
(a)
XBL 685-728

Fig. 3.

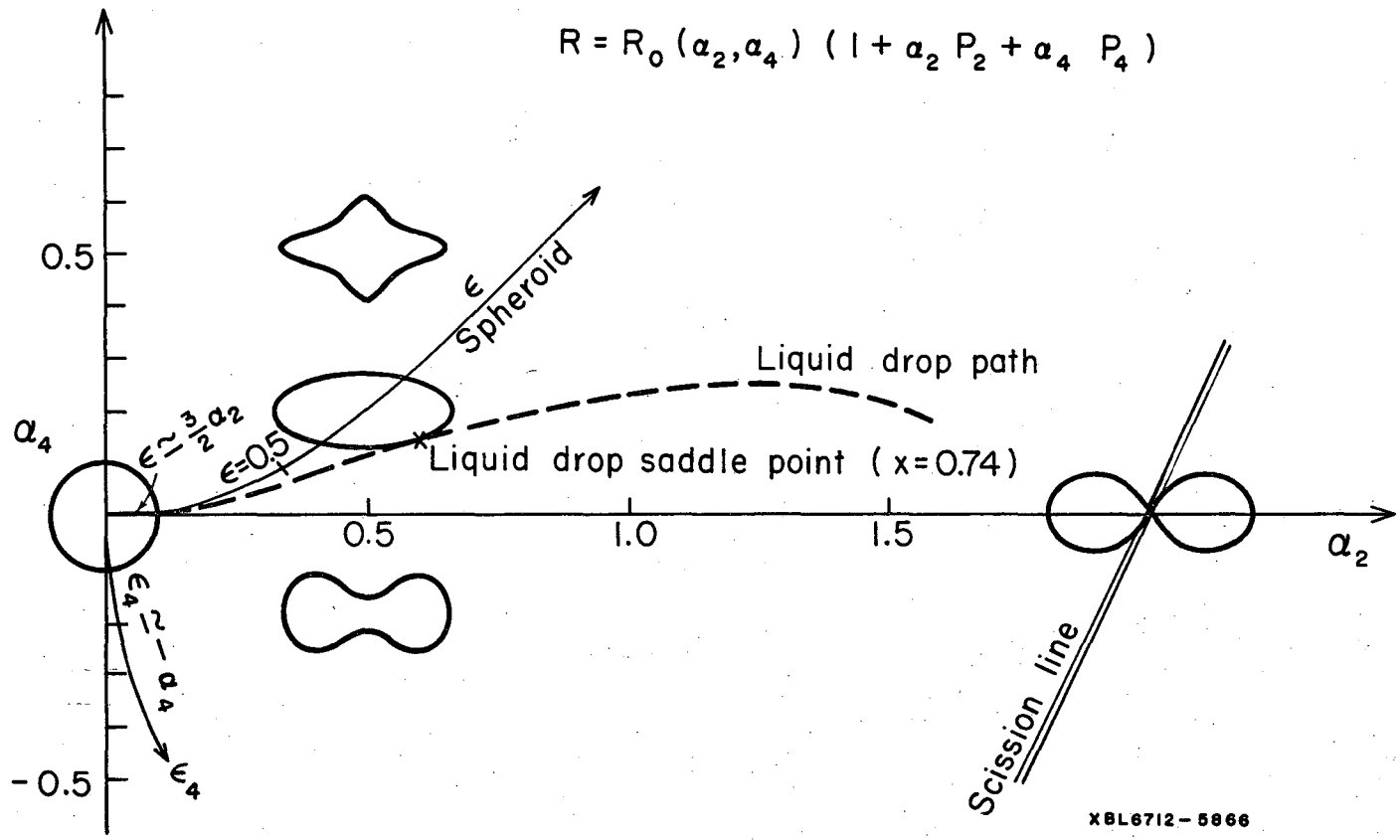
R = R0 (α2,α4) (1 + α2 P2 + α4 P4)
0.5
-0.5
α4
0.5
1.0
1.5
α2
ε Spheroid
Liquid drop path
Liquid drop saddle point (x=0.74)
ε≃3/2 α2
ε=0.5
ε4 = 2 − α4
ε4
Scission line
XBL6712-5866

Fig. 4.

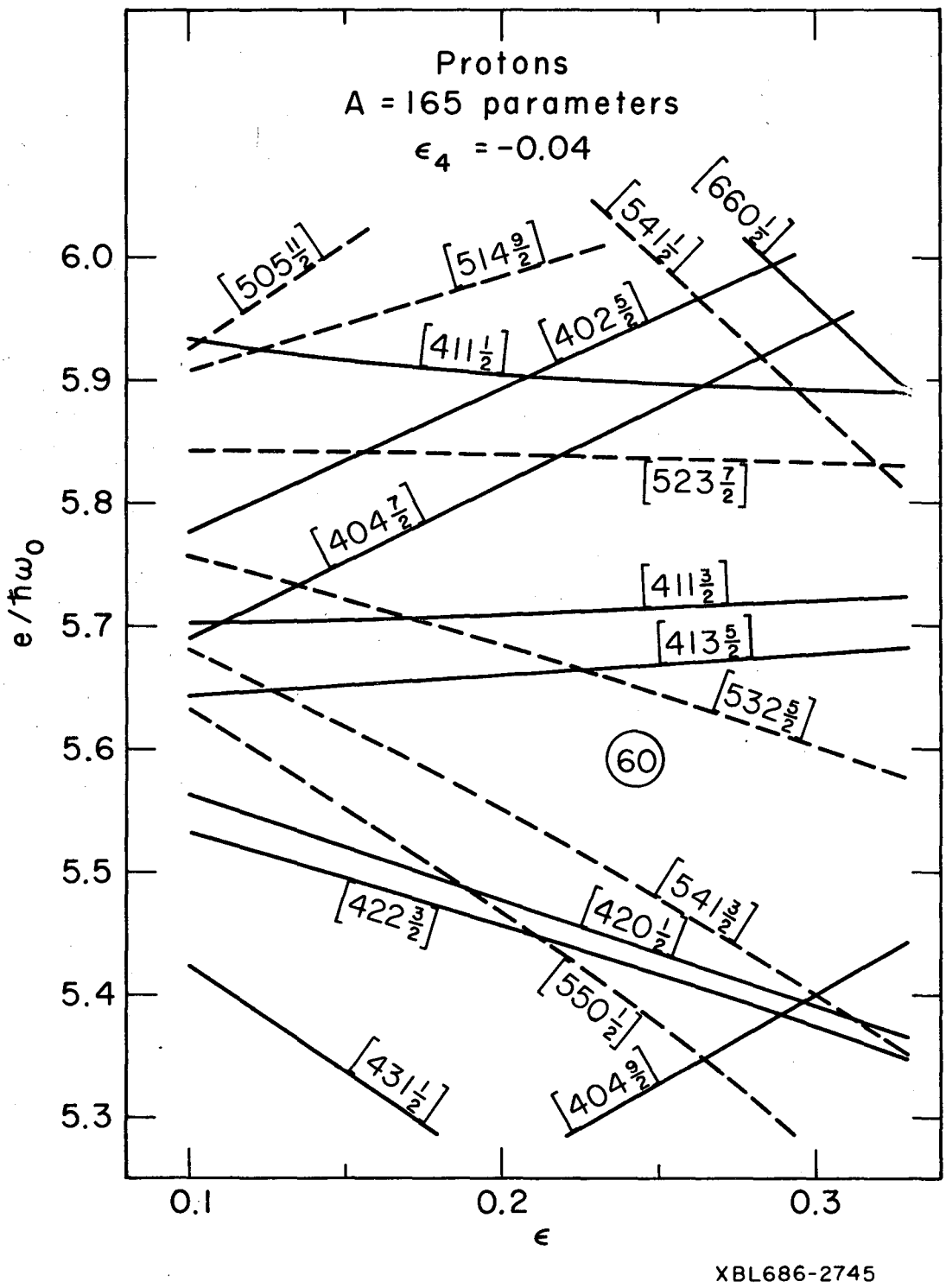
Protons
A = 165 parameters
ϵ_4 = -0.04
$[505\frac{11}{2}]$
$[514\frac{9}{2}]$
$[541\frac{1}{2}]$
$[660\frac{1}{2}]$
$[411\frac{1}{2}]$
$[402\frac{5}{2}]$
$[523\frac{7}{2}]$
$[404\frac{7}{2}]$
$[411\frac{3}{2}]$
$[413\frac{5}{2}]$
$[532\frac{5}{2}]$
60
$[541\frac{3}{2}]$
$[422\frac{3}{2}]$
$[420\frac{1}{2}]$
$[550\frac{1}{2}]$
$[431\frac{1}{2}]$
$[404\frac{9}{2}]$
6.0
5.9
5.8
5.7
5.6
5.5
5.4
5.3
$e/\hbar\omega_0$
0.1
0.2
0.3
ϵ
XBL686-2745

Fig. 5a.

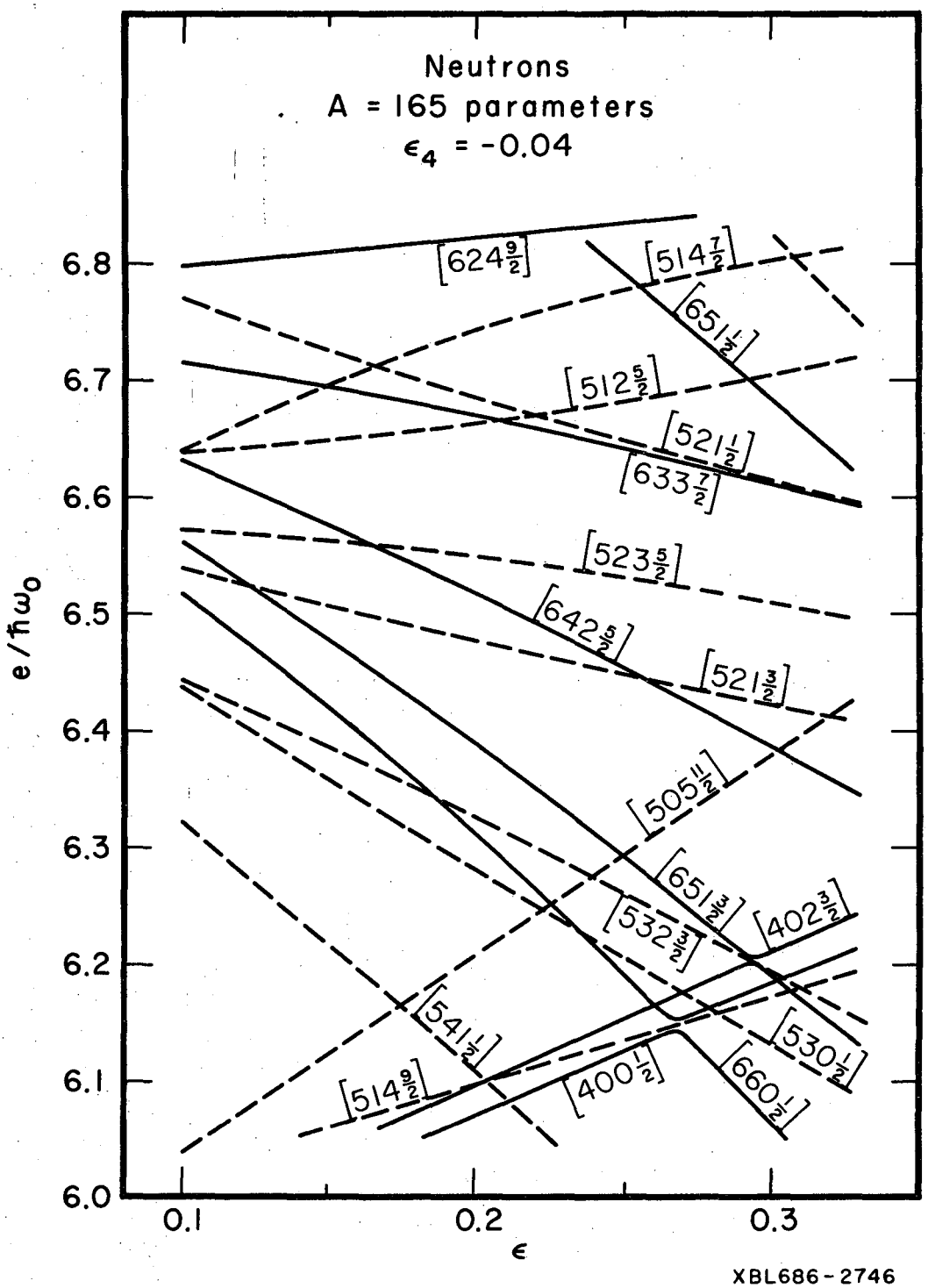
Neutrons
A = 165 parameters
ϵ_4 = -0.04
$[624\frac{9}{2}]$
$[514\frac{7}{2}]$
$[651\frac{1}{2}]$
$[512\frac{5}{2}]$
$[521\frac{1}{2}]$
$[633\frac{7}{2}]$
$[523\frac{5}{2}]$
$[642\frac{5}{2}]$
$[521\frac{3}{2}]$
$[505\frac{11}{2}]$
$[651\frac{3}{2}]$
$[532\frac{3}{2}]$
$[402\frac{3}{2}]$
$[541\frac{1}{2}]$
$[530\frac{1}{2}]$
$[514\frac{9}{2}]$
$[400\frac{1}{2}]$
$[660\frac{1}{2}]$
6.8
6.7
6.6
6.5
6.4
6.3
6.2
6.1
6.0
$e/\hbar\omega_0$
0.1
0.2
0.3
ϵ
XBL686-2746

Fig. 5b.

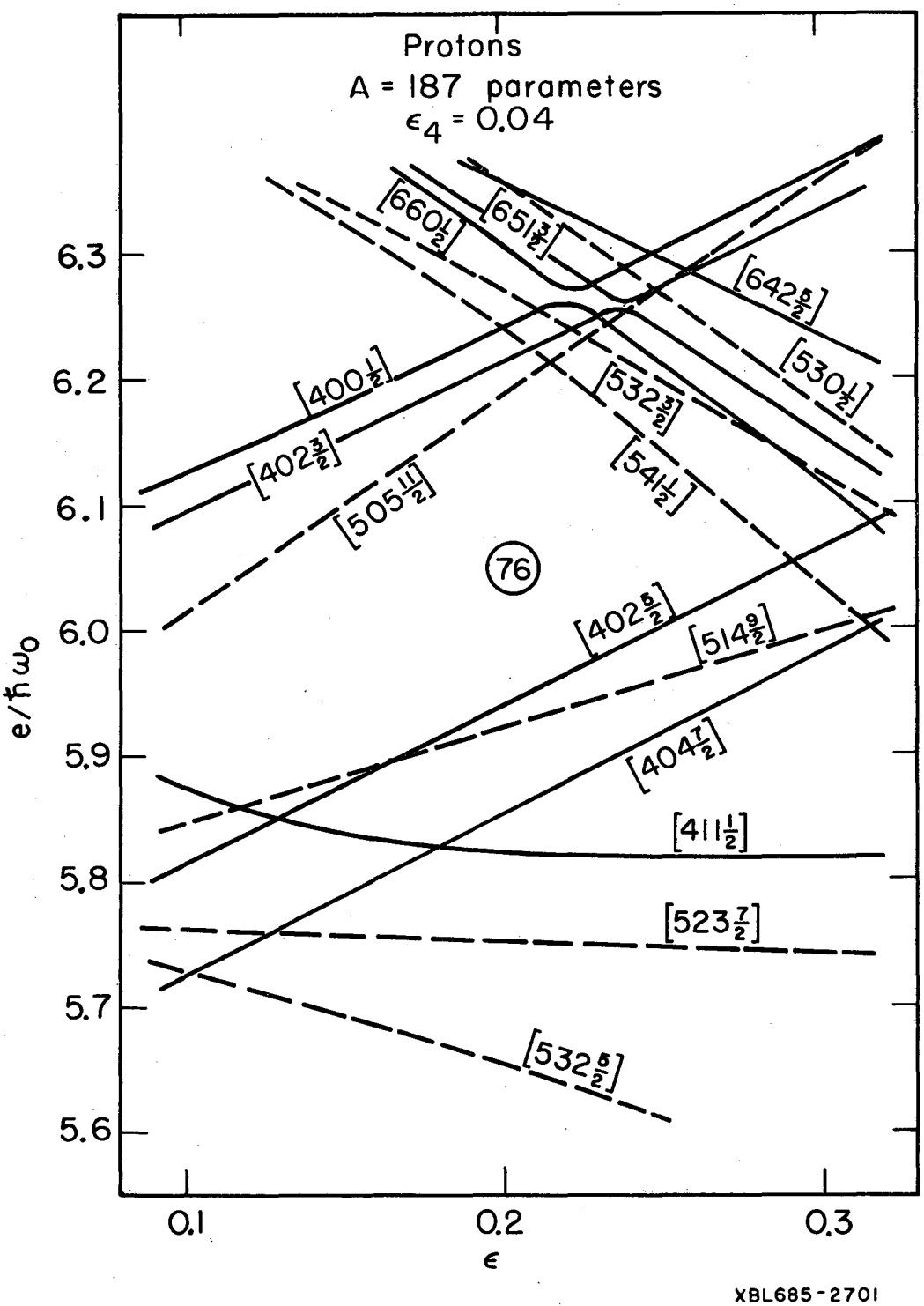
Protons
A = 187 parameters
ϵ_4 = 0.04
$[660\frac{1}{2}]$
$[651\frac{3}{2}]$
$[642\frac{5}{2}]$
$[530\frac{1}{2}]$
$[400\frac{1}{2}]$
$[402\frac{3}{2}]$
$[505\frac{11}{2}]$
$[532\frac{3}{2}]$
$[541\frac{1}{2}]$
76
$[402\frac{5}{2}]$
$[514\frac{9}{2}]$
$[404\frac{7}{2}]$
$[411\frac{1}{2}]$
$[523\frac{7}{2}]$
$[532\frac{5}{2}]$
6.3
6.2
6.1
6.0
5.9
5.8
5.7
5.6
$e/\hbar\omega_0$
0.1
0.2
0.3
ϵ
XBL685-2701

Fig. 5c.

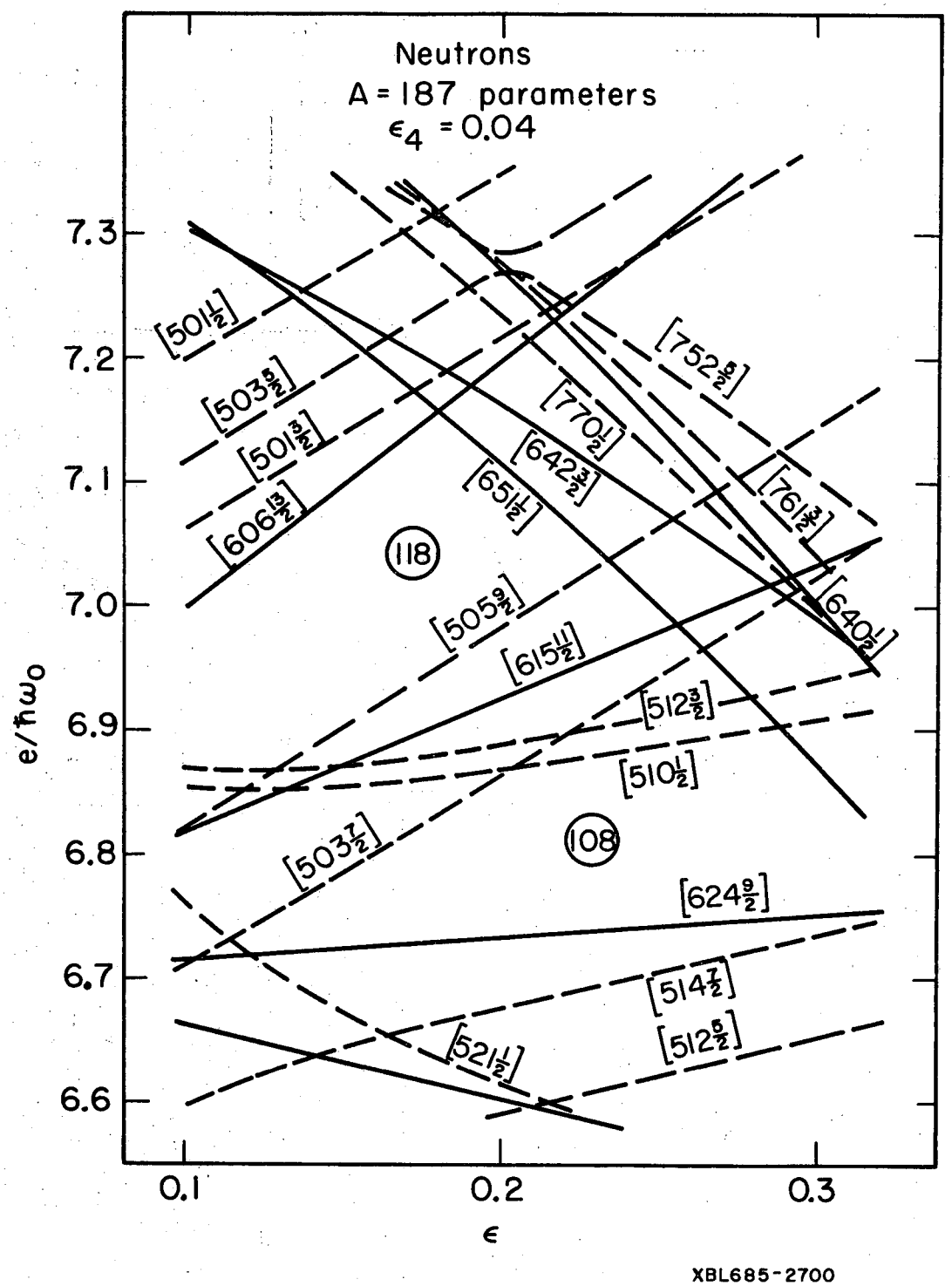
Neutrons
A = 187 parameters
ϵ_4 = 0.04
7.3
7.2
7.1
7.0
6.9
6.8
6.7
6.6
$e/\hbar\omega_0$
0.1
0.2
0.3
ϵ
$[501\frac{1}{2}]$
$[503\frac{5}{2}]$
$[501\frac{3}{2}]$
$[606\frac{13}{2}]$
$[651\frac{1}{2}]$
$[770\frac{1}{2}]$
$[642\frac{3}{2}]$
$[752\frac{5}{2}]$
$[761\frac{3}{2}]$
$[640\frac{1}{2}]$
118
$[505\frac{9}{2}]$
$[615\frac{11}{2}]$
$[512\frac{3}{2}]$
$[510\frac{1}{2}]$
108
$[503\frac{7}{2}]$
$[624\frac{9}{2}]$
$[514\frac{7}{2}]$
$[521\frac{1}{2}]$
$[512\frac{5}{2}]$
XBL685-2700

Fig. 5d.

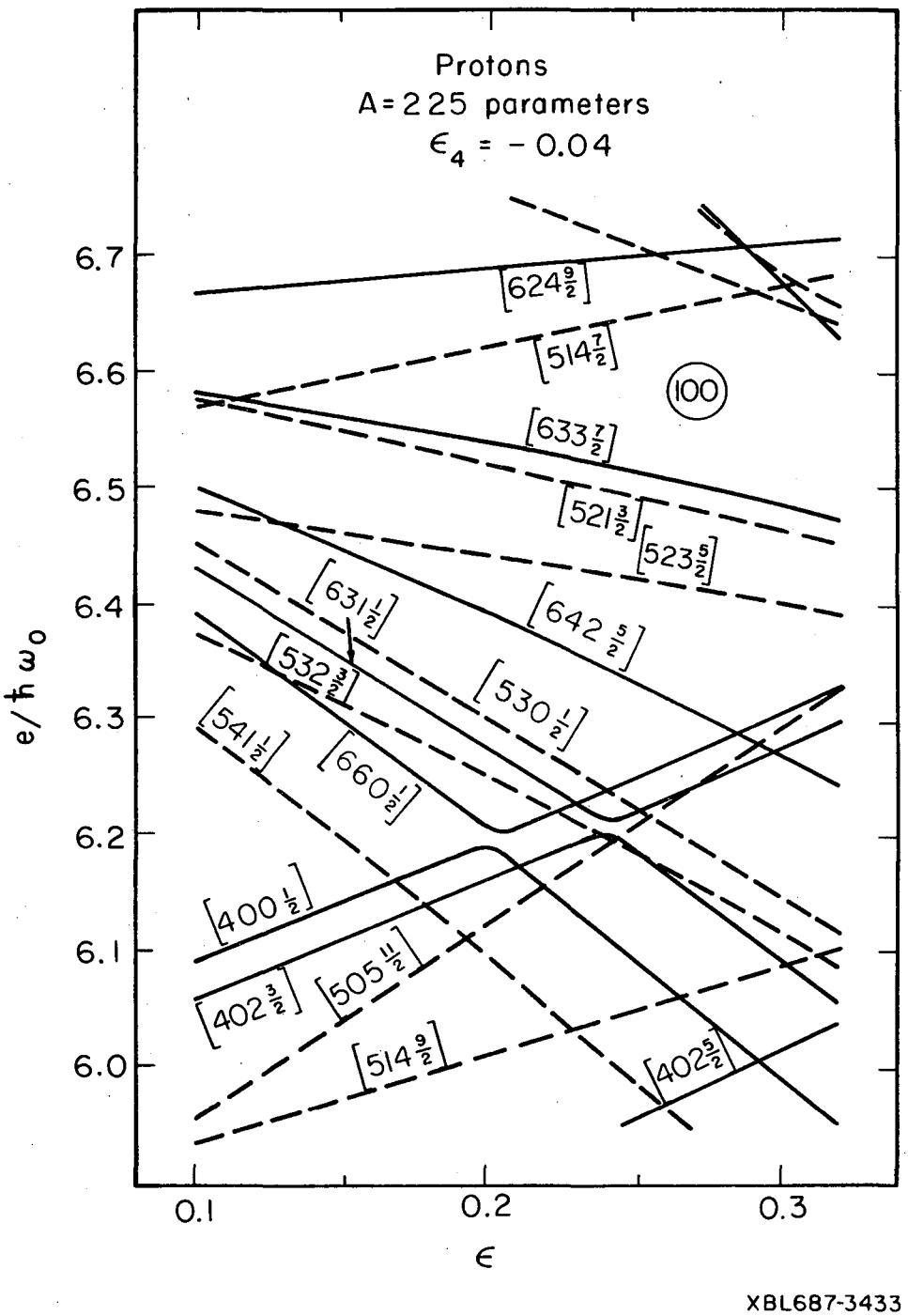
Protons
A = 225 parameters
$\epsilon_4 = -0.04$
6.7
6.6
6.5
6.4
6.3
6.2
6.1
6.0
$e/\hbar\omega_0$
0.1
0.2
0.3
ϵ
$[624\frac{9}{2}]$
$[514\frac{7}{2}]$
(100)
$[633\frac{7}{2}]$
$[521\frac{3}{2}]$
$[523\frac{5}{2}]$
$[642\frac{5}{2}]$
$[631\frac{1}{2}]$
$[532\frac{3}{2}]$
$[530\frac{1}{2}]$
$[541\frac{1}{2}]$
$[660\frac{1}{2}]$
$[400\frac{1}{2}]$
$[402\frac{3}{2}]$
$[505\frac{11}{2}]$
$[514\frac{9}{2}]$
$[402\frac{5}{2}]$
XBL687-3433

Fig. 5e.

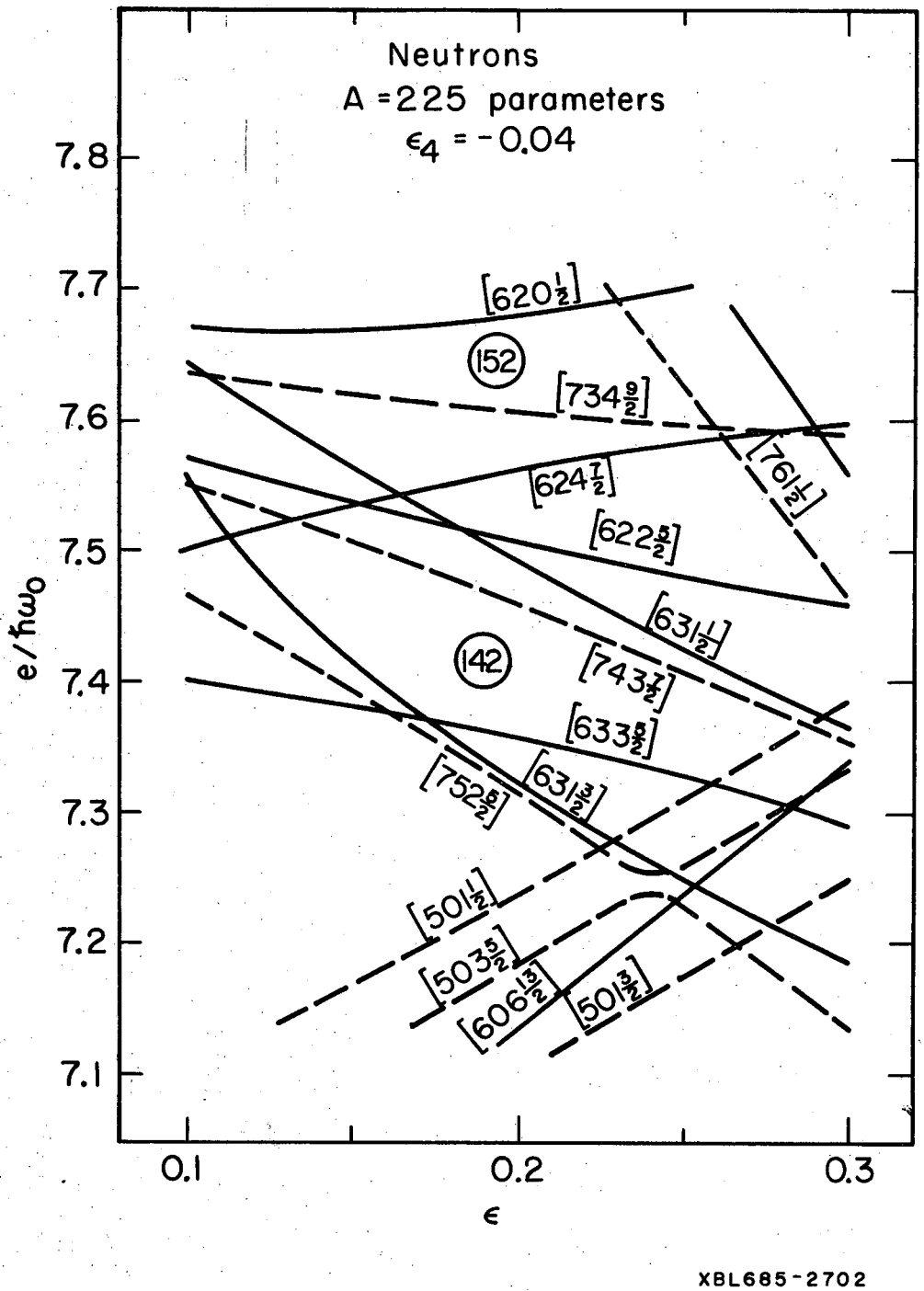
Neutrons
A = 225 parameters
$\epsilon_4 = -0.04$
7.8
7.7
7.6
7.5
7.4
7.3
7.2
7.1
$e/\hbar\omega_0$
0.1
0.2
0.3
ϵ
[620 1/2]
152
[734 9/2]
[624 7/2]
[622 5/2]
[761/2]
[631/2]
142
[743/2]
[633 5/2]
[752 5/2]
[631/2]
[501/2]
[503 5/2]
[606 13/2]
[501/2]
XBL685-2702

Fig. 5f.

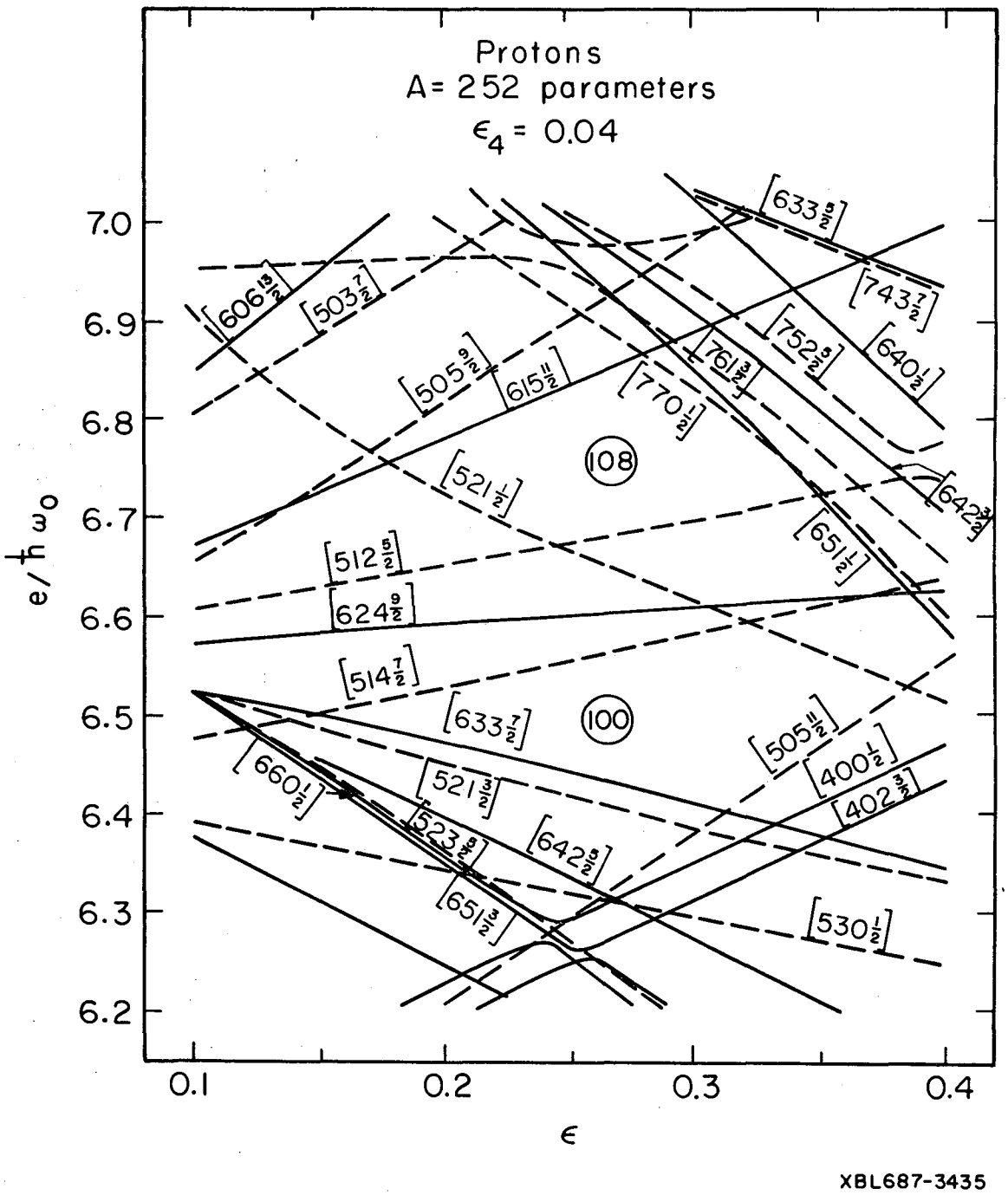
Protons
A= 252 parameters
ϵ_4 = 0.04
7.0
6.9
6.8
6.7
6.6
6.5
6.4
6.3
6.2
$e/\hbar\omega_0$
0.1
0.2
0.3
0.4
ϵ
$[606\frac{13}{2}]$
$[503\frac{7}{2}]$
$[505\frac{9}{2}]$
$[615\frac{11}{2}]$
$[770\frac{1}{2}]$
$[633\frac{5}{2}]$
$[743\frac{1}{2}]$
$[752\frac{3}{2}]$
$[761\frac{3}{2}]$
$[640\frac{1}{2}]$
108
$[521\frac{1}{2}]$
$[642\frac{3}{2}]$
$[651\frac{1}{2}]$
$[512\frac{5}{2}]$
$[624\frac{9}{2}]$
$[514\frac{7}{2}]$
$[633\frac{7}{2}]$
100
$[505\frac{11}{2}]$
$[400\frac{1}{2}]$
$[402\frac{3}{2}]$
$[660\frac{1}{2}]$
$[521\frac{3}{2}]$
$[523\frac{5}{2}]$
$[642\frac{5}{2}]$
$[651\frac{3}{2}]$
$[530\frac{1}{2}]$
XBL687-3435

Fig. 5g.

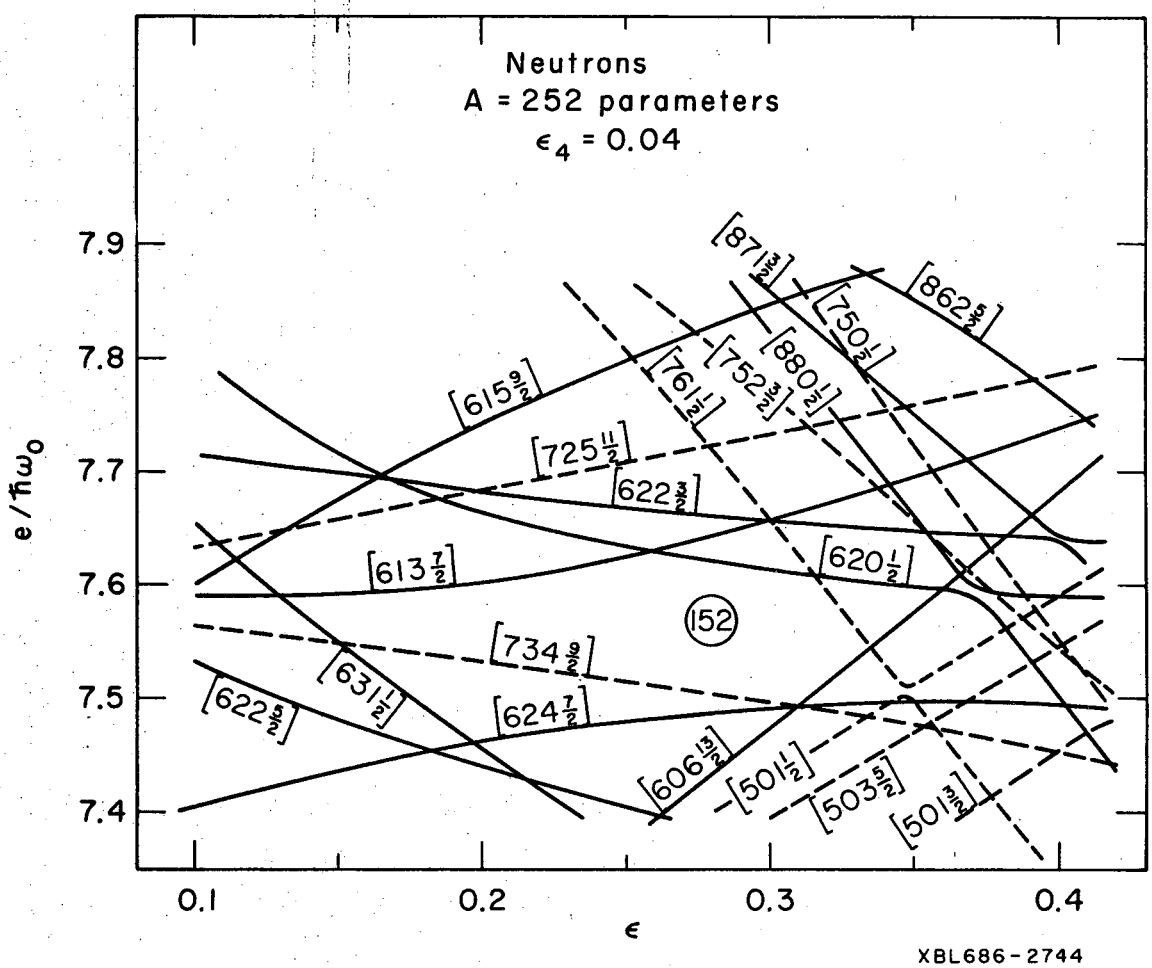
Neutrons
A = 252 parameters
ϵ_4 = 0.04
7.9
7.8
7.7
7.6
7.5
7.4
$e/\hbar\omega_0$
0.1
0.2
0.3
0.4
ϵ
[615 9/2]
[725 11/2]
[622 3/2]
[613 7/2]
[620 1/2]
(152)
[734 9/2]
[631 1/2]
[622 5/2]
[624 7/2]
[606 13/2]
[501/2]
[503 5/2]
[501 3/2]
[862 5/2]
[750 1/2]
[880 1/2]
[752 5/2]
[761/2]
XBL686-2744

Fig. 5h.

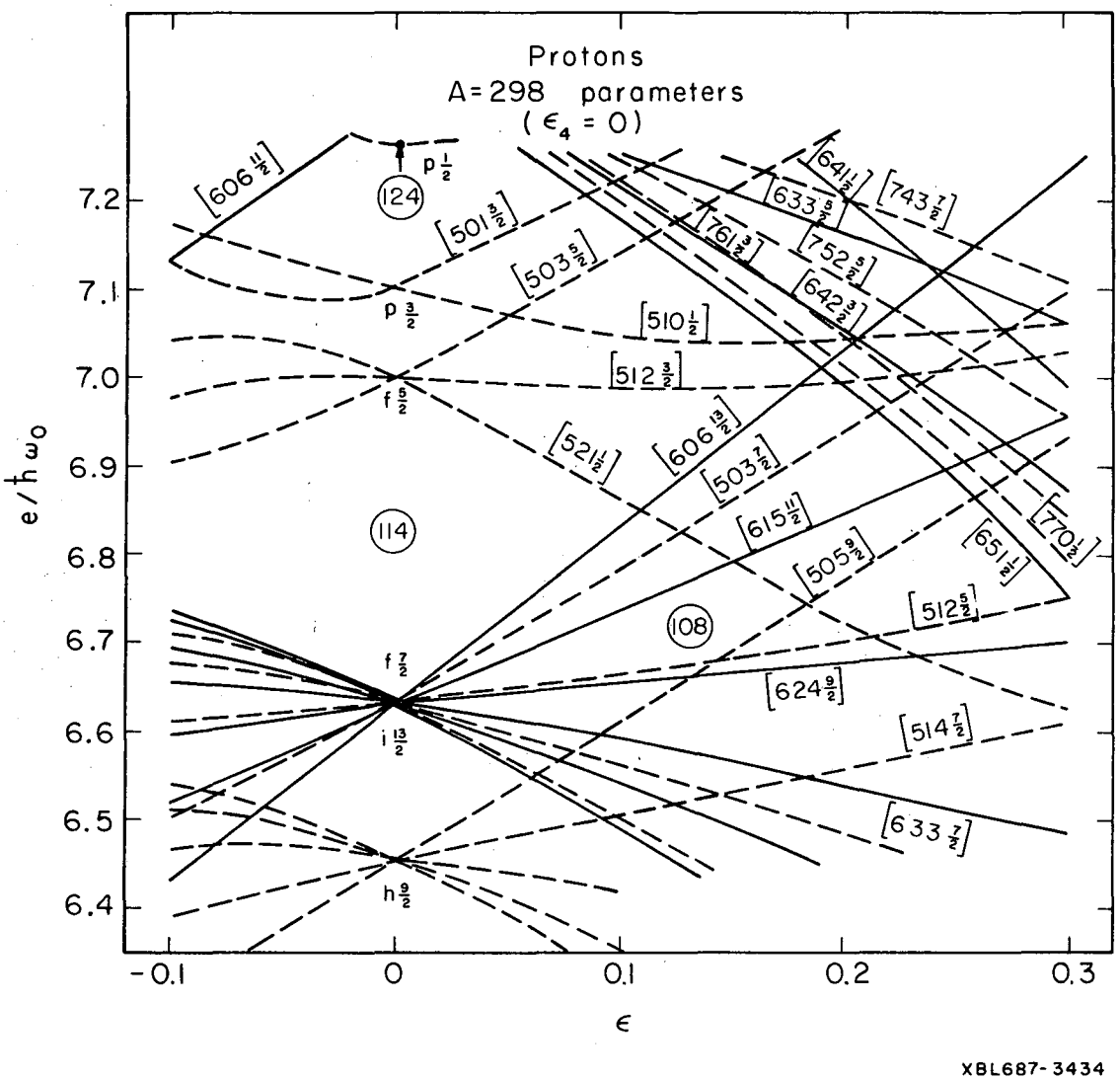
Protons
A=298 parameters
(ϵ_4 = 0)
$e/\hbar\omega_0$
ϵ
7.2
7.1
7.0
6.9
6.8
6.7
6.6
6.5
6.4
-0.1
0
0.1
0.2
0.3
[606 11/2]
p 1/2
124
[501 1/2]
[503 1/2]
p 3/2
[510 1/2]
[512 3/2]
f 5/2
[521 1/2]
[606 13/2]
[503 7/2]
114
[615 11/2]
[505 9/2]
[651 13/2]
[770 1/2]
108
[512 5/2]
f 7/2
[624 9/2]
i 13/2
[514 7/2]
[633 7/2]
h 9/2
[641 1/2]
[633 5/2]
[743 1/2]
[761 3/2]
[752 5/2]
[642 3/2]
XBL687-3434

Fig. 5i.

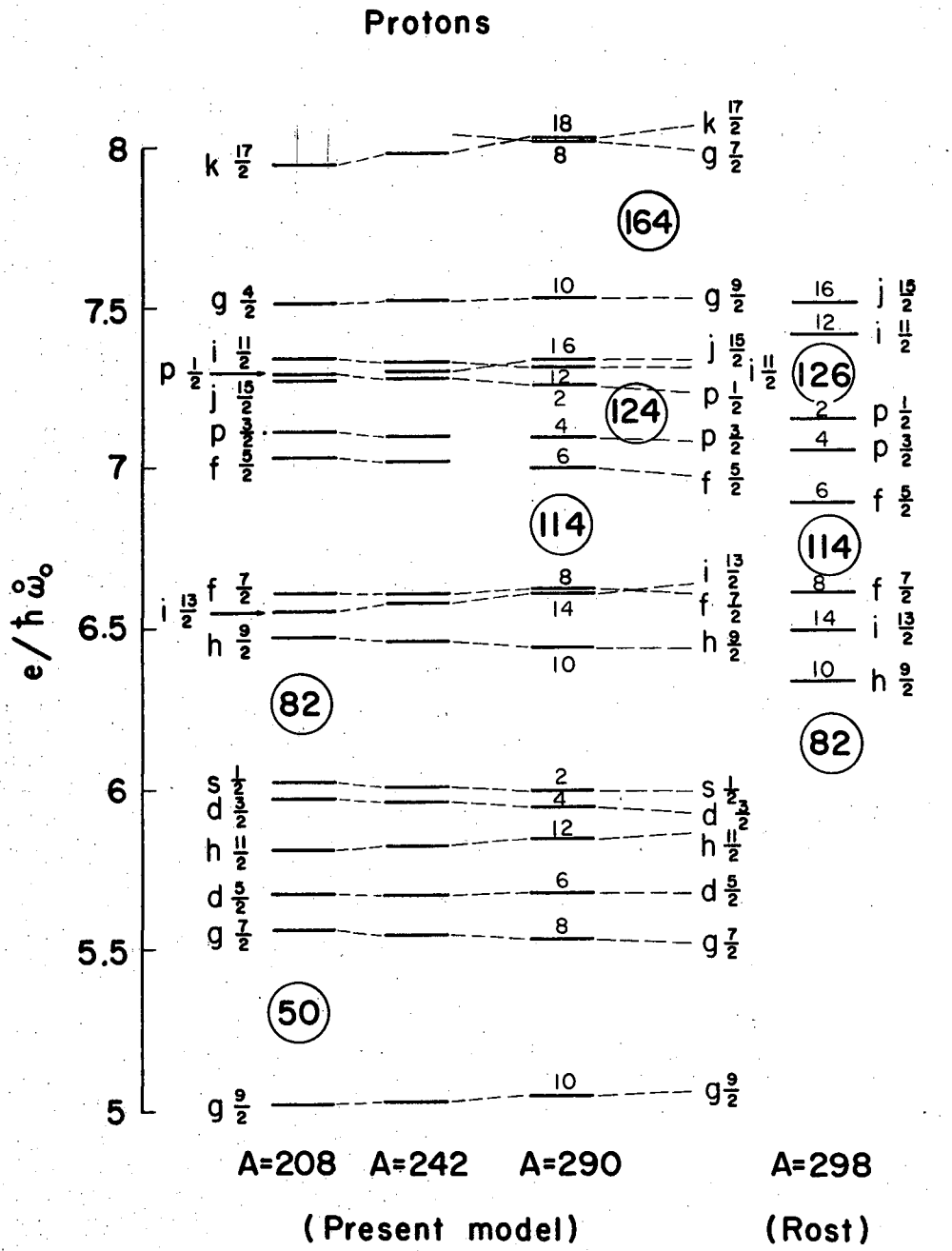
Protons
e/ħω₀
8
7.5
7
6.5
6
5.5
5
k 17/2
g 4/2
i 11/2
p 1/2
j 15/2
p 3/2
f 5/2
f 7/2
i 13/2
h 9/2
s 1/2
d 3/2
h 11/2
d 5/2
g 7/2
g 9/2
164
126
124
114
82
50
A=208
A=242
A=290
A=298
(Present model)
(Rost)
XBL682-1807

Fig. 6a.

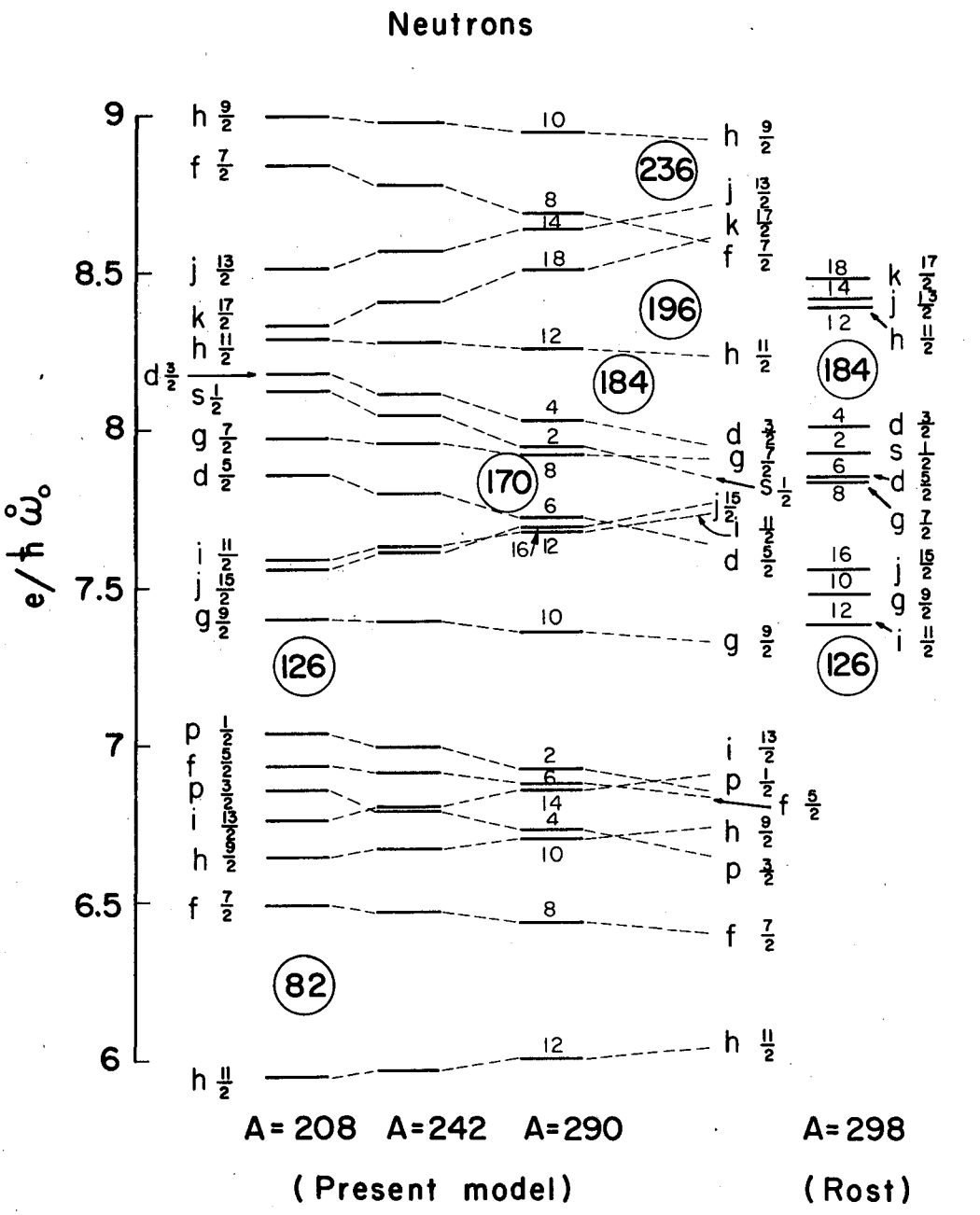
Neutrons
e/ħω₀
9
8.5
8
7.5
7
6.5
6
236
196
184
170
126
82
A= 208 A=242 A=290
A=298
(Present model)
(Rost)
XBL682-1808

Fig. 6b.

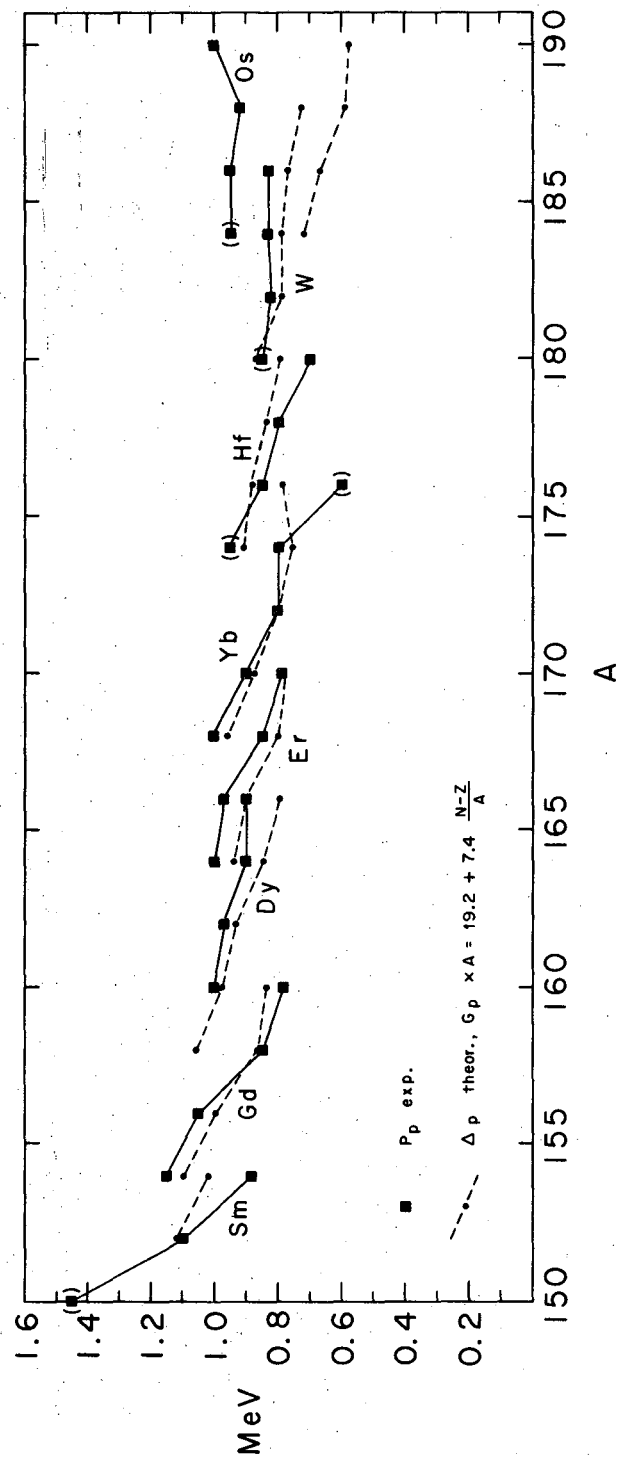
Os
W
Hf
Yb
Er
Dy
Gd
Sm
P_p exp.
Δ_p theor., $G_p \times A = 19.2 + 7.4 \frac{N-Z}{A}$
MeV
A
XBL 688-3504

Fig. 7a.

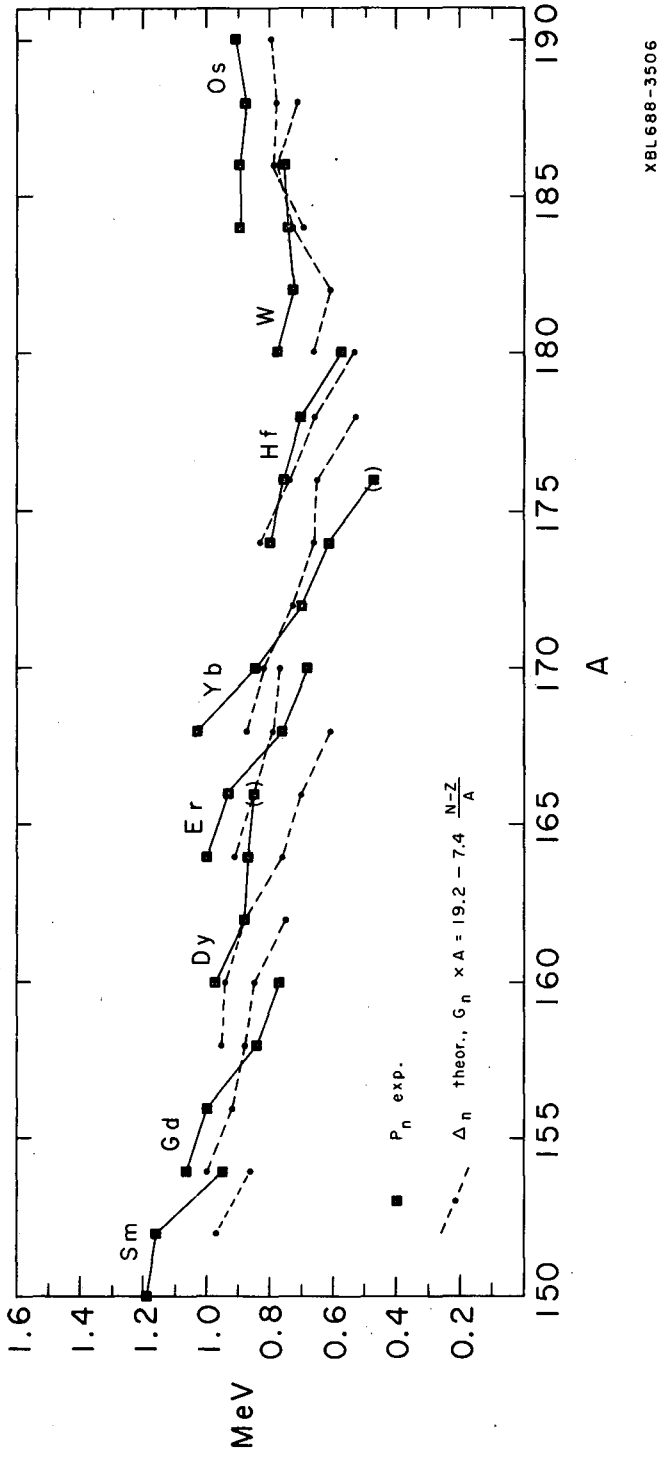
Os
W
Hf
Yb
Er
Dy
Gd
Sm
(a)
(b)
P_n exp.
Δ_n theor., G_n $\times A = 19.2 - 7.4\ \frac{N-Z}{A}$
MeV
A
XBL688-3506

Fig. 7b.

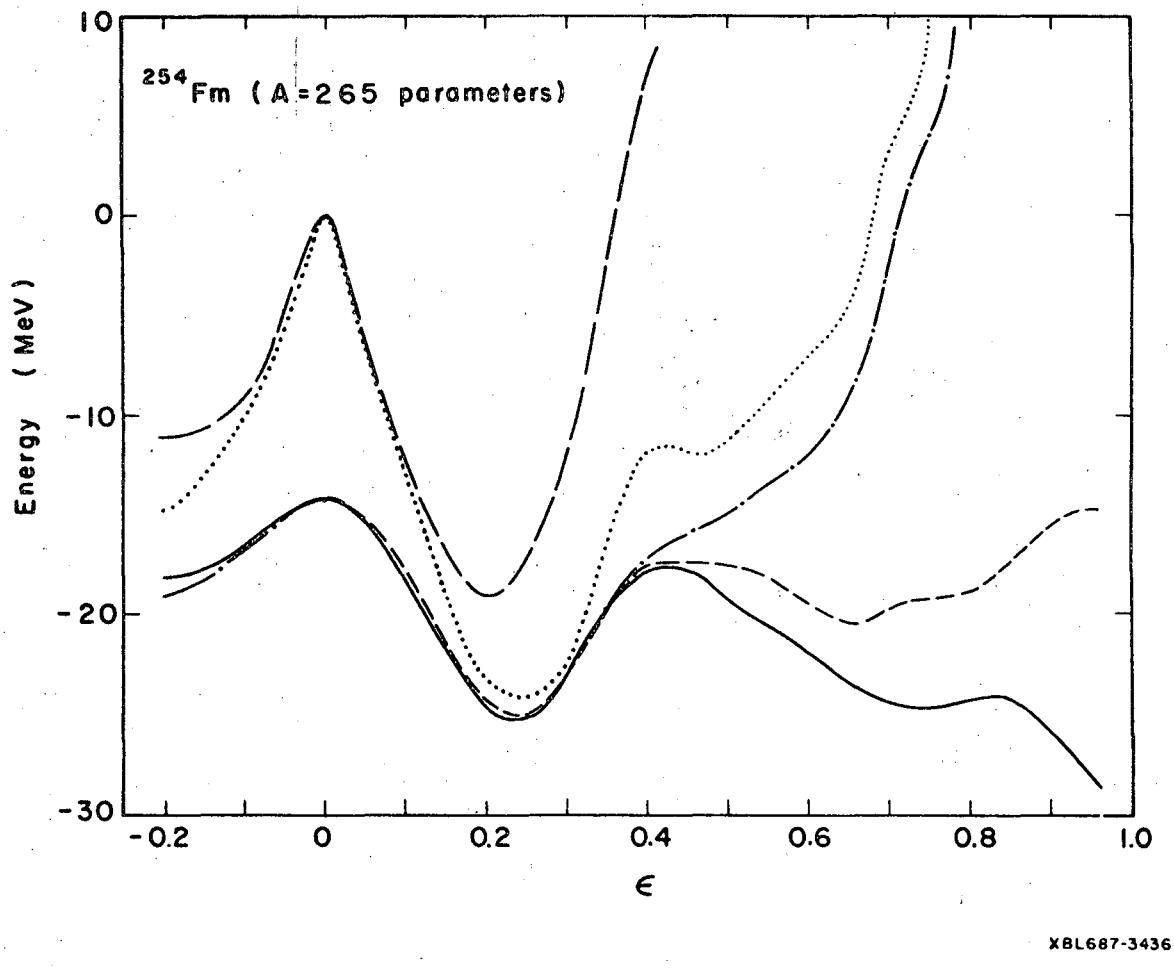
^{254}Fm (A = 265 parameters)
Energy (MeV)
10
0
-10
-20
-30
-0.2
0
0.2
0.4
0.6
0.8
1.0
ϵ
XBL687-3436

Fig. 8.

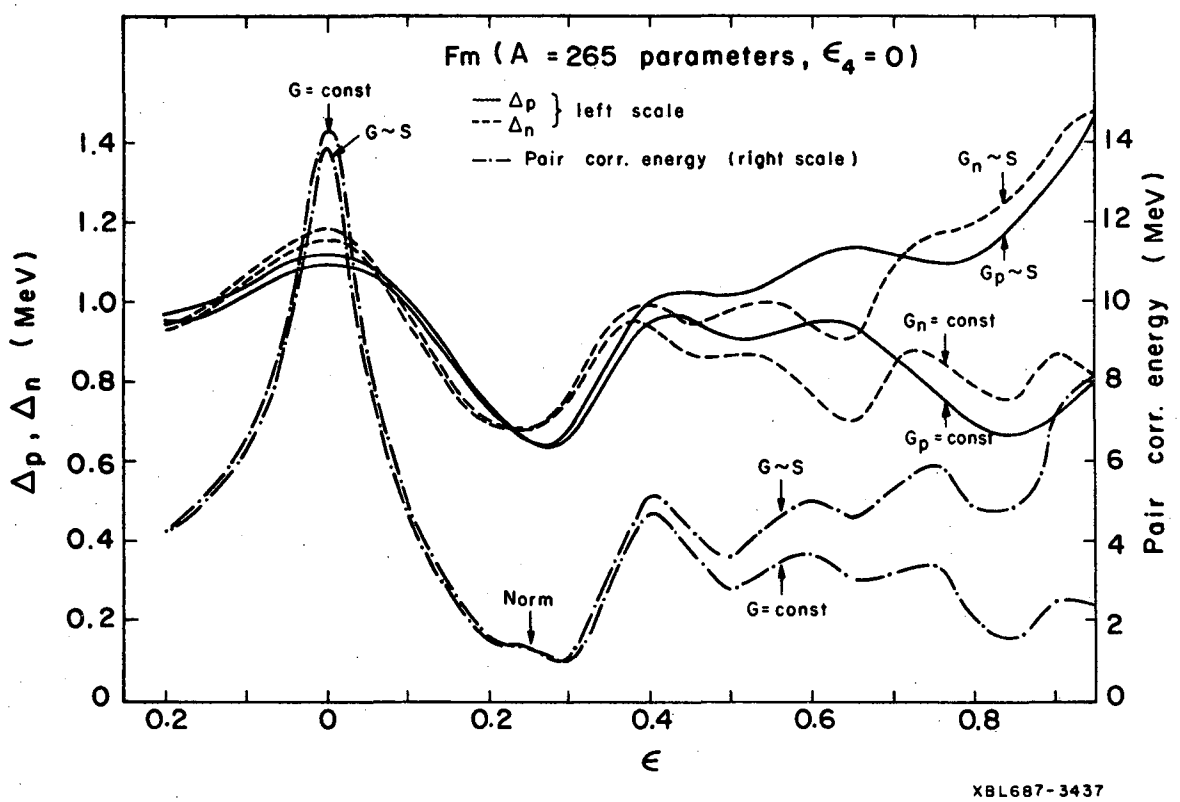
Fm (A = 265 parameters, $\epsilon_4 = 0$)
G = const
G~S
Δ_p
Δ_n
} left scale
Pair corr. energy (right scale)
$G_n \sim S$
$G_p \sim S$
G_n = const
G_p = const
G~S
G= const
Norm
Δ_p, Δ_n (MeV)
Pair corr. energy (MeV)
ϵ
XBL687-3437

Fig. 9.

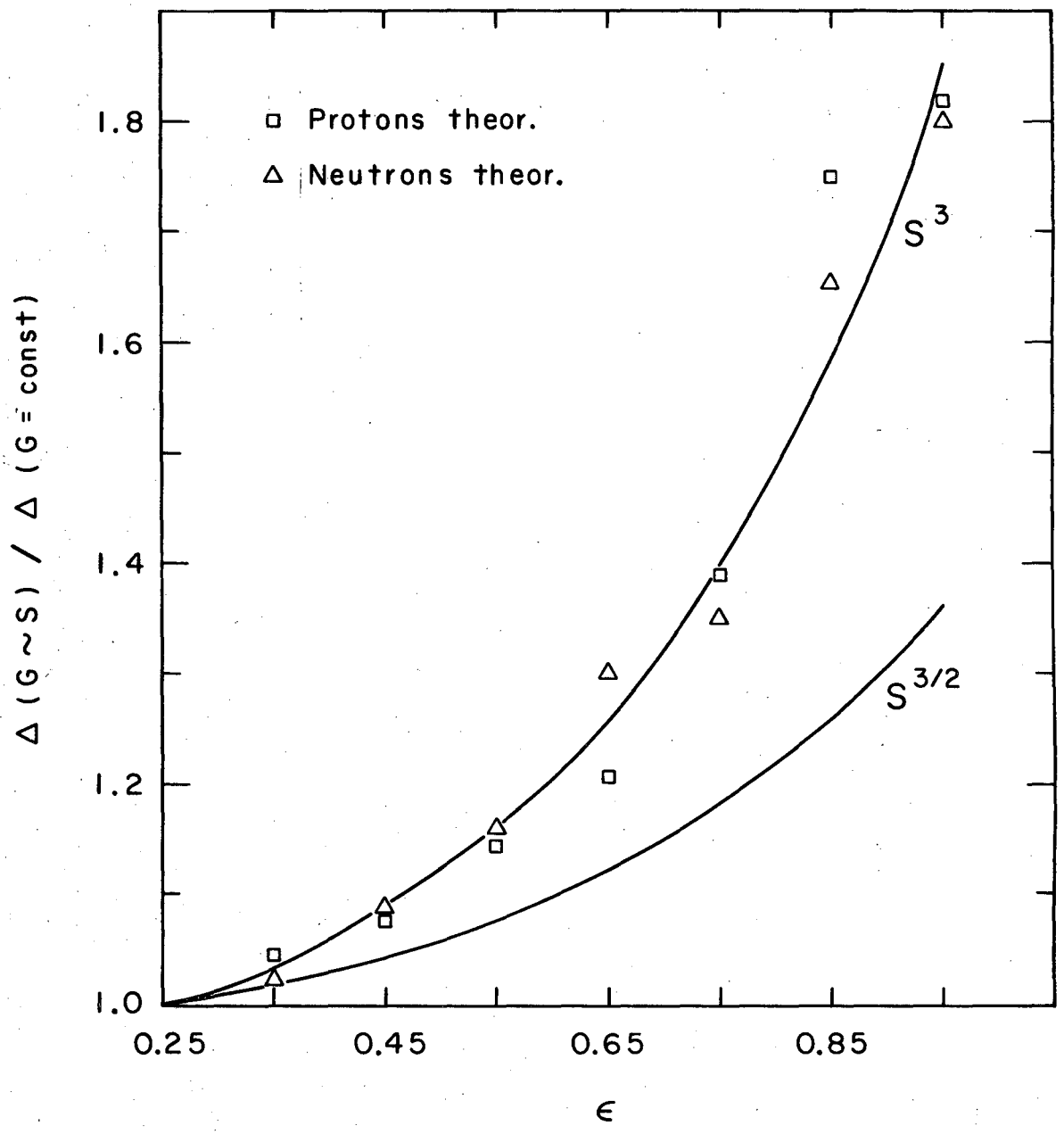
Protons theor.
Neutrons theor.
S^3
$S^{3/2}$
$\Delta (G \sim S) / \Delta (G = \text{const})$
1.8
1.6
1.4
1.2
1.0
0.25
0.45
0.65
0.85
ϵ
XBL688-3507

Fig. 10.

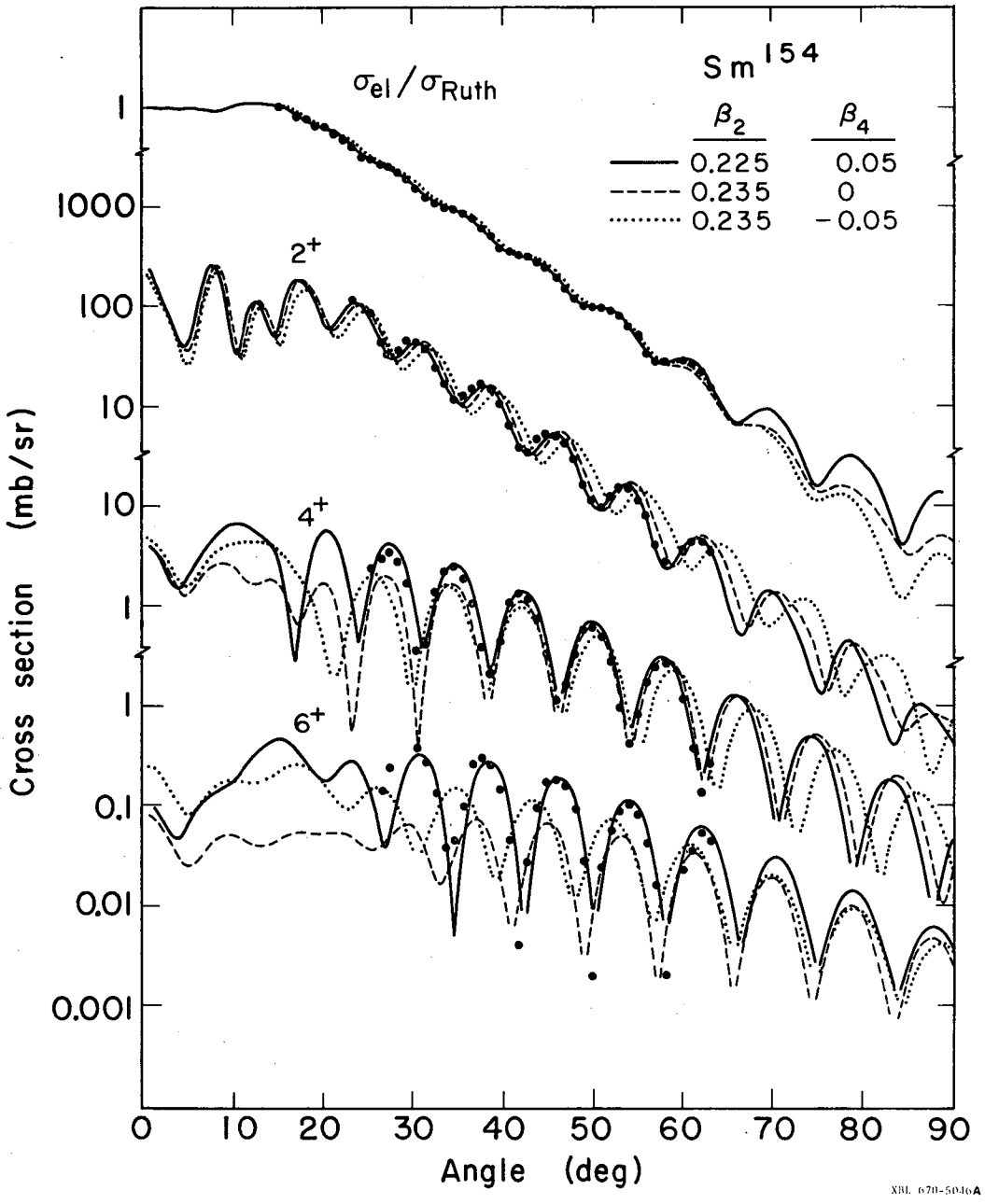
Sm 154
σel / σRuth
β2 β4
0.225 0.05
0.235 0
0.235 −0.05
2+
4+
6+
Cross section (mb/sr)
Angle (deg)
XBL 670-5046A

Fig. 11.

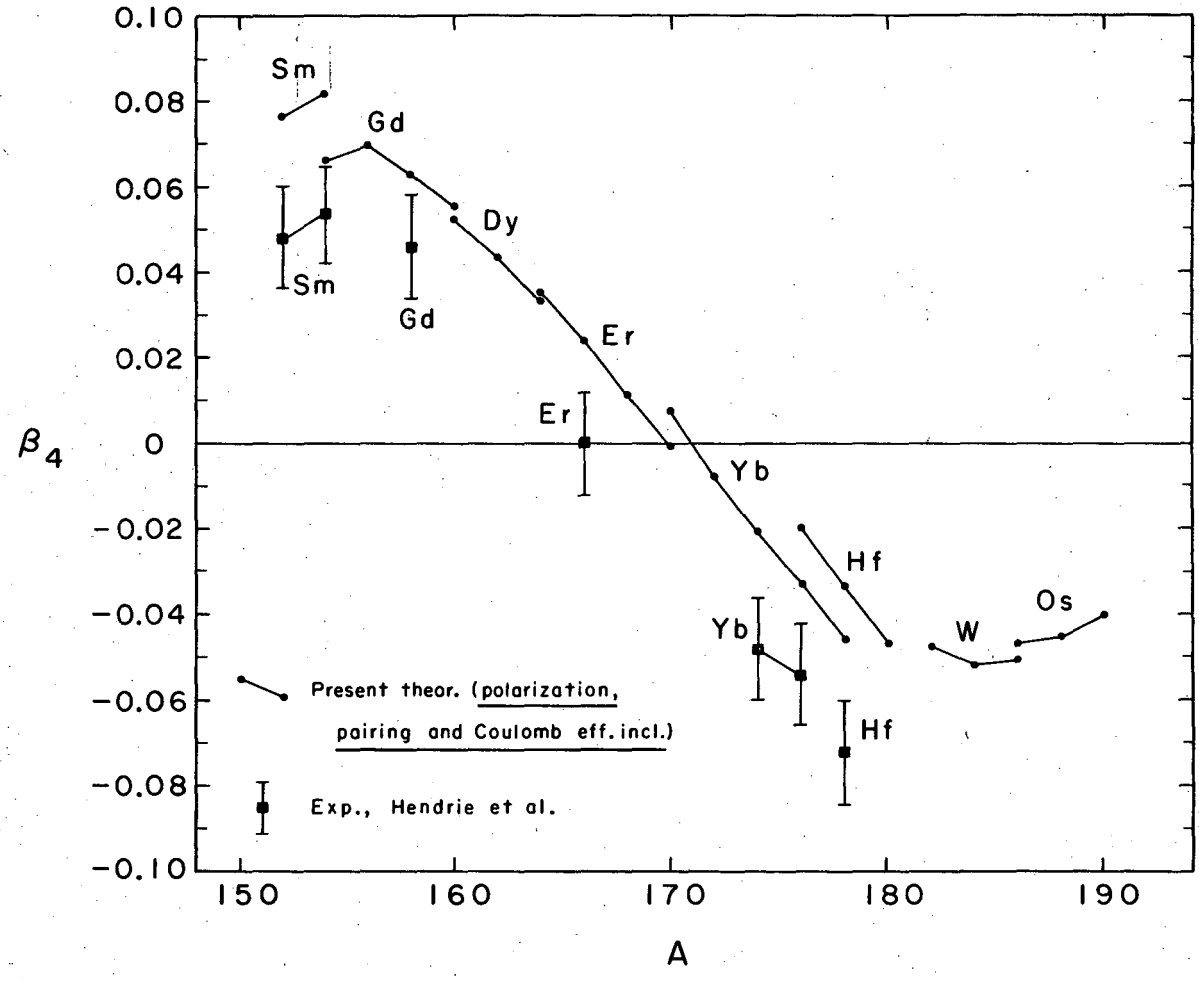
0.10
0.08
0.06
0.04
0.02
0
-0.02
-0.04
-0.06
-0.08
-0.10
β_4
150
160
170
180
190
A
Sm
Gd
Dy
Er
Yb
Hf
W
Os
Sm
Gd
Er
Yb
Hf
Present theor. (polarization, pairing and Coulomb eff. incl.)
Exp., Hendrie et al.
XBL688-3505

Fig. 12.

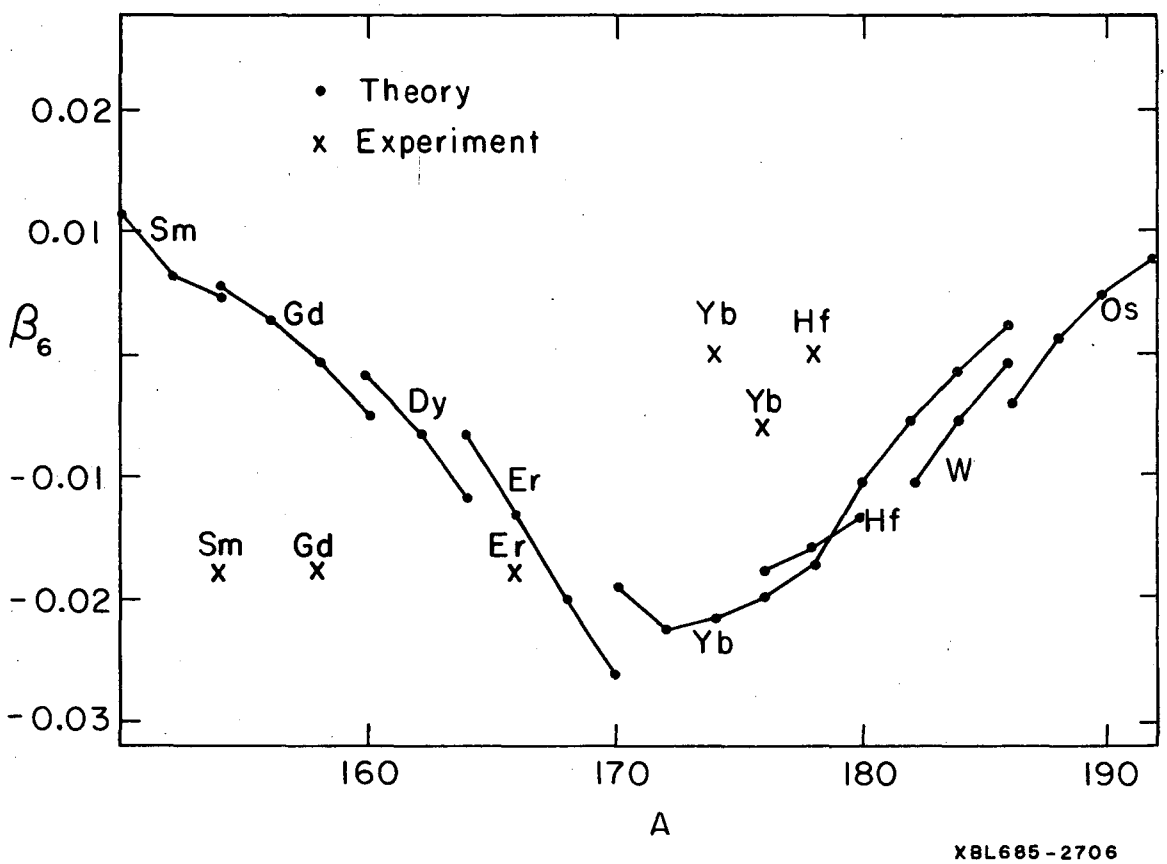
• Theory
x Experiment
0.02
0.01
-0.01
-0.02
-0.03
β_6
Sm
Gd
Dy
Er
Yb
Hf
Yb
Os
W
Hf
Yb
Sm
Gd
Er
160
170
180
190
A
XBL685-2706

Fig. 13.

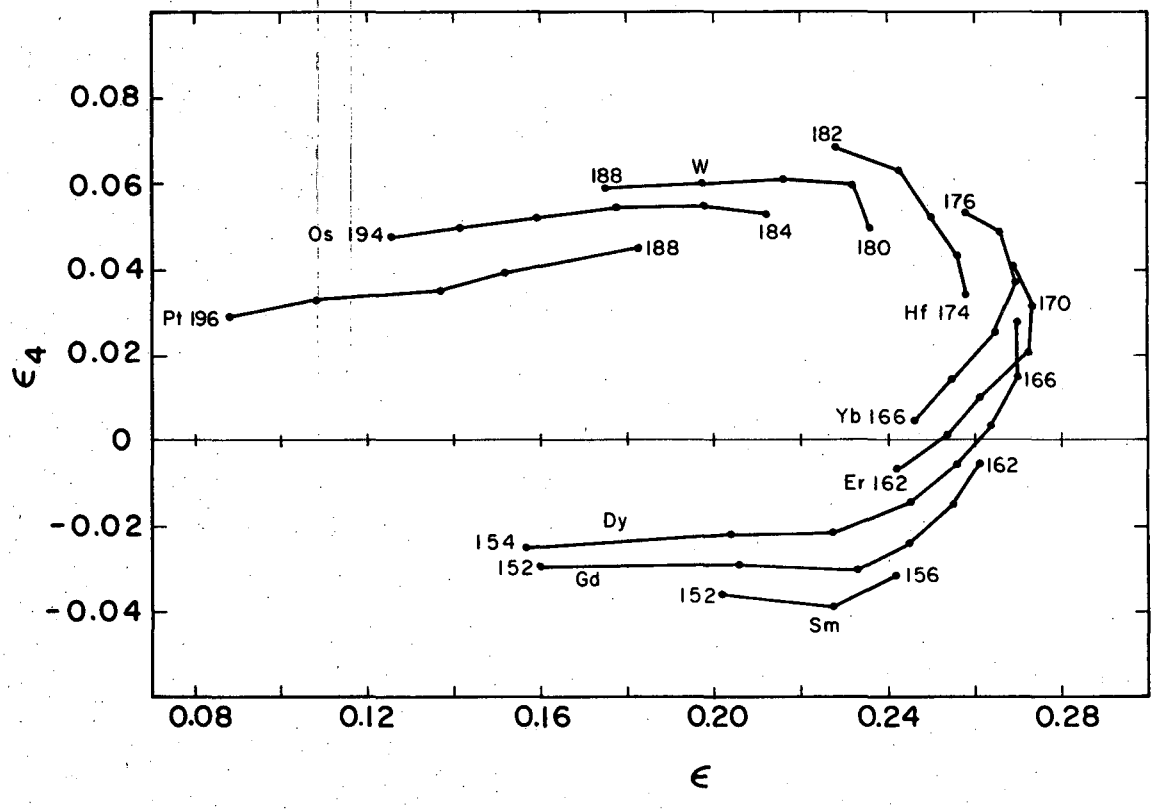
0.08
0.06
0.04
0.02
0
-0.02
-0.04
ϵ_4
0.08
0.12
0.16
0.20
0.24
0.28
ϵ
182
W
188
176
Os 194
184
180
188
Hf 174
Pt 196
170
166
Yb 166
Er 162
162
Dy
154
152
Gd
156
152
Sm
XBL687-3439

Fig. 14a.

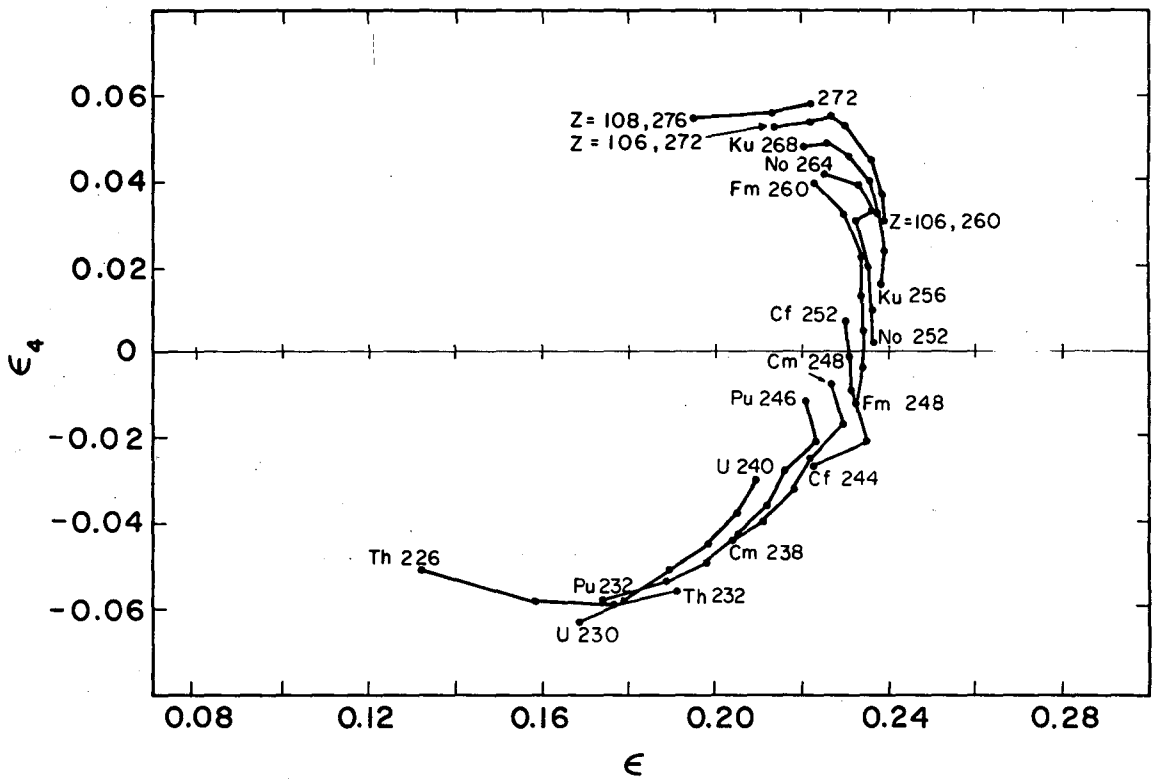
0.06
0.04
0.02
0
-0.02
-0.04
-0.06
ϵ_4
0.08
0.12
0.16
0.20
0.24
0.28
ϵ
Z= 108,276
Z = 106,272
272
Ku 268
No 264
Fm 260
Z=106,260
Ku 256
Cf 252
No 252
Cm 248
Fm 248
Pu 246
U 240
Cf 244
Cm 238
Th 226
Pu 232
Th 232
U 230
XBL687-3438

Fig. 14b.

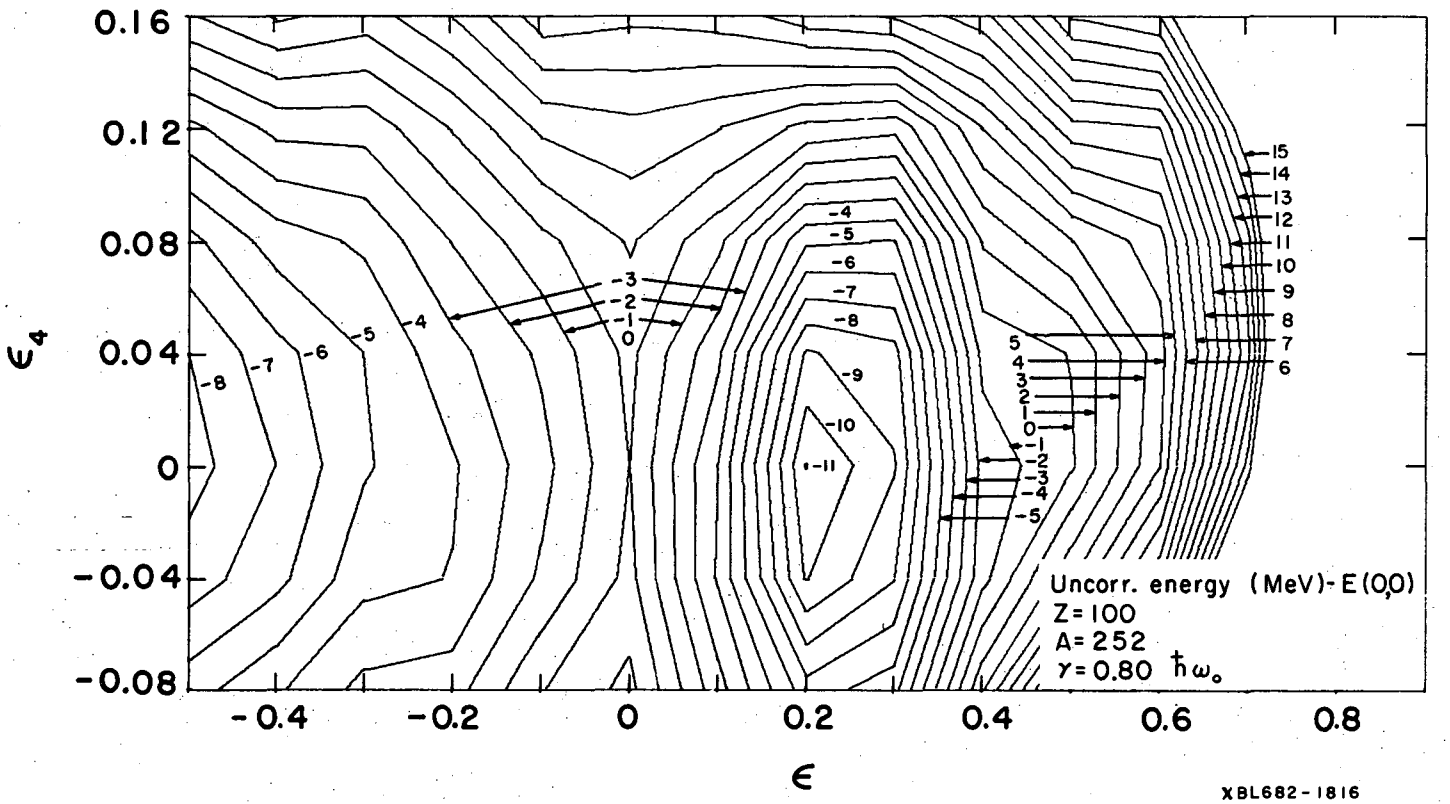
0.16
0.12
0.08
0.04
0
-0.04
-0.08
ϵ_4
-0.4
-0.2
0
0.2
0.4
0.6
0.8
ϵ
Uncorr. energy (MeV)- E(0,0)
Z= 100
A= 252
γ= 0.80 $\hbar\omega_0$
XBL682-1816

Fig. 15.

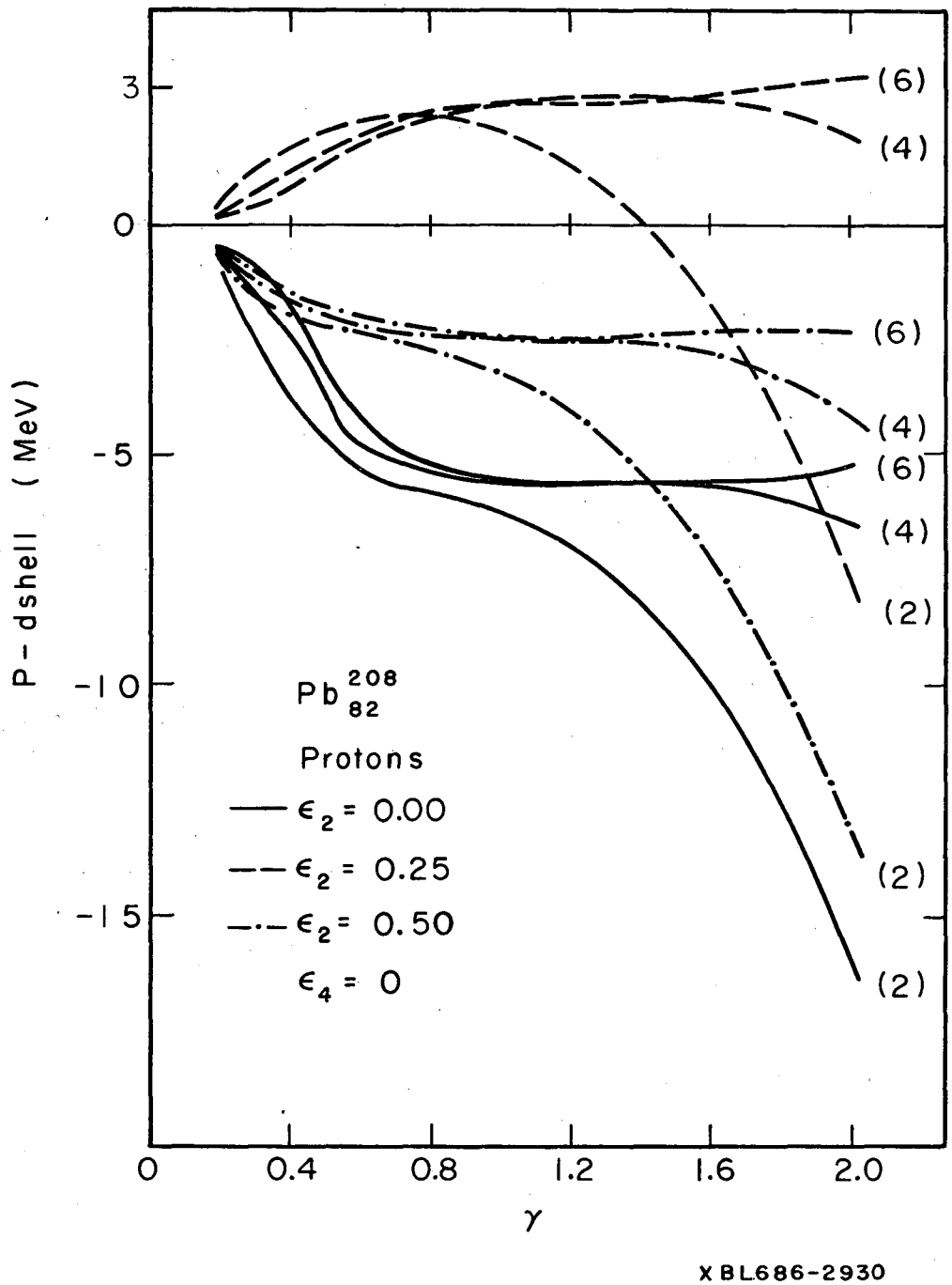
3
0
-5
-10
-15
P-dshell (MeV)
0
0.4
0.8
1.2
1.6
2.0
γ
(6)
(4)
(6)
(4)
(6)
(4)
(2)
(2)
(2)
Pb 208 82
Protons
ε2 = 0.00
ε2 = 0.25
ε2 = 0.50
ε4 = 0
XBL686-2930

Fig. 16.

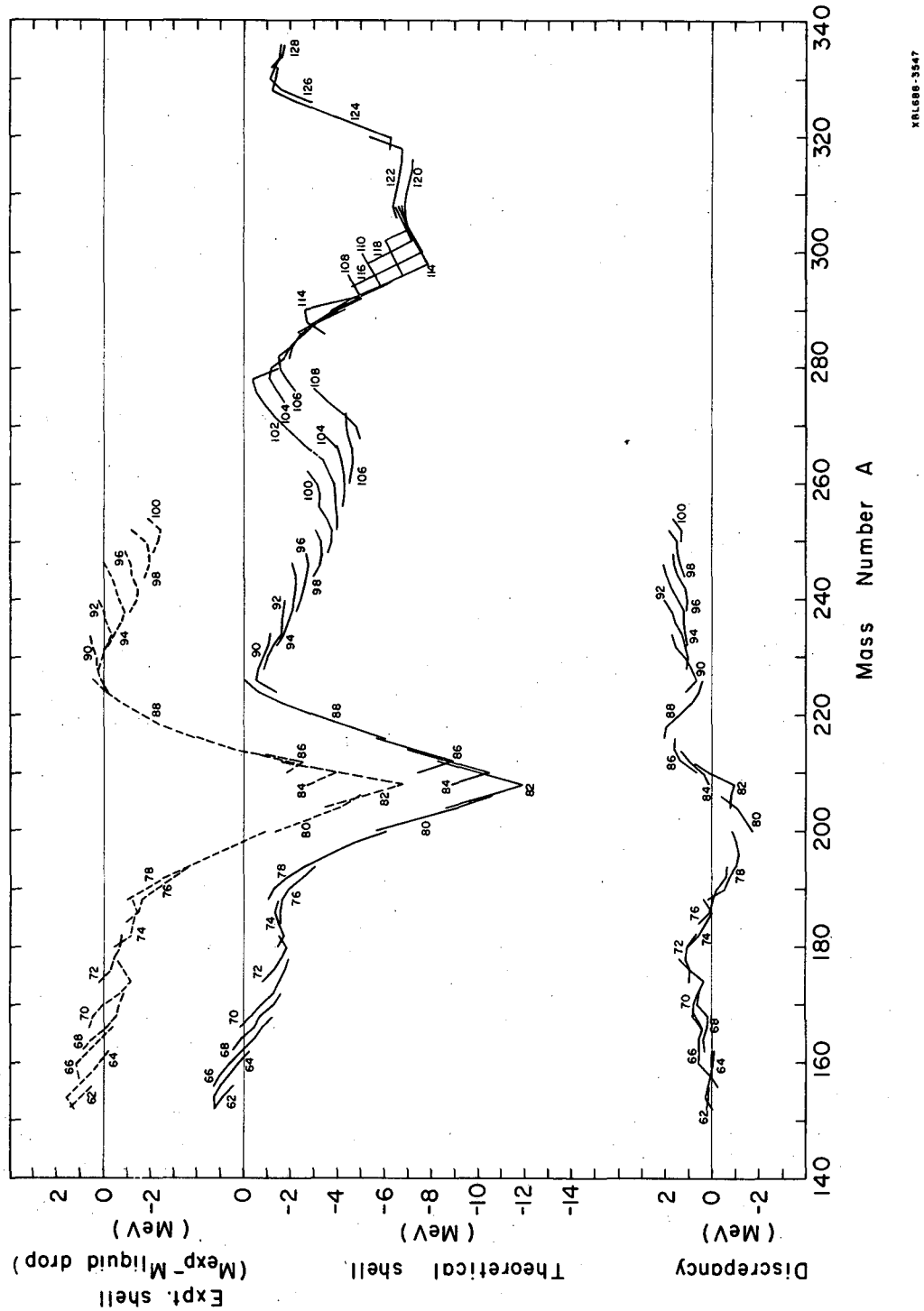
Expt. shell
(Mexp-Mliquid drop)
(MeV)
Theoretical shell
(MeV)
Discrepancy
(MeV)
Mass Number A
XBL688-3547

Fig. 17

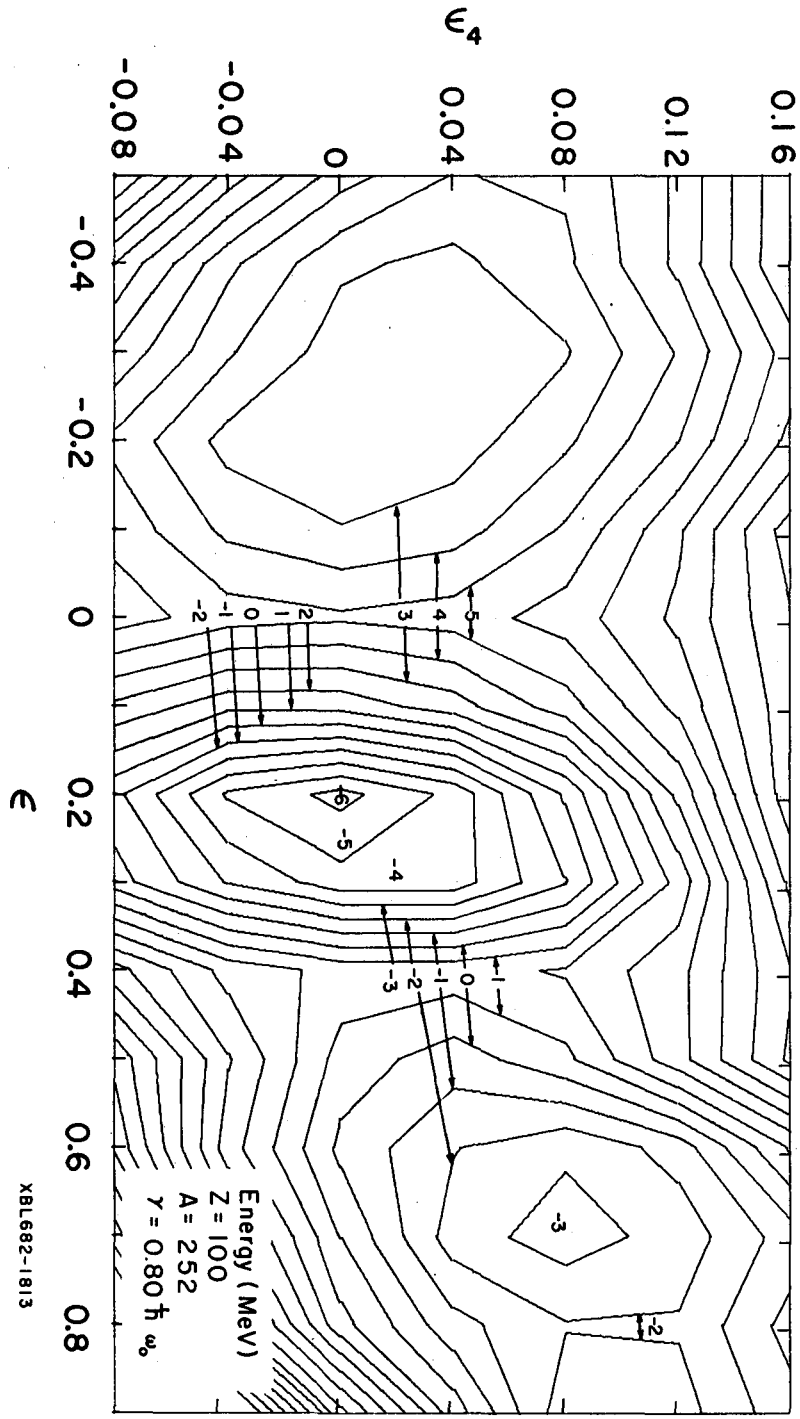
ϵ_4
0.16
0.12
0.08
0.04
0
-0.04
-0.08
ϵ
-0.4
-0.2
0
0.2
0.4
0.6
0.8
Energy (MeV)
Z = 100
A = 252
γ = 0.80 ħ ω₀
XBL682-1813

Fig. 18a.

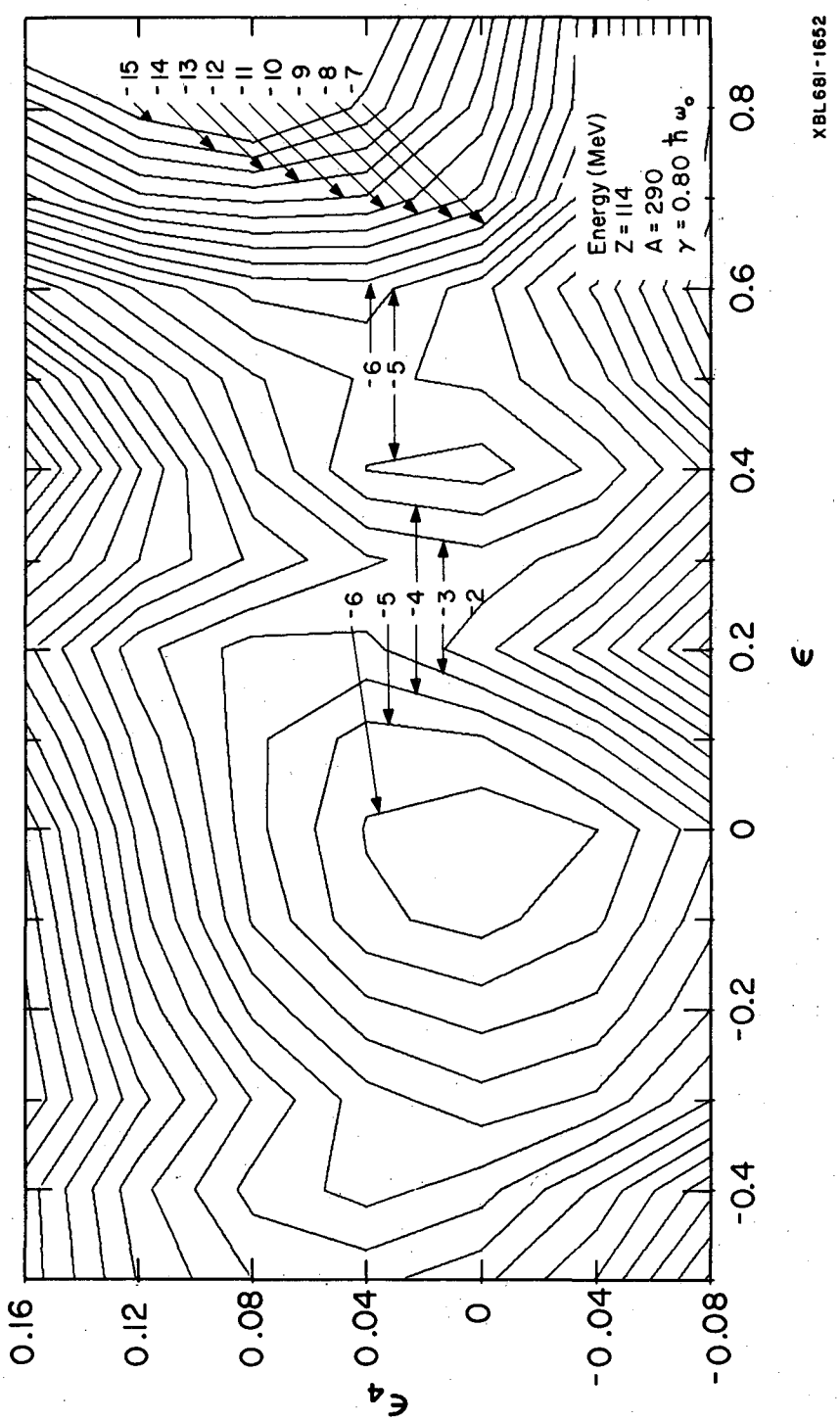
Energy (MeV)
Z = 114
A = 290
γ = 0.80 ħω₀
-15
-14
-13
-12
-11
-10
-9
-8
-7
-6
-5
-6
-5
-4
-3
-2
0.16
0.12
0.08
0.04
0
-0.04
-0.08
ε₄
0.8
0.6
0.4
0.2
0
-0.2
-0.4
ε
XBL681-1652

Fig. 18b.

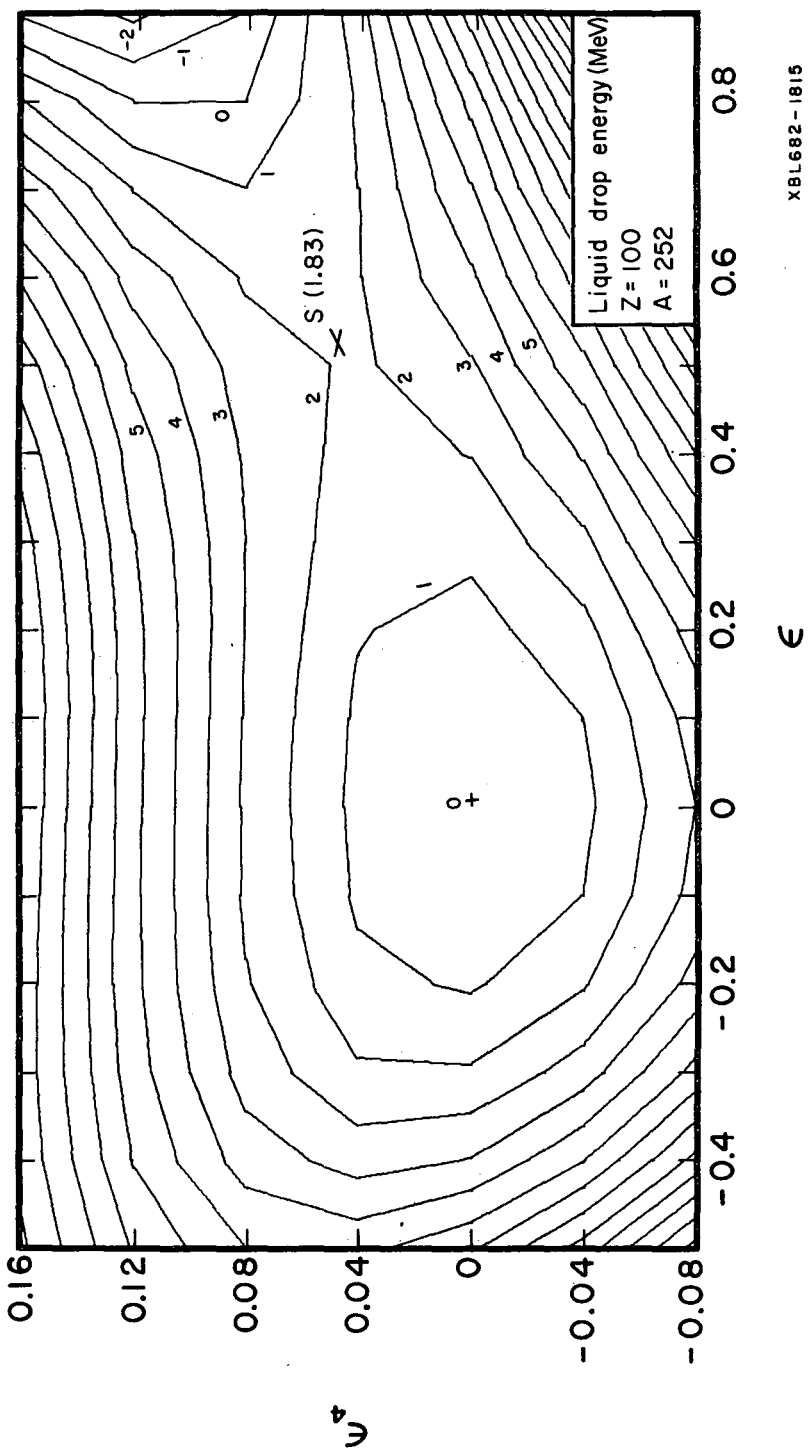
Liquid drop energy (MeV)
Z = 100
A = 252
S (1.83)
0.16
0.12
0.08
0.04
0
-0.04
-0.08
0.8
0.6
0.4
0.2
0
-0.2
-0.4
ϵ_4
ϵ
XBL682-1815

Fig. 19a.

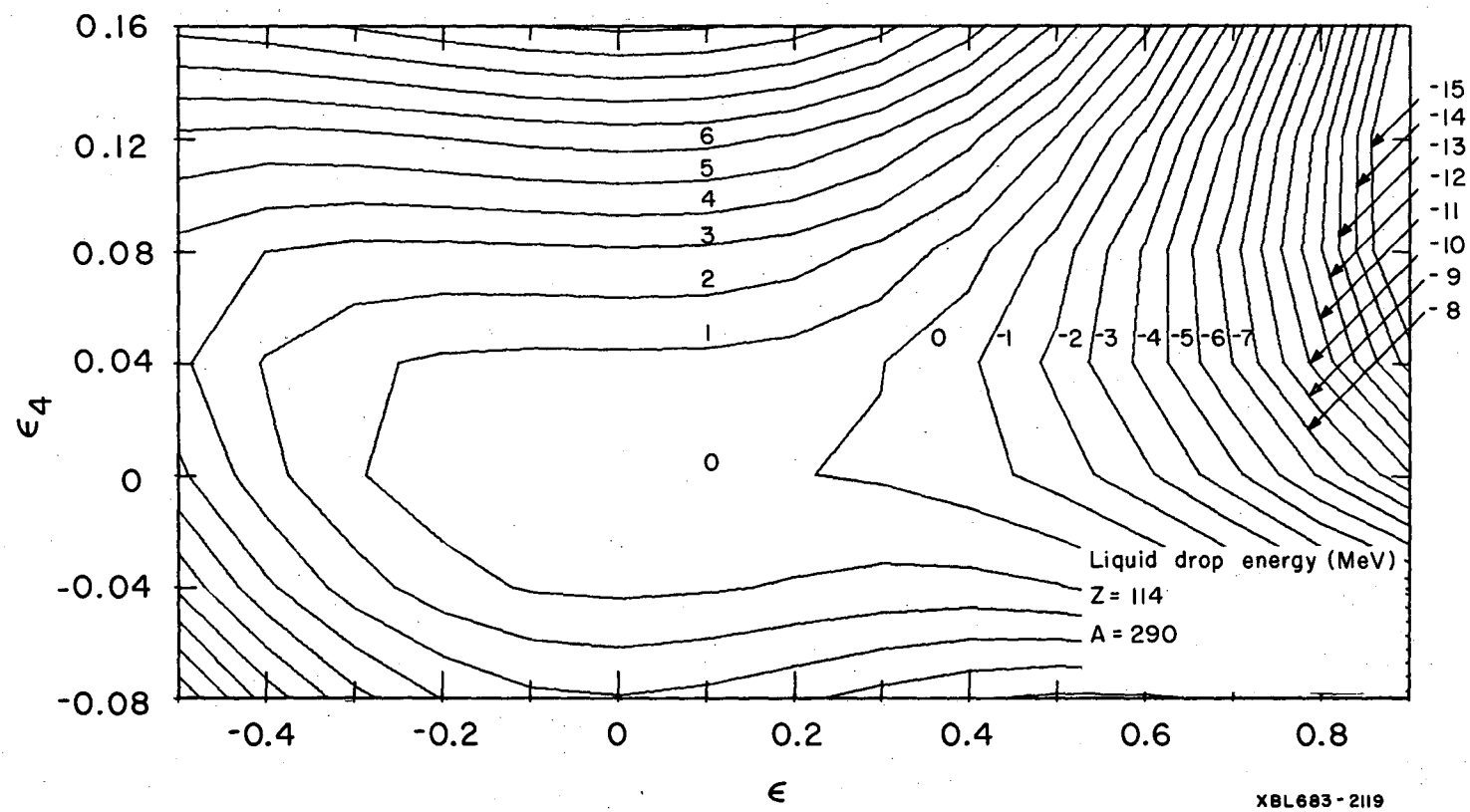
0.16
0.12
0.08
0.04
0
-0.04
-0.08
ϵ_4
-0.4
-0.2
0
0.2
0.4
0.6
0.8
ϵ
6
5
4
3
2
1
0
0
-1
-2
-3
-4
-5
-6
-7
-15
-14
-13
-12
-11
-10
-9
-8
Liquid drop energy (MeV)
Z = 114
A = 290
XBL683-2119

Fig. 19b.

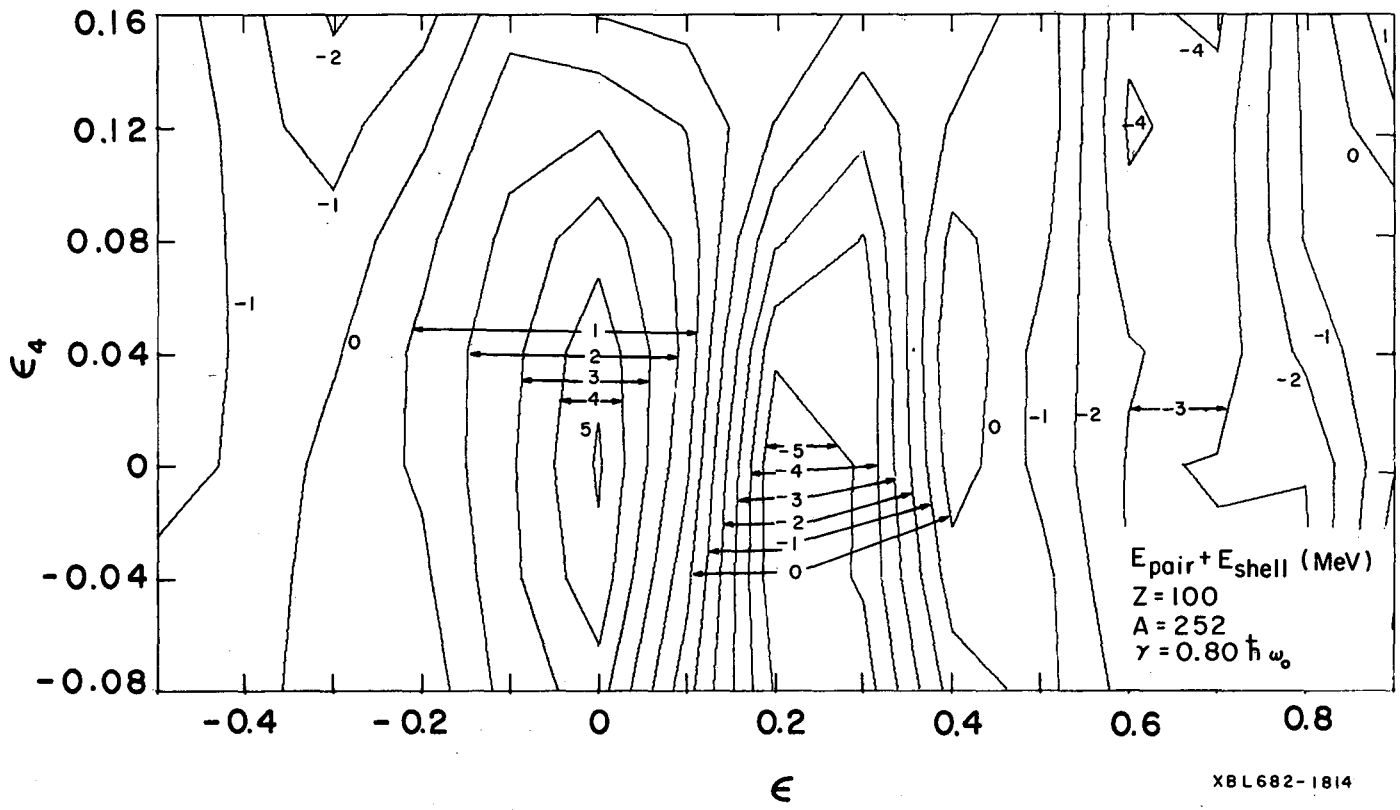
0.16
0.12
0.08
0.04
0
-0.04
-0.08
ϵ_4
-0.4
-0.2
0
0.2
0.4
0.6
0.8
ϵ
$E_{pair} + E_{shell}$ (MeV)
Z = 100
A = 252
$\gamma = 0.80\ \hbar\omega_0$
XBL682-1814

Fig. 20a.

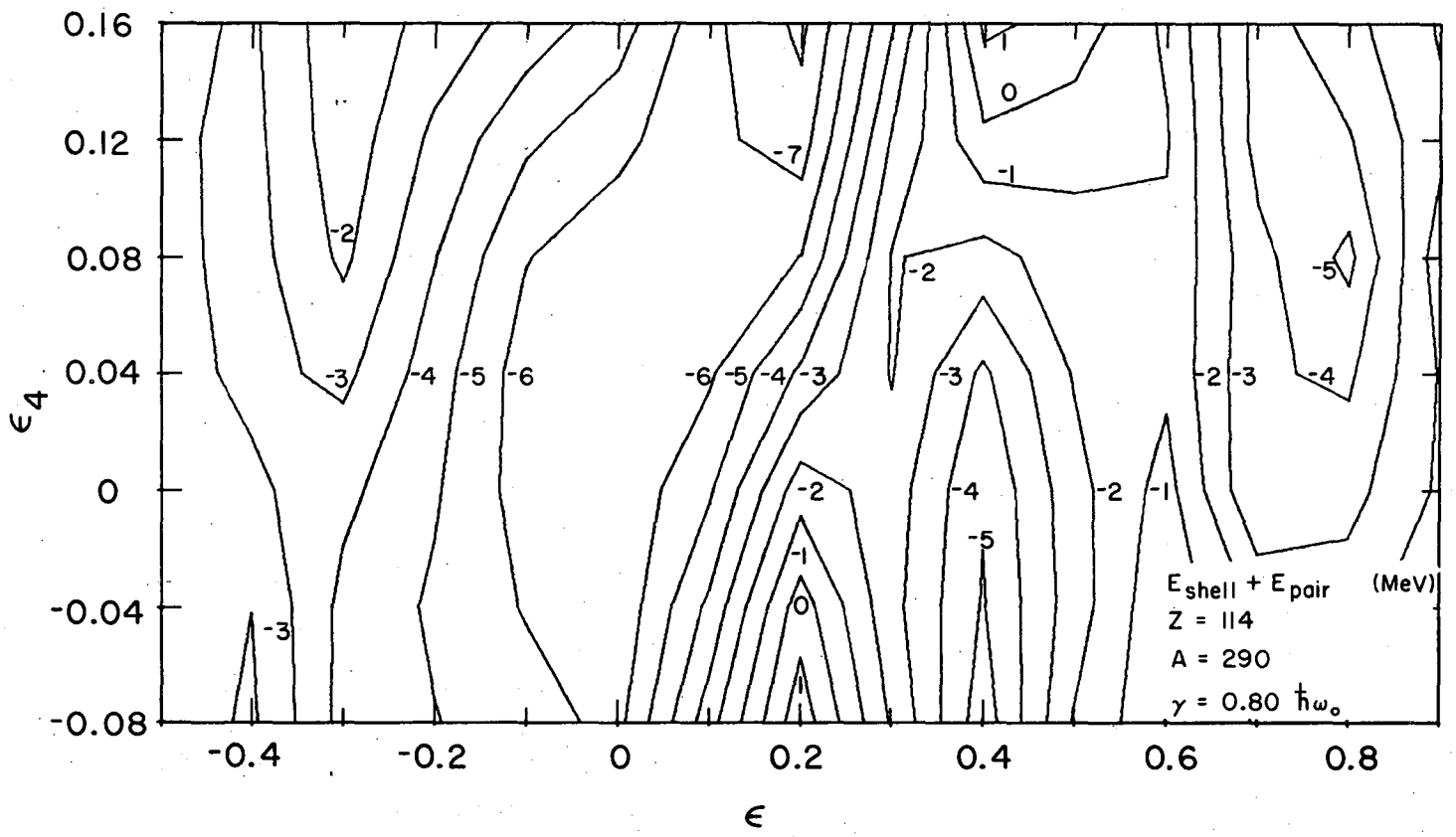
0.16
0.12
0.08
0.04
0
-0.04
-0.08
ϵ_4
-0.4
-0.2
0
0.2
0.4
0.6
0.8
ϵ
$E_{shell} + E_{pair}$ (MeV)
Z = 114
A = 290
γ = 0.80 $\hbar\omega_o$
XBL683-2118

Fig. 20b.

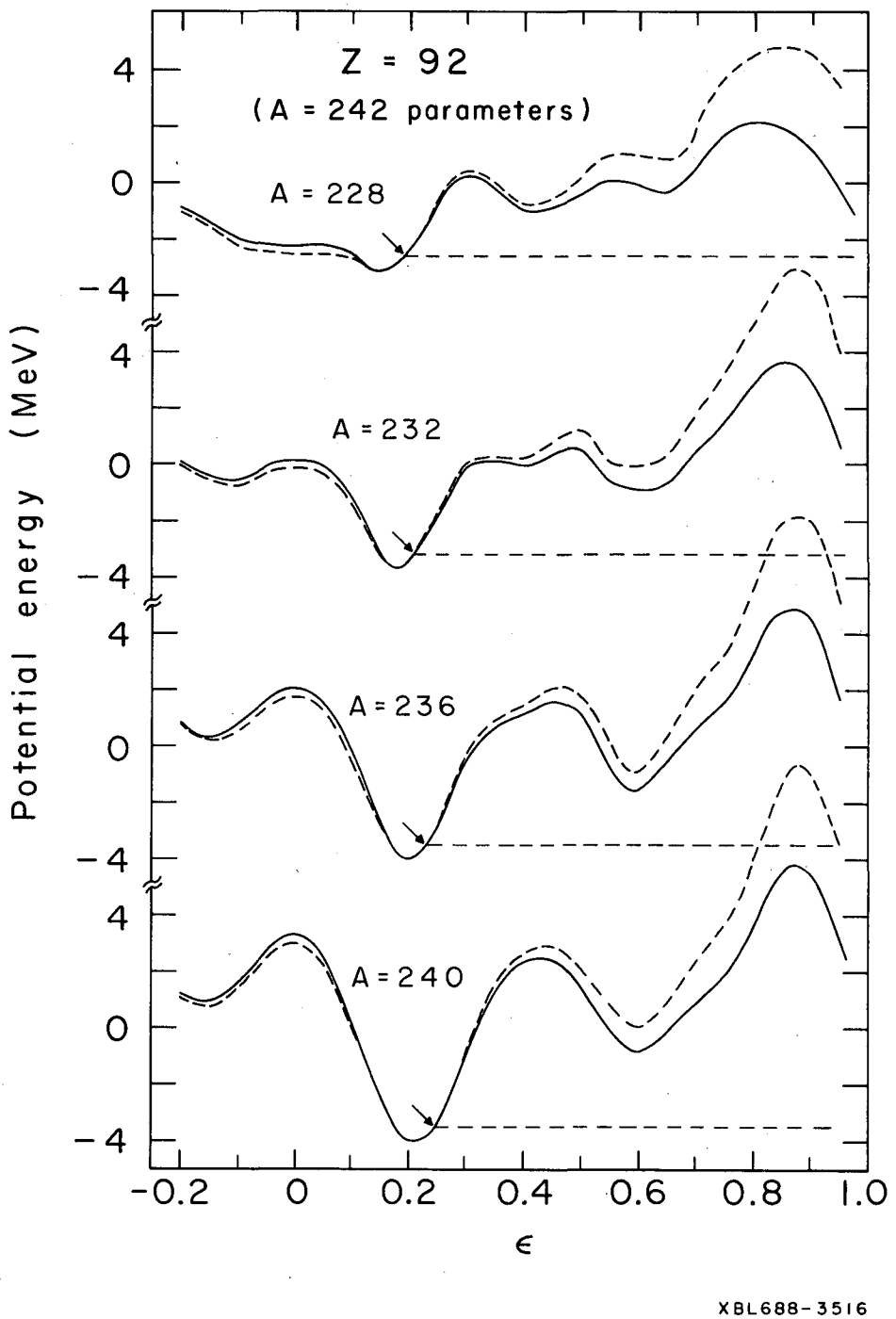
Z = 92
(A = 242 parameters)
A = 228
A = 232
A = 236
A = 240
Potential energy (MeV)
4
0
-4
-0.2
0
0.2
0.4
0.6
0.8
1.0
ϵ
XBL688-3516

Fig. 21a.

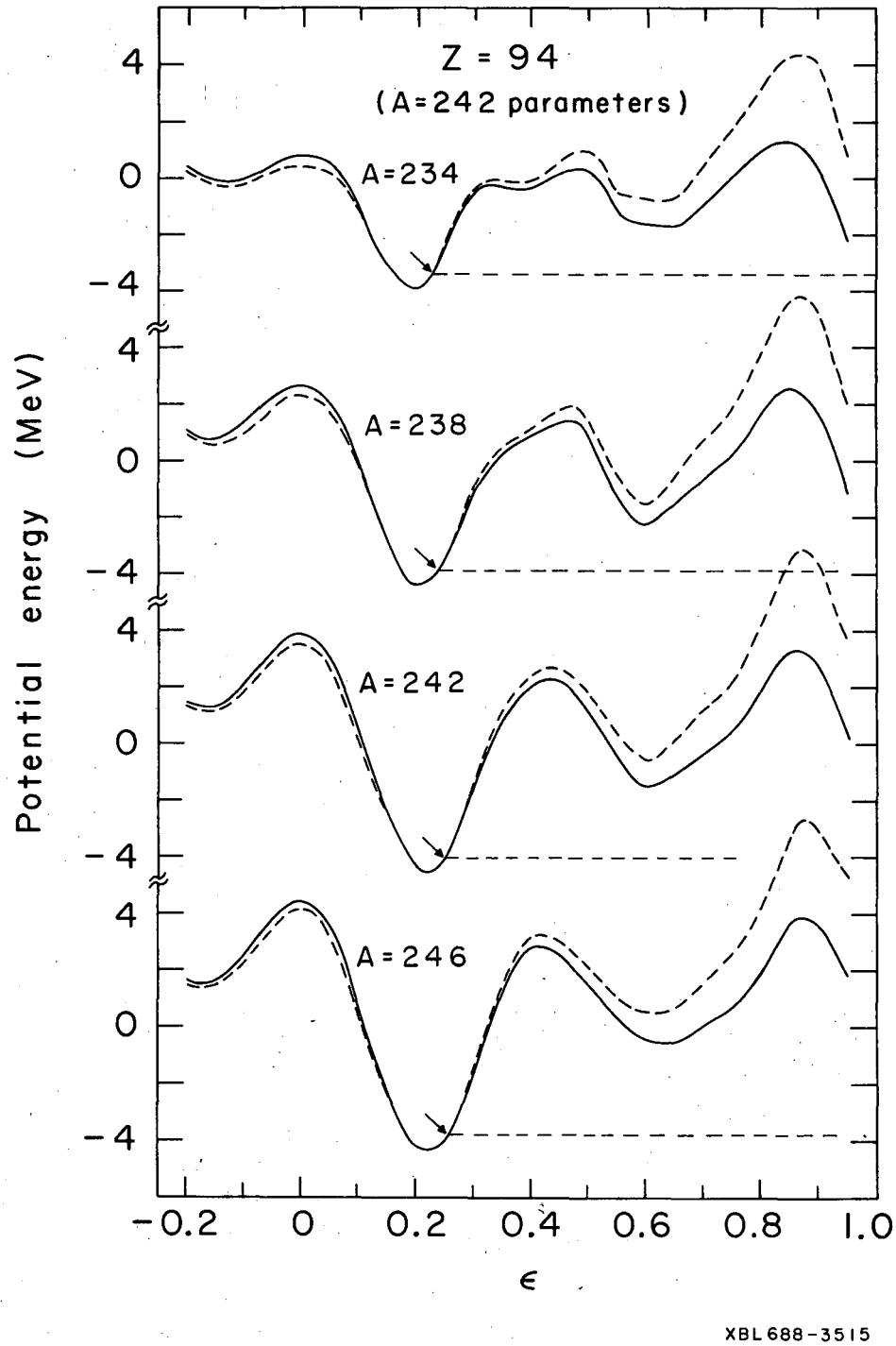
Z = 94
(A=242 parameters)
A=234
A=238
A=242
A=246
Potential energy (MeV)
4
0
-4
-0.2
0
0.2
0.4
0.6
0.8
1.0
ϵ
XBL688-3515

Fig. 21b.

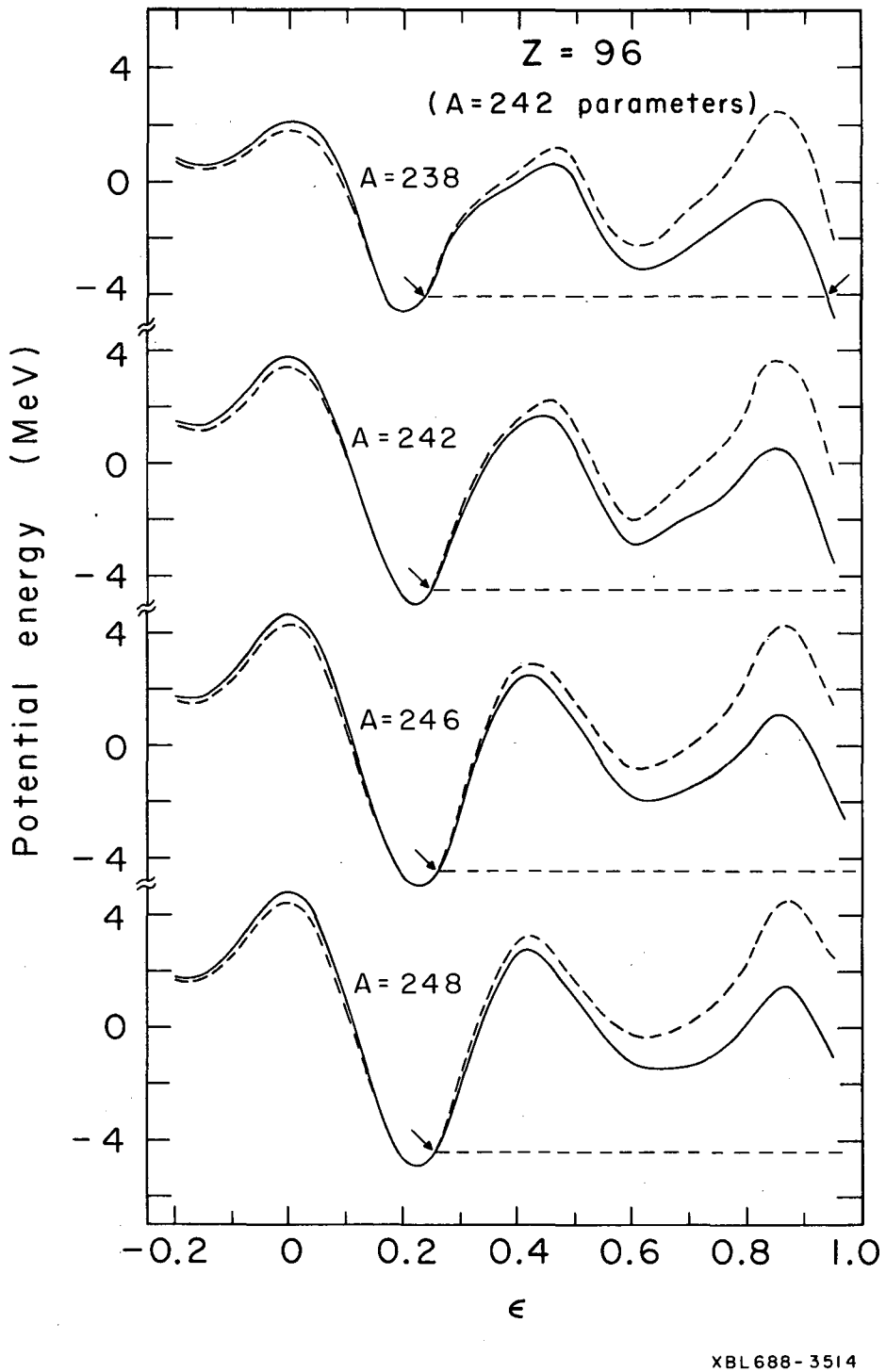
Z = 96
(A=242 parameters)
A=238
A=242
A=246
A=248
Potential energy (MeV)
4
0
-4
-0.2
0
0.2
0.4
0.6
0.8
1.0
ϵ
XBL688-3514

Fig. 21c.

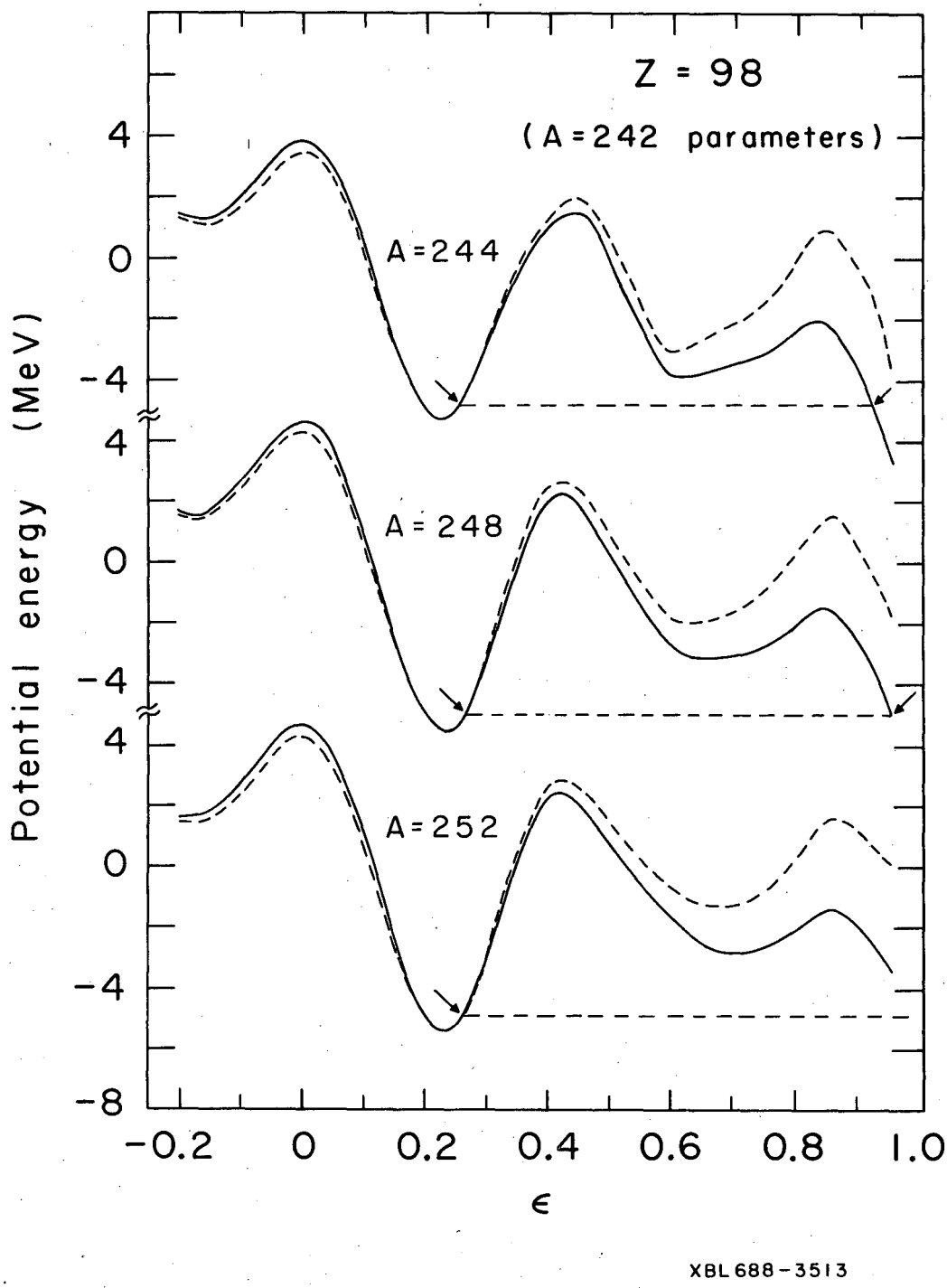
Z = 98
(A=242 parameters)
A=244
A=248
A=252
Potential energy (MeV)
4
0
-4
4
0
-4
4
0
-4
-8
-0.2
0
0.2
0.4
0.6
0.8
1.0
ϵ
XBL688-3513

Fig. 21d.

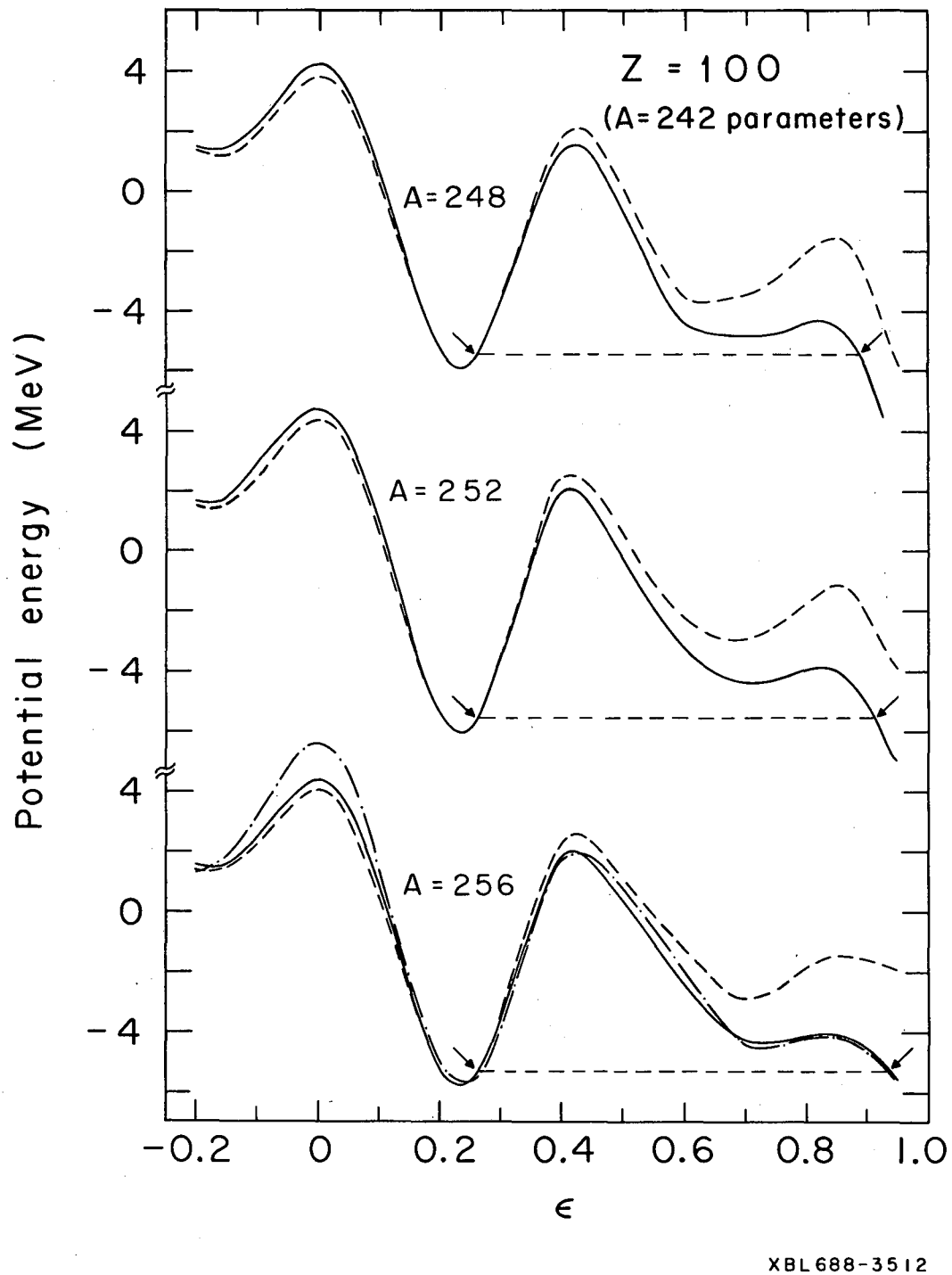
Z = 100
(A= 242 parameters)
A=248
A=252
A=256
Potential energy (MeV)
4
0
-4
-0.2
0
0.2
0.4
0.6
0.8
1.0
ϵ
XBL688-3512

Fig. 2le.

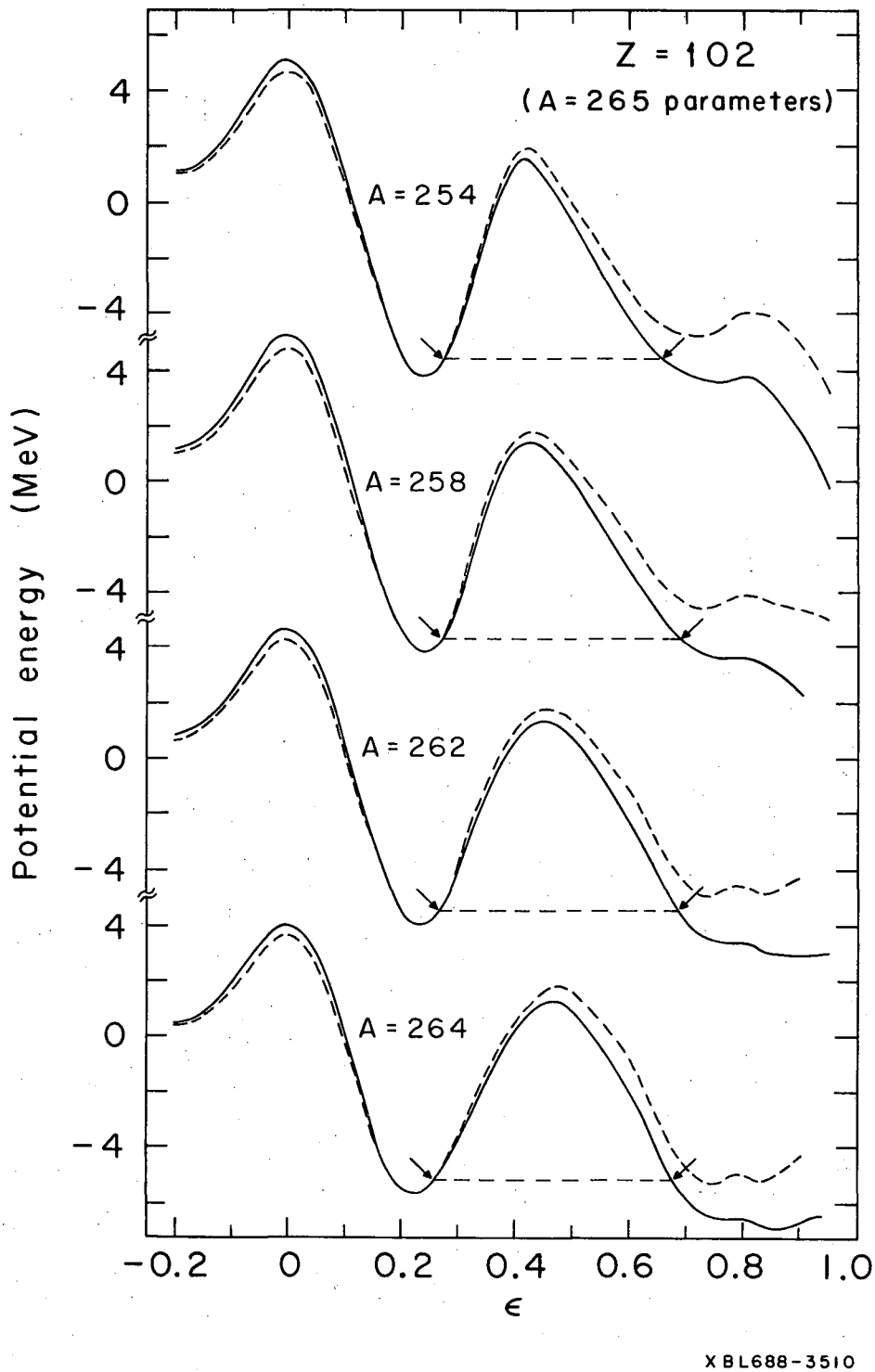
Z = 102
(A = 265 parameters)
A = 254
A = 258
A = 262
A = 264
Potential energy (MeV)
4
0
-4
-0.2
0
0.2
0.4
0.6
0.8
1.0
ϵ
XBL688-3510

Fig. 21f.

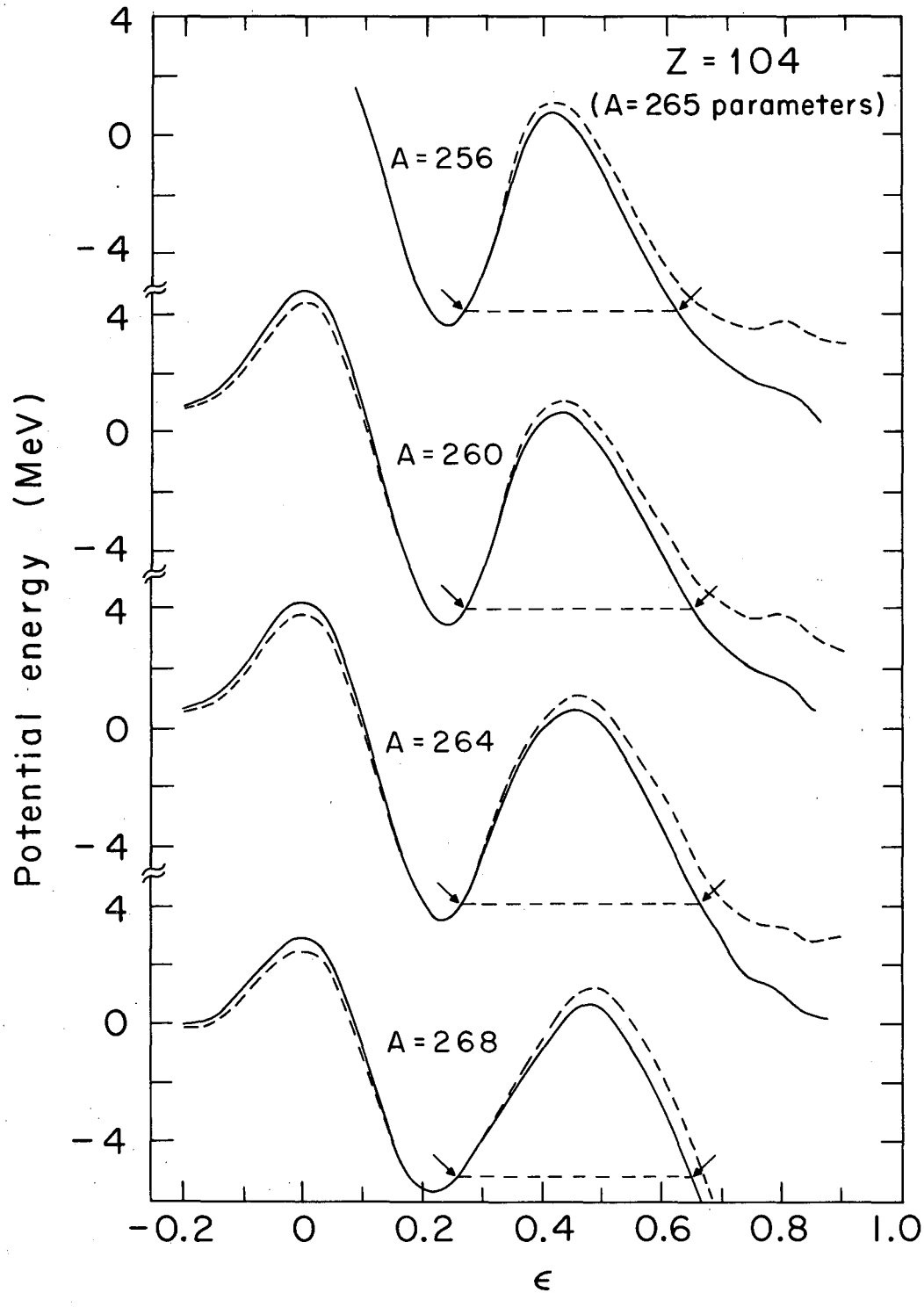
Z = 104
(A= 265 parameters)
A = 256
A = 260
A = 264
A = 268
Potential energy (MeV)
4
0
-4
-0.2
0
0.2
0.4
0.6
0.8
1.0
ϵ
XBL688-3509

Fig. 21g.

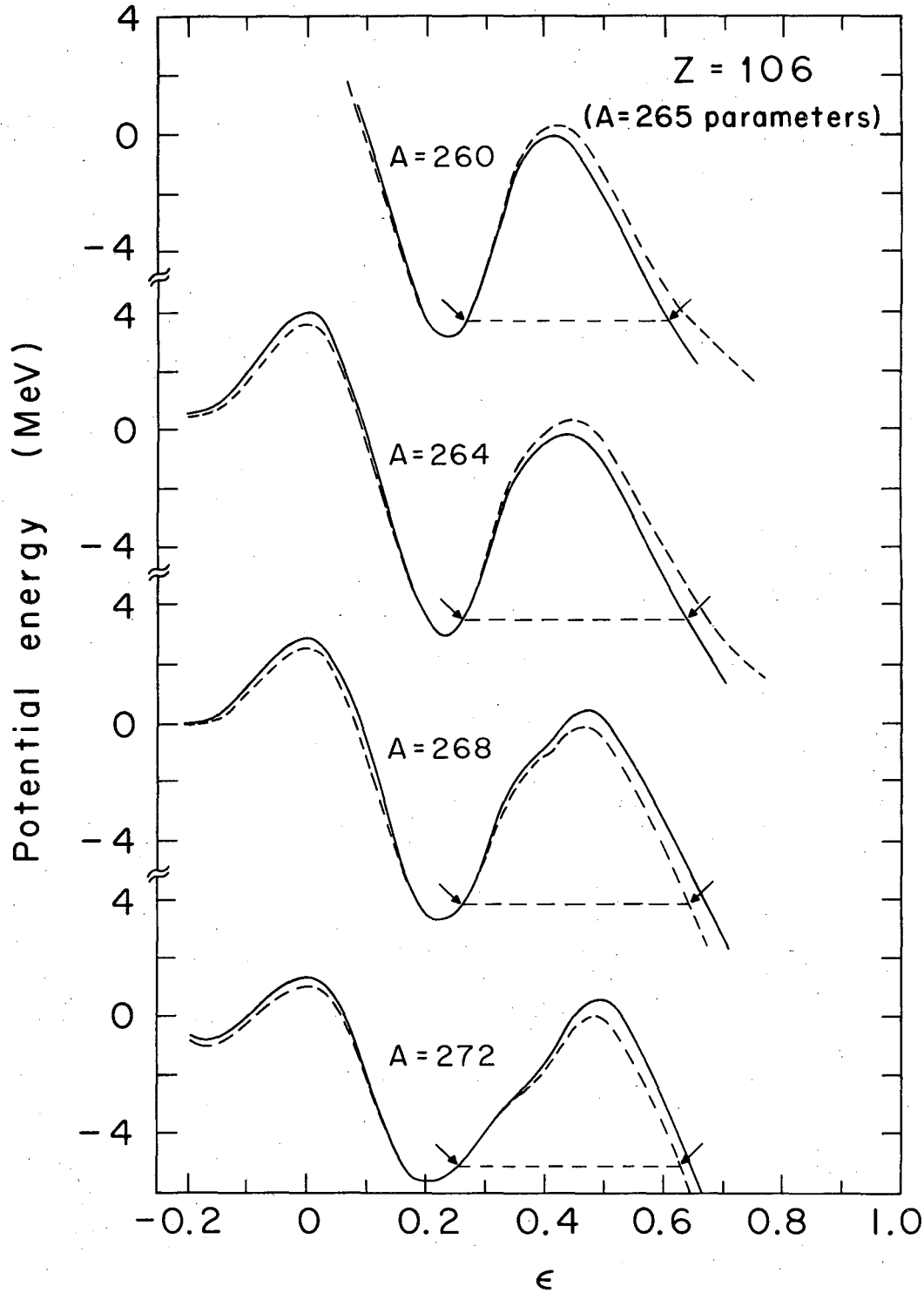

Fig. 21h.

XBL688-3508

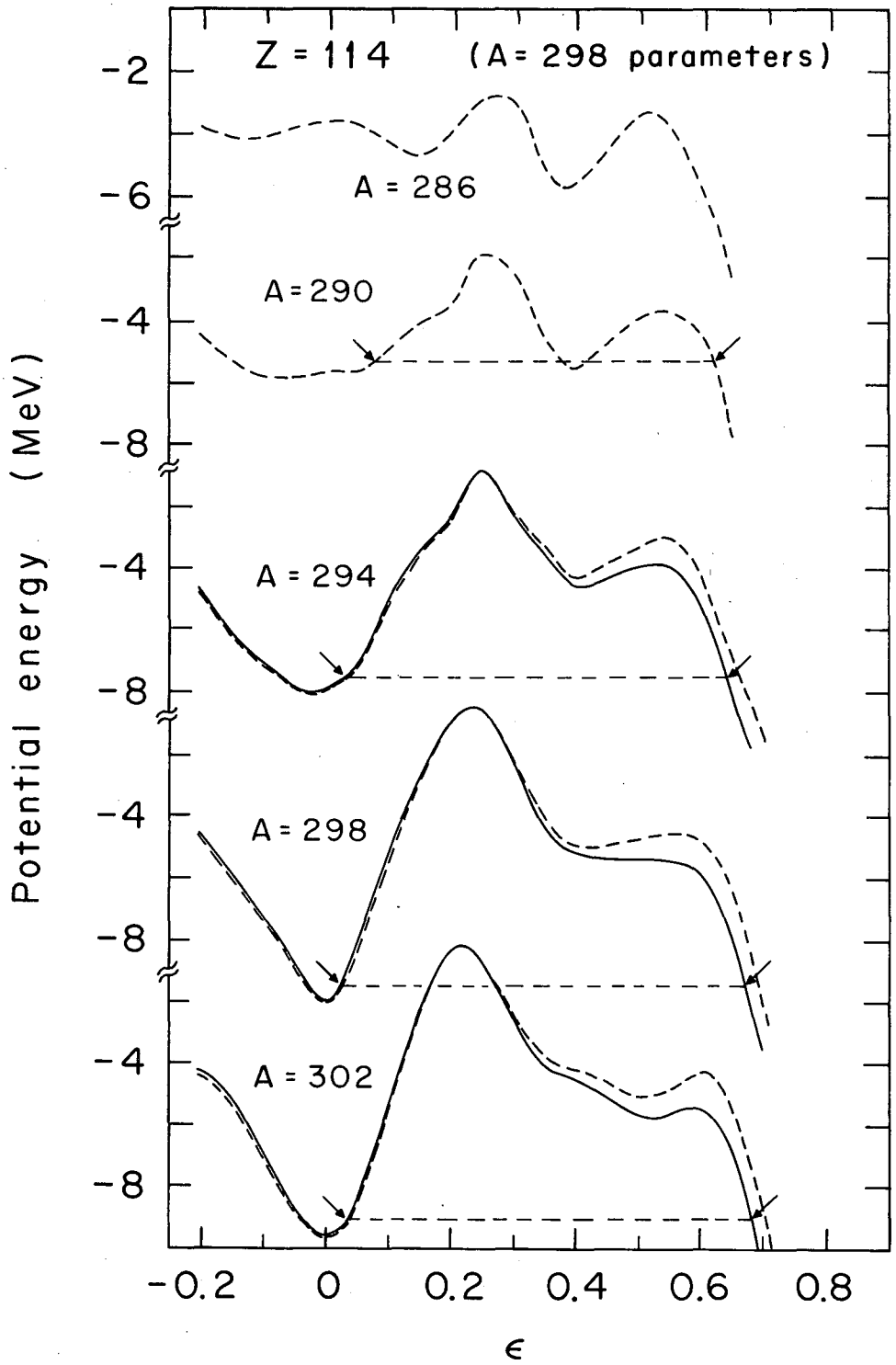

XBL688-3530

Fig. 22a.

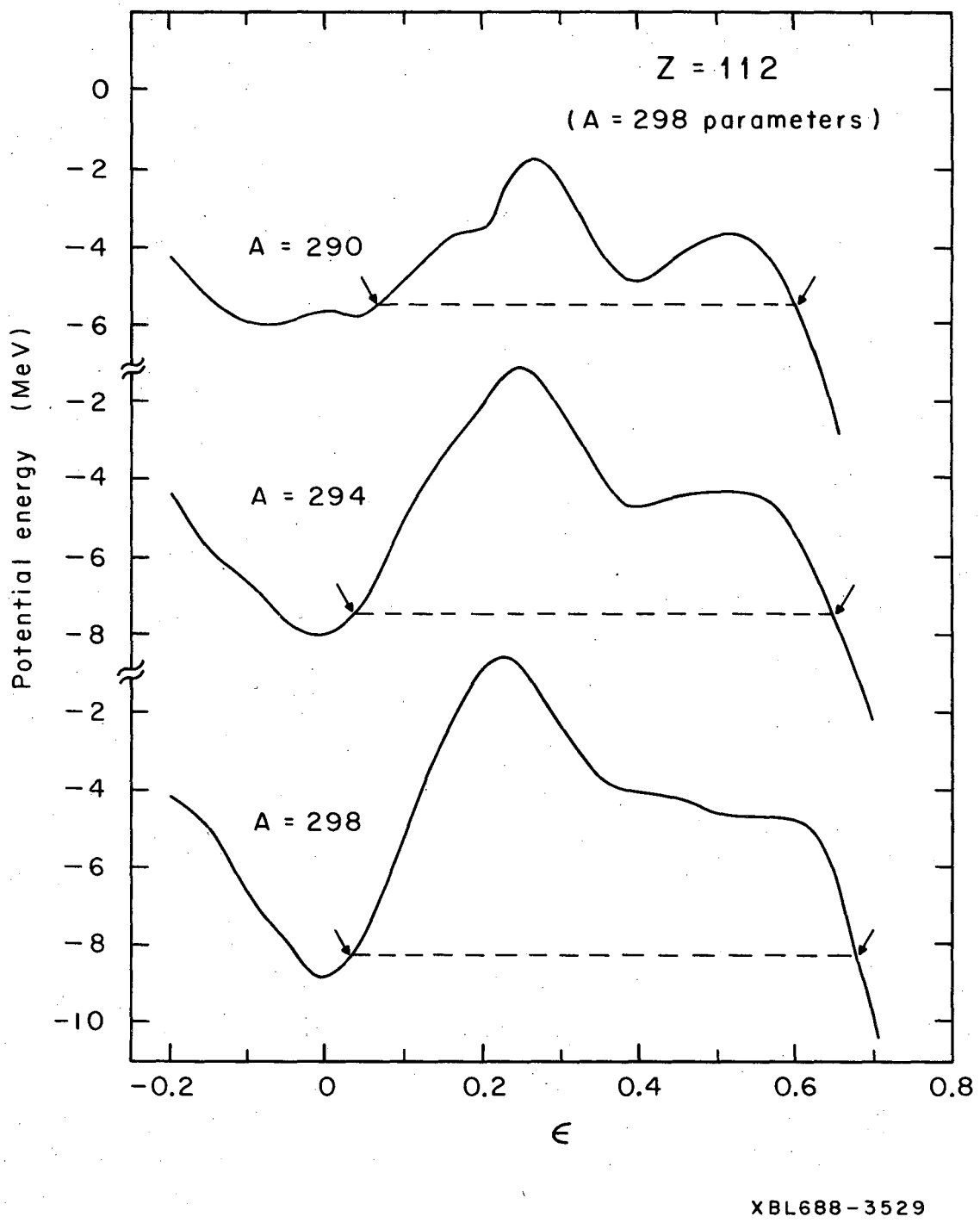
Z = 112
(A = 298 parameters)
A = 290
A = 294
A = 298
Potential energy (MeV)
0
-2
-4
-6
-2
-4
-6
-8
-2
-4
-6
-8
-10
-0.2
0
0.2
0.4
0.6
0.8
ϵ
XBL688-3529

Fig. 22b.

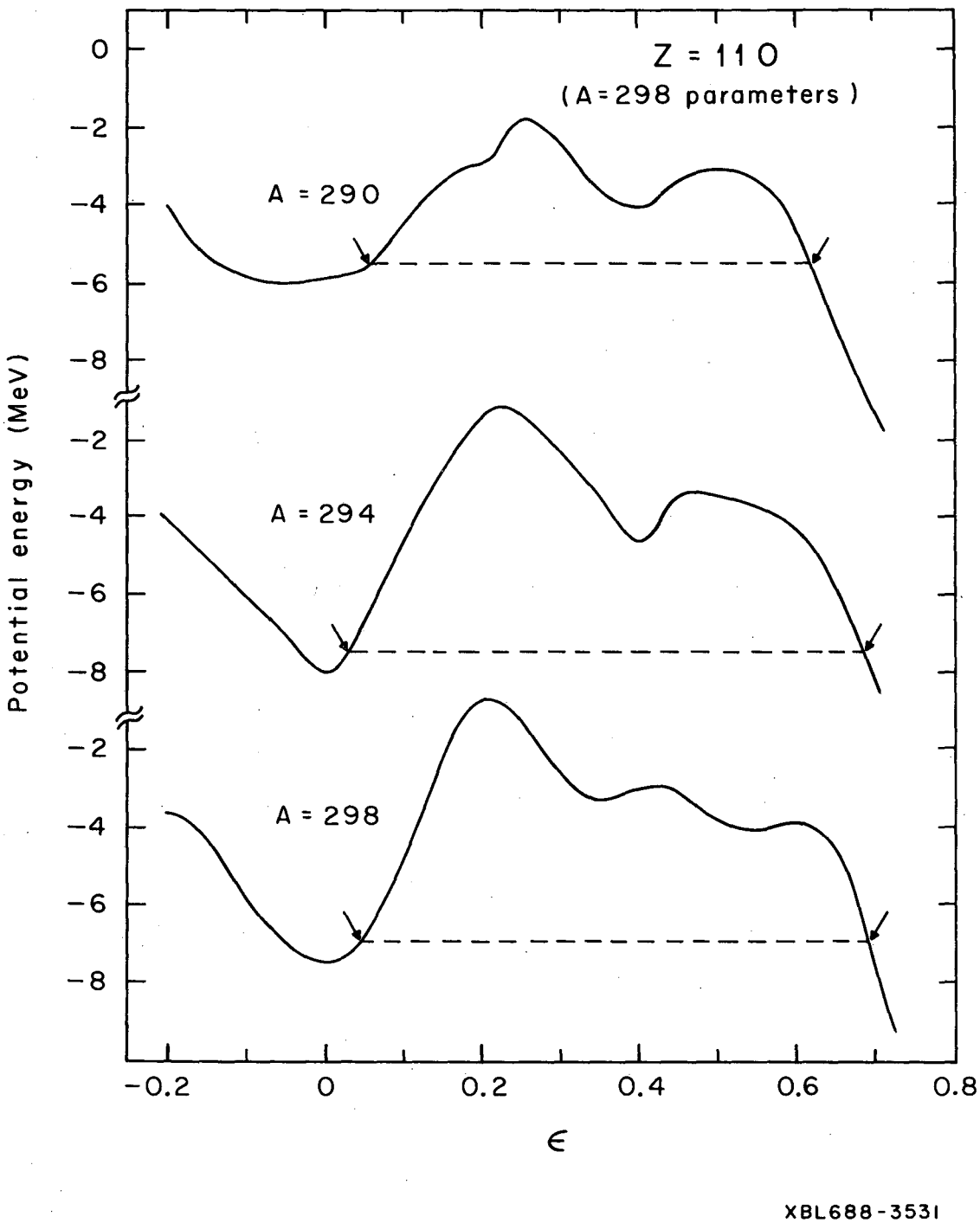
Z = 110
(A=298 parameters)
A = 290
A = 294
A = 298
Potential energy (MeV)
0
-2
-4
-6
-8
-0.2
0
0.2
0.4
0.6
0.8
ϵ
XBL688-3531

Fig. 22c.

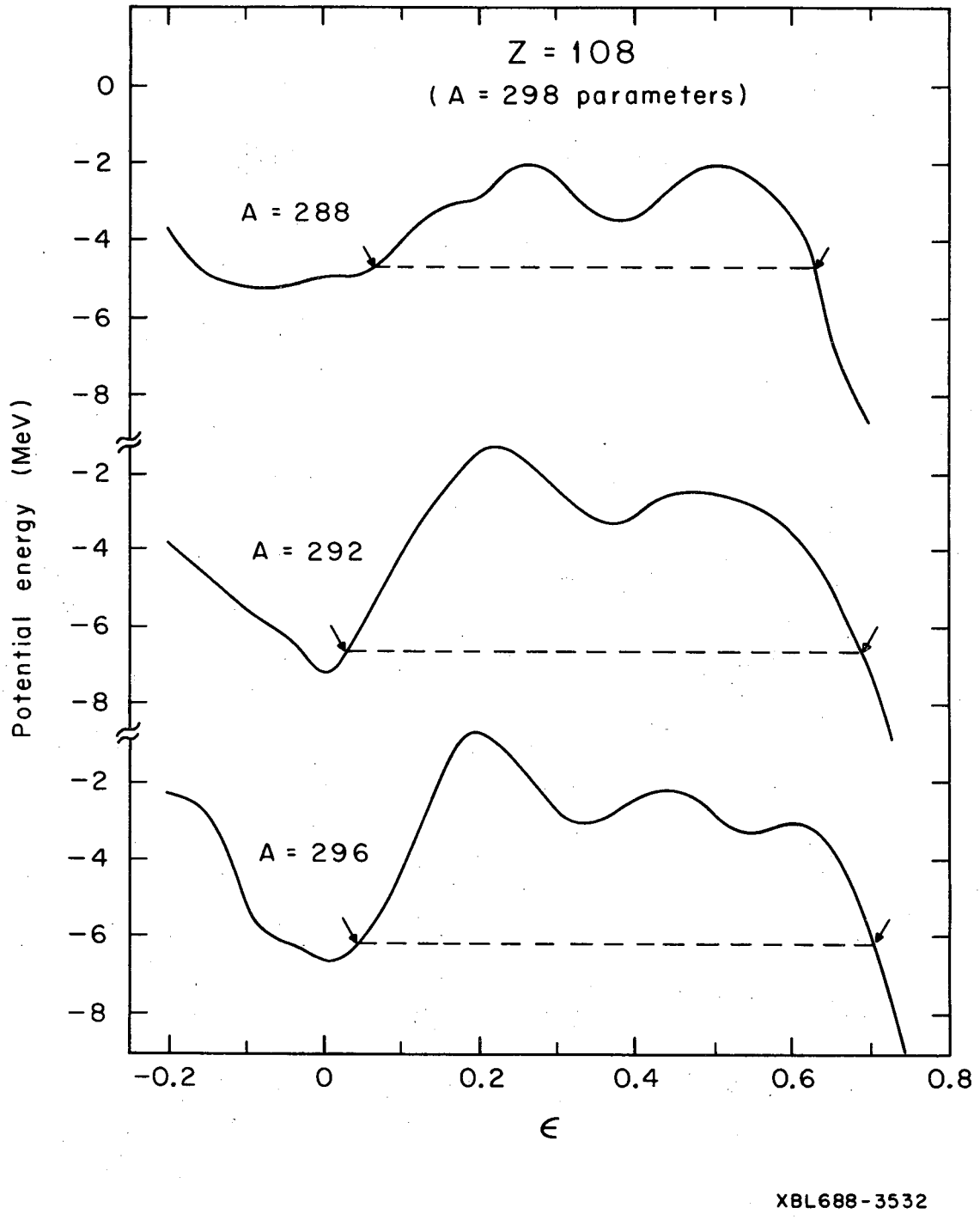
Z = 108
(A = 298 parameters)
A = 288
A = 292
A = 296
Potential energy (MeV)
0
-2
-4
-6
-8
-2
-4
-6
-8
-2
-4
-6
-8
-0.2
0
0.2
0.4
0.6
0.8
ϵ
XBL688-3532

Fig. 22d.

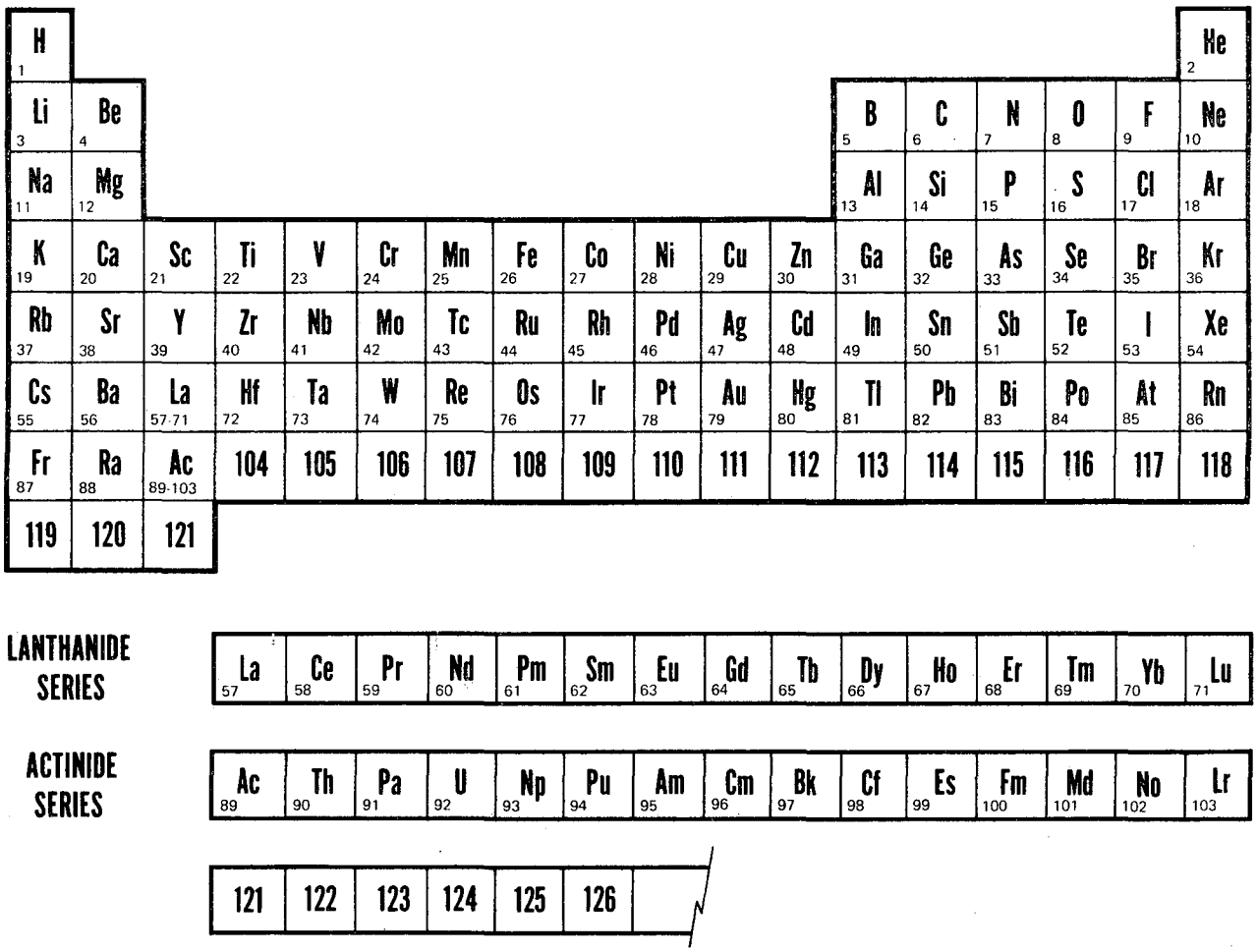
H 1
He 2
Li 3
Be 4
B 5
C 6
N 7
O 8
F 9
Ne 10
Na 11
Mg 12
Al 13
Si 14
P 15
S 16
Cl 17
Ar 18
K 19
Ca 20
Sc 21
Ti 22
V 23
Cr 24
Mn 25
Fe 26
Co 27
Ni 28
Cu 29
Zn 30
Ga 31
Ge 32
As 33
Se 34
Br 35
Kr 36
Rb 37
Sr 38
Y 39
Zr 40
Nb 41
Mo 42
Tc 43
Ru 44
Rh 45
Pd 46
Ag 47
Cd 48
In 49
Sn 50
Sb 51
Te 52
I 53
Xe 54
Cs 55
Ba 56
La 57-71
Hf 72
Ta 73
W 74
Re 75
Os 76
Ir 77
Pt 78
Au 79
Hg 80
Tl 81
Pb 82
Bi 83
Po 84
At 85
Rn 86
Fr 87
Ra 88
Ac 89-103
104
105
106
107
108
109
110
111
112
113
114
115
116
117
118
119
120
121
LANTHANIDE SERIES
La 57
Ce 58
Pr 59
Nd 60
Pm 61
Sm 62
Eu 63
Gd 64
Tb 65
Dy 66
Ho 67
Er 68
Tm 69
Yb 70
Lu 71
ACTINIDE SERIES
Ac 89
Th 90
Pa 91
U 92
Np 93
Pu 94
Am 95
Cm 96
Bk 97
Cf 98
Es 99
Fm 100
Md 101
No 102
Lr 103
121
122
123
124
125
126

Fig. 25.

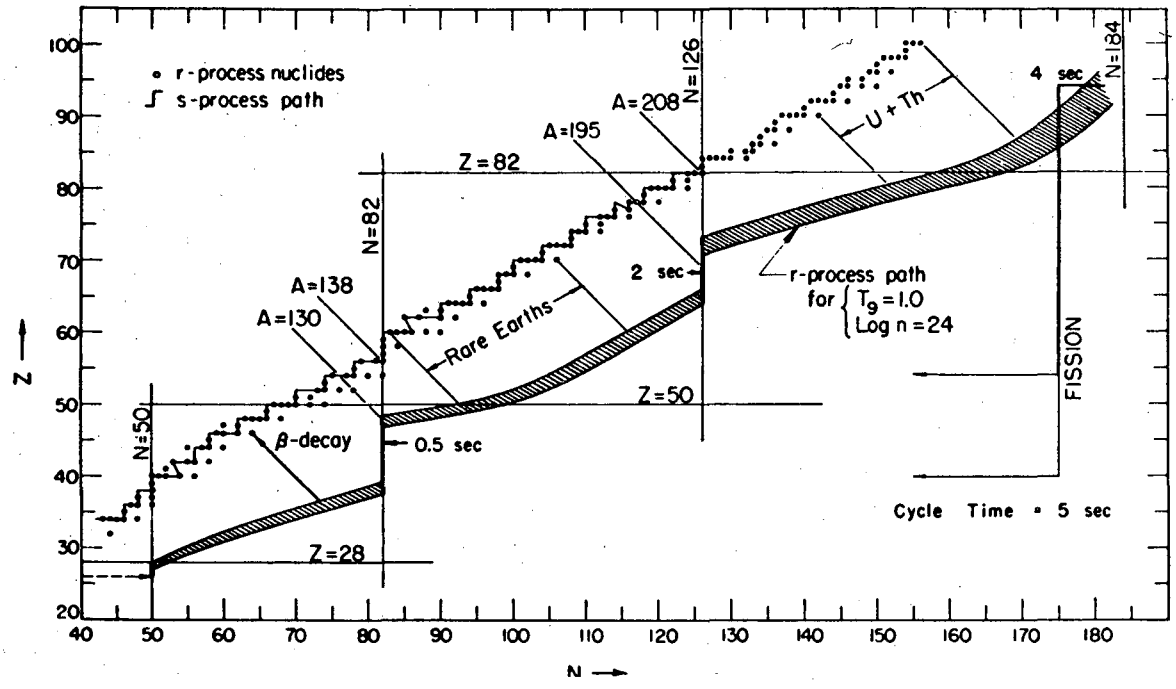

XBL 688-5648

Fig. 26.

TECHNICAL INFORMATION DIVISION
LAWRENCE RADIATION LABORATORY
UNIVERSITY OF CALIFORNIA
BERKELEY, CALIFORNIA 94720